CF

Development and Validation of an Electrical Energy Harvesting System Utilising the Seebeck Effect for use in AUV/Submarines

By

Jordan James Kelly

In collaboration with

Delkia

Abstract

Thermoelectric Generators (TEGs) utilise the Seebeck effect which can directly convert heat energy into electricity. When a temperature difference is created across the TEG modules, an electromotive force will be generated if the modules are connected in an electric circuit with a load. As the planet aims to reduce its carbon footprint clean methods of generating electricity are increasing in demand, and therefore so is the research into the use of TEG modules.

This research aimed to determine how TEGs could be used in utilising the temperature difference between the inside of a small submarine and the water which surrounds it and predict how much electrical power could be produced. This was done using both Ansys software and physical experiments. A test rig was built to emulate the conditions which would be experienced by the TEG modules in a submarine, with a warmer constant temperature on one side and the other side cooled by flowing chilled water. Many materials and the potential addition of heat transfer fins were tested, and all experimental tests performed were then simulated in Ansys Fluent and Thermal Electric to ascertain how accurate the simulations represent real-world results. The tests were performed from temperatures ranges between approximately $5°C \leq T \leq 20°C$, it was decided that all temperatures $17°C$ and below simulated in Ansys would give a fair representation of how much power the TEGs could produce.

Using the information from these tests and simulations, scaled up models we simulated in Ansys to model the TEG modules in a submarine section. These results showed that the use of heat transfer fins was not necessary due to the thickness of the submarine wall and the velocity at which the submarine would travel. At a temperature difference of $15°C$ between the inside of the submarine and the water flowing around it, four TEG modules connected in series can be expected to produce 0.35W.

Table of Contents

List of Figures

List of Tables

Acknowledgements

Nomenclature

A- Cross-Sectional Area

C_f- Skin Friction Coefficient

C_p- Specific Heat Capacity

e_{fin}- Fin Thickness

h- Average Heat Transfer Coefficient

h_{H2Ofin}- Heat Transfer Coefficient of Fin

I- Current

k- Thermal Conductivity

L- Length of Plate

L_{fin}- Fin Length

Nu- Nusselt Number

Pr- Prandtl Number

Q- Flow Rate

$\dot{q}$- Heat Transfer Rate

R- Resistance

Re- Reynolds Number

T- Temperature

ΔT- Temperature Difference

U- Overall heat transfer coefficient

U_τ- Shear Velocity

U_{bulk}- Bulk Fluid Velocity

V- Voltage

w_{fin}- Fin Width

z- Figure of Merit

α- Seebeck Coefficient

η- Auxiliary Parameter

λ- Thermal Conductance

ρ- Density

σ- Electrical Conductivity

τ_W- Wall Shear Stress

τ-Thomson Coefficient

δ- Boundary Layer Thickness

μ- Dynamic Viscosity

π- Peltier Coefficient

Introduction

1.1 Background

The world is changing. After years of relentlessly burning fossil fuels for energy and releasing harmful gases into the Earth's atmosphere scientists across the globe have detected the damage caused and predict a worrying future if things were to stay the same. According to (NCDC, 2020), the average surface temperature has risen 1.18ºC since the late 19th century due to human activity which is producing greenhouse gases. To the average person 1.18ºC in over a hundred years may not sound a lot but the damage is frightening, and projections are only showing this to keep rising. The rising temperature is causing glaciers to retreat and Arctic Sea ice to melt which is causing sea levels to rise and endanger coastlines and low-lying cities. Extreme events such as river flooding are happening at an increasingly alarming rate due to the warming climate a study by (Manuela I. Brunner, 2021) confirms, this shows how not only the coastal cities are affected. Climate change will not only damage communities and threaten people with flooding, but the high temperatures are also increasing the likelihood of droughts and temperatures which cause risk to health. For example, in the United Kingdom in 2022 the temperatures in some areas saw record highs, even reaching 40.3ºC in Lincolnshire. This temperature in a country such as England where houses do not generally have air-conditioning and are designed to keep heat in is not just uncomfortable but can endanger the lives of residents, especially the elderly and vulnerable population. A study by (Raju, 2022) found that this specific heatwave was made at least ten times more likely due to human made climate change. Figure 1 shows graphs depicting the highest temperature experience in the UK each year (a) and the highest two-day average temperature experienced each year (b). It is clear to see that the extremity of temperature the UK is experiencing is trending upwards as both graphs show a positive correlation.
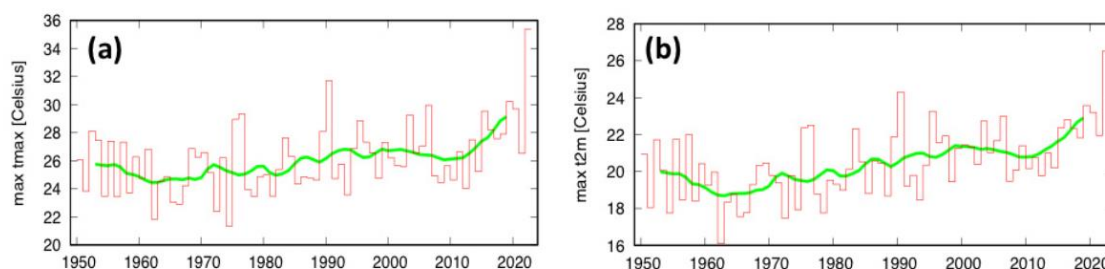
Figure 1 (WWA, 2022):UK max temperature experienced each year (a) and UK two-day average max temperature (b)

It is common knowledge across the globe that there must be change for the benefit of planet, and it is clear to see in recent years on a large scale what is being done, from renewable energy such as solar and wind, to the gradual drive away from fossil fuelled vehicles. What may not be as clear to the public is the smaller forms of reducing carbon footprint by converting waste energy from a system into a usable form. Systems such as regenerative braking in vehicles help convert kinetic energy into usable electrical energy.

Sustainable- "capable of being maintained or continued at a certain rate or level" (OED, 2022). It is clear to the modern public that the burning of fossil fuels is not sustainable for the future of energy production, what may not be obvious is that electric power via batteries is not a solution for every energy problem. Largely due to the increase in popularity of

electric vehicles, the demand for lithium to be used in the batteries has risen rapidly. Currently the raw materials for producing Lithium-Ion batteries are not being mined at a rate fast enough to keep up with demand which is causing prices to ascend rapidly, as shown by figure 2.
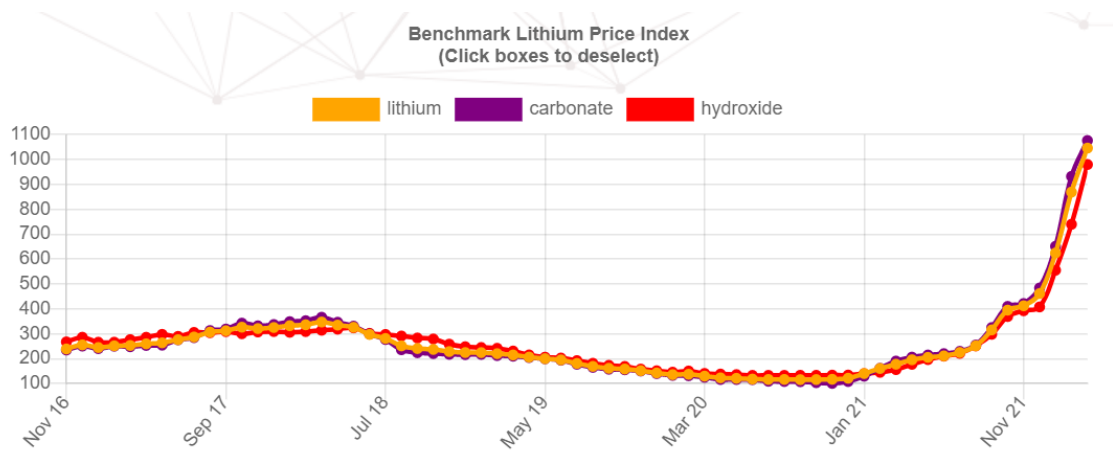
Figure 2 (Benchmark Minerals, 2021): Price index for raw materials used in Lithium-Ion batteries

A solution to reducing the need for batteries is to have methods of electrical power generation which are directly linked to a system, rather than having to use a battery to store the electrical power.

One form of renewable energy conversion which is not used for mass electricity production in the sense that wind turbines are is Thermoelectric Generators converting heat energy directly to electrical. These generators are currently used in limited applications, most of which are used to utilise waste heat lost from a system. Although this technology is not new and rare comparatively with other renewable energy generators, there has been an increase in interest in recent years due to its little to no maintenance required among other advantages.

1.2 Project Focus

Submerged water vehicle such as Autonomous Underwater Vehicles (AUVs) and small Submarines are common across the globe now and are used for many purposes for example surveying the seabed. The temperature of the Oceans/Seas decrease with depth. This project aimed to utilise the temperature difference between the inside of an AUV and the water surrounding it by means of thermoelectric generation. This project focused on both physical and mathematical modelling (using ANSYS Workbench) to test the system. A system like this would make a greener alternative to using another battery or recharging a battery.

1.3 Problem Statement

This investigation aimed to confirm the hypothesis, if thermoelectric generators produce electricity via utilising temperature differences across systems, then they will be viable additions to submarines to generate additional usable power to either be stored or power a submarines sub-system.

1.4 Aims & Objectives

The main aim of this project was to determine whether the use of Thermoelectric Generators to harvest electricity from the temperature difference between the inside of an AUV and the water surrounding is viable for extending mission time or powering an electrical subsystem, economically and logistically.

To fulfil the aim of this project the following key objectives must be achieved:

- A suitable test rig which would accurately simulate the conditions the AUV will experience must be built. This should mimic the effect of different methods of heat exchange on the vessel, to ascertain which Is most effective. The system needed to be waterproof and possible to replicate in Ansys.
- A control panel needed to be manufactured to accurately control and measure parameters when tests were performed on the TEGs.
- The extra power which will be used due to changes to the geometry of the AUV must be calculated to determine the net power produced by the system. This will allow understanding of whether the system is beneficial. This is not necessary if the geometry does not need to be changed.
- A parameter study would take place to determine how the material of the heat exchange surface and extra geometry such as heat transfer fins would affect the power output of the TEGs. This data helps with the design of the scaled-up system.
- The real-world results need to be compared with simulation results to determine how accurate the simulations are. The test rig is be deemed accurate if the power produced in the simulations is within the standard error of the physical test results. The standard error is calculated by dividing the standard deviation of the results by the square root of the number of samples.
- Using the information from the comparison of the test rig and the simulations of it, further simulations need to be done to see how the TEGs may perform when scaled up in an actual AUV/Submarine. This would involve determining the best orientation/locations for the TEGs and deciding on if the potential power they can produce would make it worth implementing them into submarines economically and logistically in the future.

1.5 Delkia Role in Project

Delkia are a company which specialise in systems integration focusing within the aerospace, clean energy, and maritime industries. The company played a large role in supporting the project financially by contributing funding towards the project. However, arguably even more valuable to the project was the resources and support provided by their engineers throughout the project, especially when designing and manufacturing the control unit which was completed at the Delkia workshops. The company also provided useful resources such as dimensions for submarines, which made scaling up the system to fit a real world design more accurate.

2 Literature Review

2.1 Autonomous Underwater Vehicles (AUVs)

Autonomous Underwater Vehicles (AUVs) are a class of vehicle which are designed to operate underwater without the need for any crew onboard. The specifications of these vehicles vary greatly depending on its desired use. AUVs range from small gliders which can be propelled by changes to its buoyancy such as (Douglas C. Webb, 2001) to much larger battery propelled AUVs. Many of these larger electric propelled AUVs can only be submerged for up to 48 hours or shorter due to the limited power that the batteries can carry.

2.2 AUV/Submarine Environment

Most AUVs are designed to operate in large bodies of water such as the seas and oceans. The temperature of these bodies of water changes with depth due to the water at the surface being influenced by factors such as amount of sunlight and local air temperature. Figure 3 shows temperature data recorded by (Carl Freitas, 2021) in the North Sea off the coast of Norway.
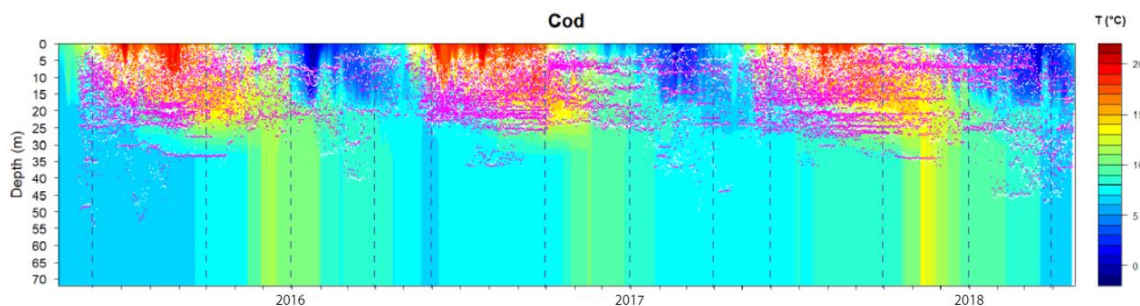
Figure 3 (Carl Freitas, 2021): Sea temperature by depth and month in the North Sea off the coast of Tved, Norway and the location of Cod at these measurements (pink dots).
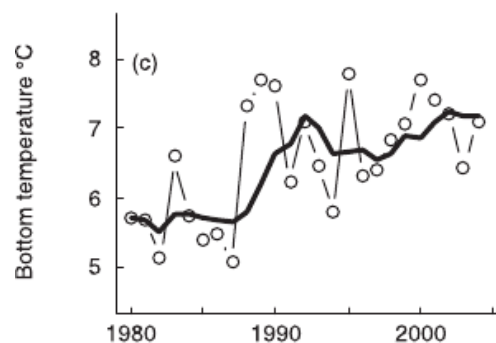
Figure 4(Nicholas K. Dulvy, 2008): Mean winter bottom temperature of the North Sea from 1980-2008.

From looking at Figure 3 it appears that the water 35m deep and below averages a temperature of about 7⁰C and even hits lows of approximately 4⁰C. The water at depths of less that 35m fluctuates in temperature much more, this is due to the air/wind temperature on the surface having an effect. The water at the surface can reach near 1⁰C in the winter months.

Figure 4 shows the recorded mean temperature at the bottom of the North Sea through winter which further supports figure 3 that the mean temperature is approximately 7⁰C, although this data is a decade old it correlates with the recent data shown in figure 3.

2.3 The History of Thermoelectric Generators

Thermoelectric Generators (TEGs) work by converting heat energy into electrically energy directly without any mechanical work. This effect was discovered by Thomas Johann Seebeck in 1821 when he found that if two dissimilar metals were connected in circuit and a temperature gradient was maintained across the metals, then an Electromotive force is produced. This is known as the Seebeck effect.

Later in 1834, Jean Charles Athanase Peltier discovered what would be the reverse of the Seebeck effect, if two dissimilar materials were connected in circuit and a current was passed through, a temperature difference across the material junctions would appear as heat would travelled away from the cold junction to the hot. This became known as the Peltier effect and is very important in refrigeration technology.

The third and final thermoelectric effect discovered to date was in 1854 by William Thomson, later known as Lord Kelvin from 1892. The effect that Thomson discovered differed in a sense from the prior two as it is present in a single material rather than a thermocouple. It is the effect in which when an electric current passes through a homogenous material with a temperature difference across it in circuit causing heat to either be released or absorbed. Thomson not only discovered this effect (the Thomson effect), but he also derived relationships between the thermoelectric effects, known as the Kelvin relations. The Peltier coefficient (π) and Seebeck coefficient (α) are related by equation (1).

$$\pi_{PN} = \alpha_{PN}T \qquad\qquad (1)$$

The P and N subscripts refer to the positive and negative elements in the thermocouple respectively. The Thomson coefficients (τ) of a thermocouple can be related to the Seebeck coefficient by equation (2).

$$\tau_P - \tau_N = T \cdot \frac{d\alpha_{PN}}{dT} \qquad\qquad (2)$$

This phenomenon largely remained unused in practical technologies as the power output was very small. According to (Davide Beretta, 2019) in the first half of the 20th century research into the use of semiconductors began. This revolutionised the potential for practical uses of TEGs as semiconductor materials much higher power outputs than what was previously seen, although still low comparatively with other forms of electrical generation methods.

2.4 Physics of Semiconductors

A good TEG will have three properties: high Seebeck coefficient 'α', high electrical conductivity 'σ', and low thermal conductivity 'λ'. This is shown by equation (3) determining the value of the figure of merit 'z' for an individual material (Goldsmid, 2017).

It is believed that the figure of merit was first referenced by Edmund Altenkirch in 1909 (Kar, 2016).

$$z = \alpha^2 \cdot \frac{\sigma}{\lambda} \qquad (3)$$

The reason semiconductors have been favoured as TEG materials is that it is possible to optimise the three properties which affect the figure of merit with different techniques, one of which involves doping the materials to increase the charge concentration. To understand how doping benefits, the band theory must be understood.

Electrons are contained in states in different bands of energy within the crystal lattice of a semiconductor. The Fermi level in the band theory is defined as the energy level at which there is a 50% probability of occupation of an electron at any temperature. Figure 5 shows how the location of the Fermi level in comparison the both the Conduction band and Valence band affect what polarity the semiconductor is.
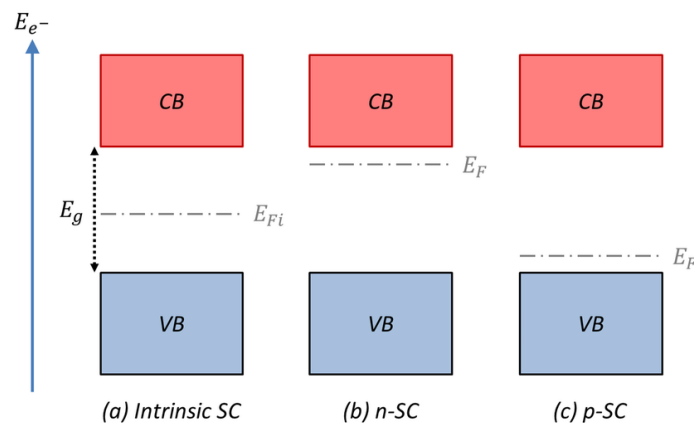
Figure 5 (Rioult, 2015): Fermi energy level location in intrinsic, n-type, and p-type semiconductors

The electrical conductivity and Seebeck coefficient are dependent on how close the Fermi level is from the bands. If the Fermi level is closer to the Conduction Band, then the amount of quasi-free electrons outweighs the number of holes and vice versa. Doping with elements that act as electron donors will increase charge carrier concentration in n-type semiconductors, whilst doping with elements which act as electron acceptors will increase the charge carrier concentration in p-type semiconductors.

Another method of optimising a semiconductors figure of merit which was first proposed by (Dresselhaus, 1993) in which they investigated the effect of nanomanufacturing the semiconductor material into one dimensional nanowires. When the thickness of the material becomes incredibly small (2 or 1 dimensional), the figure of merit rises due to an increase in the effective density of states at the Fermi level. This discovery had a positive impact on the electronic properties of TEGs in theory, however according to a book by (Oliver Eibl, 2015) this initial research was not as useful in practice as nanomanufacturing thermoelectric materials to reduce into superlattices to reduce thermal conductivity, which in turn rises the ZT (Dimensionless Figure of Merit) value.

It is common knowledge throughout the science community which bulk semiconductor materials perform best at which temperature ranges; much of the modern research being carried out for semiconductors is into increasing the properties of these materials via means of dopants and nano structuring superlattices.

2.5 Current Thermoelectric Generators & their applications

2.5.1 Background

TEGs are an attractive concept due to their low maintenance, low noise, and usefulness on capturing waste heat there is a lot of research conducted for these technologies. The main aim which researchers try to achieve when developing TEG materials is to produce a material with a high dimensionless figure of merit (ZT) for the temperature which it will operate at. Most TEGs used in the real world are some form of semiconductor. Figures 6 & 7 shows a comparison of the ZT of some of the most common semiconductors used at a range of temperatures.
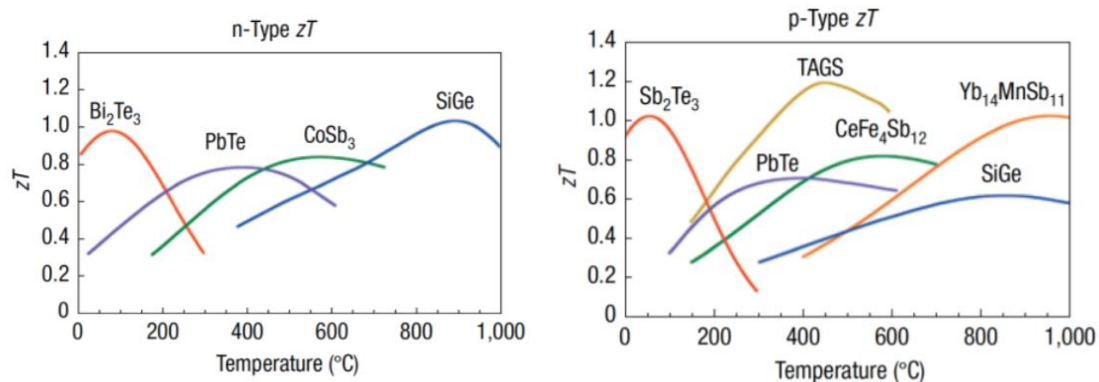
Figure 6 & Figure 7(Snyder G.J., 2008): ZT of some common semiconductor materials based on operating temperature.

2.5.2 Common Applications for TEGs

One of the most important applications for TEGs is in the aerospace industry where TEGs convert heat released from the decay of a radioactive isotope to generate electricity for spacecrafts and satellites, semiconductor materials would be chosen for this application of TEG. This method of TEG has been in use for a long time as proven by a patent by (Jordan, 1958).

A few decades later the use of TEGs was implemented into the automotive industry to convert waste heat from exhaust gases into usable electricity, the first patent for this type of system to my knowledge was by (Bass & C., 1993). TEGs in automobile exhausts use semiconductors. An earlier patent from (Kiekhaefer, 1965) aimed to directly convert waste heat directly from an internal combustion engine into electricity using TEGs however this method does not appear to be as common as the use in the exhaust system.

TEGs are also used in electronic systems to recover waste heat from batteries/circuits to power other electrical components. A system using this technology was patented by (Suski, 1996) which converted heat generated from a semiconductor circuit into usable electricity. A new approach with this technology is to convert waste heat from circuits in mobile phones into usable electricity, this system was invented by (Jorge Luis Rosales, 2018).

There has also been research into the use of TEGs in building to recover heat from pipes containing hot water from the boiler (X.F. Zheng, 2014), this however is not common practice today.

There has been lots of research into TEGs in wearable devices for sport or medical purposes to utilise humans body heat to generate electricity. These devices usually power sensors which measure medical data from a person or can be used to examine data of a person playing sport and the main characteristic of these devices is that the TEG must be flexible, which has encouraged research into polymer and thin-film technologies. These types of TEGs are further discussed by (Thielen M., 2017).

2.5.3 Maximum Power Point Tracking (MPPT)

TEGs compared to other forms of generators do not generate a massive amount of power therefore it is crucial to make sure the TEG is operating at its maximum power point by means of Maximum Power Point Tracking (MPPT). MPPT aims to track the specific voltage and current values which will produce the highest power output for the TEG at its instantaneous operating conditions for a variable power source. This has been used for more common variable power sources such as photovoltaic solar systems for some time. Figure 8 shows graphically the locations for the MPP (Maximum Power Point) at different temperatures particular TEG module. Two key papers on the use of this in TEGs are (Jensak Eakburanawat, 2005) and (Marcos Compadre Torrecilla, 2019). MPPT requires and control unit using an algorithm which will adjust the voltage using a SEPIC (Single-Ended Primary-Inductor Convertor) to achieve the maximum power output. SEPIC type convertors are favoured for this as they can step voltage both up and down.
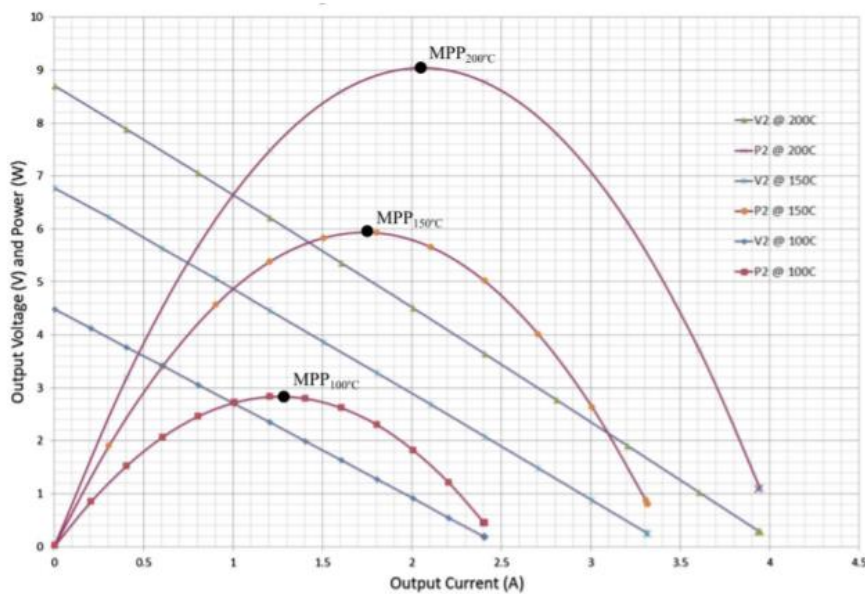
Figure 8(O. Maganga, 2014): MPP at different temperatures for module GM25-127-14-10 from European Thermodynamics.

19

2.5.4 Thermoelectric Modules

There are many TEG modules available to buy, these are not built for a specific application but instead consist of too thermally conductive ceramic plates either side of an array of thermoelectric pellets of both p-type and n-type. These can come in a range of sizes, operating temperature, expected power outputs, and prices.

2.6 Novel Thermoelectric Technologies

2.6.1 TEGs in AUVs

The idea of using the thermal energy stored in the ocean to power AUVs is not a new idea, a recent paper by (Guohui Wang, 2020) reviews what attempts have been made so far into this area. This review shows that most of the research into this area so far is into the use of PCMs utilising the oceans temperature gradient to adjust the buoyancy of an AUV.

The use of TEGs in AUVs has been researched by only two papers to the authors knowledge, (J.R. Buckle, 2013) and (J. Falcão Carneiro, 2018). The first of these papers (J.R. Buckle, 2013), aimed to model a TEG system for an AUV using MATLAB & Simulink. He modelled a system in which the TEGs heat emitting side was directly in contact with the water and an energy store material of stainless-steel was used. (J. Falcão Carneiro, 2018) aimed to build on the research from (J.R. Buckle, 2013) and simulate a model with different energy store materials. Furthermore, (J. Falcão Carneiro, 2018) believed aluminium heat transfer fins would be required to act as a heat sink. Both papers however target underwater gliders rather than battery powered AUVs and neither of these papers perform any physical simulations.

2.6.2 Uses of Software for Analysing TEGs

Each year simulation software is becoming more capable, (Ayman Eldesoukey, 2019) utilised ANSYS Fluent software to analyse which position in a chimney could generate the most power for a TEG module. This research did a mesh study to determine the variation in TEG power based upon number of elements to see what mesh size is required for accurate results. This same software could be used for simulating waters flow over a TEG built into a structure to determine its best position and if it benefits from additional structures (such as heat transfer fins).

Work by (Artur Wodołazski, 2021) also used Ansys CFD (Computational Fluid Dynamics) software Fluent to analyse a TEG cooled by an air heat sink, in this meshes were trialled in a study to find a mesh of the highest quality, this produces more accurate simulation results. A k-epsilon model was used in this research however this does not translate that this model is suitable for the research in the report as water will be the fluid for this research as opposed to air.

Ansys is a very useful software not only for analysing a system with CFD, but it also provides useful tools for Finite Element Modelling (FEM) of systems. A paper by (P. Ziolkowski, 2010) showed how TEG performance could be analysed using FEM using Ansys, the software capabilities and accuracy will have improved since this work with Ansys always updating its software.

A paper by (A. S. Korotkov, 2017) presented how on a more modern version of Ansys workbench, FEM software could be used to analyse TEGs, the practical applications of the software and potential uses for it and compared the results with that of simulations used

from COMSOL Multiphysics software. This research concluded that Ansys was especially useful software for analysis as it can solve various physical problems. This paper concluded how the use of Ansys to analyse TEG modules is especially useful for determining the most effective operating conditions for the module. The models simulated in this paper on Ansys used median temperature conditions on the TEG modules, as opposed to heat flux or convection conditions. The paper also stated that the use of temperature dependence on the material properties increased a correction of up to 15%. Another paper by the same author from that year (Alexander Korotkov, 2017) went further in comparing experimental data with the results obtained using Ansys FEM software for analysis TEGs. This research concluded that Ansys provides reliable data on power outputs of TEGs using different temperature conditions and load resistances.

A paper by (Saleh, 2021) used a modern version of Ansys from 2021 to model a TEG module and determine how much power could be produced by it with very low temperature difference of a few degrees Celsius across the module. This research used four conditions in the Thermal-Electric simulations, three temperatures across the system and a low voltage condition. The use of the three temperatures rather than just a hot and a cold side condition could increase the accuracy of simulations slightly, although the effect could be minor.

Ansys is not the only software which can be utilised for simulating TEGs, COMSOL can also be used to simulate thermoelectric effects. Research by (R. Kiflemariam, 2014), (S. Mahmoudinezhada, 2019), and (Murat Emre Demira, 2017) used COMSOL to simulate Solar-TEG hybrid-based systems. (S. Mahmoudinezhada, 2019) compared its results from COMSOL with experiment, the results showed close agreement with each other. Although COMSOL clearly appears to also provide accurate data, Ansys was chosen due to the favourable reasons given in (A. S. Korotkov, 2017), the ease of using Ansys for both CFD simulations and Thermal-Electric makes for uncomplicated transfer of data between the two.

A paper by (Topal, 2011) showed how COMSOL Multiphysics could be used to model a TEG with a fluid flow providing forced convection. The paper proved that the use of forced convection via fluid flow increased the amount of power generated by 3.5 times.

Other notable research using COMSOL Multiphysics to model TEGs includes (Sun Jin Kim, 2014), (Tulaev, 2019), and (Jaegle, 2007).

Unlike the previous papers, one piece of research by (Abolhasan Khajepoura, 2017) used a combination of Ansys, COMSOL, and MCNP to simulate TEG powered by a radioisotope heat source. The authors described the use of a combination of these software as enabling them to precisely design various types of radioisotope heat sources.

Ansys have many guides to help use their software to its maximum capabilities, (Ansys, 2009) gives a guide on how to perform successful FLUENT simulations for an older version of the software, however the points are still valid with the present version.

2.6.3 Novel Semiconductor Materials

With a materials performance as a TEG being dependant on operating temperature research must be done to create materials tailored to these desired temperatures. This project is focused on TEGs operating about room temperature or slightly below. Many materials are known to perform well at room temperature such as Bismuth Telluride and Antimony Telluride; a lot of the research aims to use these base compounds and improve their performance by doping them with other elements or nano-manufacturing them to increase

their ZT value. A largely cited article by (Rama Venkatasubramanian, 2001) claimed to have developed p-type Bi2Te3/Sb2Te3 based superlattices with a ZT of 2.4 at room temperature, a record high recorded at the time. Research by (Cheng Jin An, 2017) claimed to have developed an organic TEG using directly spun carbon nanotubes with multiple molecular dopants which had the best maximum power factor for organic materials to date and was similar rating to bismuth telluride. (Hyeongdo Choia, 2018) claimed to develop a method of developing TEG materials which was reliable, flexible, and easily reproducible in results due to the materials being screen printed. (Seong Eun Yang, 2021) claimed to have developed materials consisting of $Bi_xSb_{2-x}Te_3$ with record high efficiencies of 8.7%, fabricating it by 3D printing. A material developed by (Dehua Hu, 2020) is an n-type perylene bisimide which claimed to have record-high induced thermoelectric properties induced by Soret effect.

2.6.4 Novel Non-Semiconductor Materials

With semiconductor elements often being rare and therefore relatively expensive, there has been some research into the potential for ceramic or polymer-based TEG materials. Research by (Nesrine Jaziri, 2021) developed a ceramic based low temperature TEG design to harvest heat from power circuits which produced 81µW at ΔT=114ºC which was deemed acceptable for this paper and is a large power output for a ceramic based TEG of its size however it still does not compare to the capabilities of semiconductors today. A lot of the research into ceramic based TEGs is into the use of them in very high temperature applications due to their high melting points, some of these key investigations include (Geppert, 2014), (G. Constantinescu, 2013), and (Gabriel Constantinescu, 2021); although this does not make these technologies relevant to the objectives of this report (room temperature operation). One of the main problems with ceramics when compared to semiconductors is their very high electrical resistivities which reduce the figure of merit value. This means that although they may have a place in future thermoelectric technologies, they will not be suitable for this project.

Polymers as thermoelectric materials as discussed are a desire for the future due to them being cheaper like ceramics, however unlike ceramics, there is a lot of excitement about the ability for flexible polymer-based TEGs. Research by (Ming He, 2013) discussed how improving the ZT of polymer-based materials involves the same type of techniques as with semiconductors such as doping and nanomanufacturing. It also stated however, that at the time of writing (2013) the maximum recorded ZT to date of polymer-based materials was 0.25, which is very low compared to the semiconductors of the time (some ZT > 2). A polymer investigated by (Kim, 2016) recorded a ZT of 0.32 which to the authors knowledge was a record for a polymer at the time. However, to the authors knowledge the best ZT recorder for a polymer-based material was by (Cong Jiang, 2021) which recorded ZT≈1.1, which is competitive with a lot of semiconductor values and has excellent flexibility. Even with the advances in polymer-based TEG technology, semiconductors still have much more data supporting higher ZT values than 1.1 and therefore the correct semiconductors will produce a higher output than the polymer-based materials.

2.6.5 Other Novel TEG applications

With TEGs showing clear potential to be used in systems with a natural temperature difference across an interface, there has been plenty of research into implementing them. A paper by (D. Samson T. O., 2010) aimed to utilise the temperature difference found on the

outside of an aeroplane and its inner fuselage to generate electricity via the Seebeck effect. In this paper specifically simulations were performed to mimic the conditions which would be experienced for the TEGs in an aircraft. Following this paper, (D. Samson M. K., 2011) was released where further simulations were done to refine the shape and size of the energy store and a prototype was created ready for testing with a power management system. Finally, in (D. Samson M. K., 2012) the prototype was tested in a real flight on an aeroplane. The final results concluded both that the simulations were accurate representations of how the system would perform and that the system was reliable for its purpose.

2.7 Heat Transfer

2.7.1 Calculations

Calculating the heat transfer in the situation of forced convection over a flat plate does not have a set method and is in fact still being researched to find the most accurate method of calculating the heat transfer coefficient. It is especially difficult to approximate the heat transfer coefficient in the turbulent regions of flow. Another issue when calculating the heat transfer coefficient is that the Prandtl number of water varies massively with temperature changes therefore estimating the exact Prandtl number can be difficult. The Prandtl number, named after Ludwig Prandtl, is a measure of the ratio momentum diffusivity to thermal diffusivity (Nuclear Power, 2022).

One paper by (Lienhard, 2020) calculates average heat transfer coefficients by integrating across the "transition point" which allows a good estimation of heat transfer coefficients for flows with turbulent behaviour and across the transient region.

There are well documented methods of calculating the heat transfer coefficient in a laminar region of flow, a book by (Mayhew, 1992) contains a method which produce results which agrees with (McConkey, 1993) method. The Nusselt, named after Wilhelm Nusselt, is the ratio of convective to conductive heat transfer across a boundary and is therefore essential in finding the heat transfer coefficient. The equation for Nusselt number (Nu) over a flat plate is the same in both (Mayhew, 1992) & (McConkey, 1993) and can be found in equation 4.

$$Nu = 0.332 \cdot (\text{Pr})^{\frac{1}{3}} \cdot (Re)^{\frac{1}{2}} \tag{4}$$

Both books differ slightly on the way they display the equation the calculate the heat transfer coefficient however the results are the same. The average heat transfer coefficient according to (McConkey, 1993) is calculated using equation 5 where λ is fluid thermal conductance and L is the length of the plate.

$$h = 2\left(\frac{Nu \cdot \lambda}{L}\right) \tag{5}$$

This method was used in this research for the calculations when the flow is laminar. Finally, the heat transfer rate can be calculated using equation 6

$$\dot{q} = hA\Delta T \qquad\qquad (6)$$

2.7.2 Computational Fluid Dynamics Turbulence Models

CFD software allows highly accurate analysis of complex heat transfer problems which involve a moving fluid. When it comes to analysing heat transfer with turbulent flow, there are many different methods as there is no set way of calculating the fluids behaviour, only methods of prediction. The different methods yield different results and have great differences in the amount of time they take to simulate. There is not one method that is more accurate in all situations, the method of turbulence modelling should be chosen based upon the model being simulated. In Ansys there are many turbulence models which generally come in different variations. Some of these models include:

k-ε: The k-ε turbulence model is one of the most common turbulence models used due to the speed in which simulations can be produced as it only uses two equations and does not require as fine a mesh near the boundary as the k-ω model. The two transport equations used in this model aim to obtain the turbulent kinetic energy (k) and its rate of dissipation (ε). The work previously mentioned by (Artur Wodołazski, 2021) used the k-ε model when simulating wind flow over a heat sink for a TEG model. A study by (Mohamed Elkhmri, 2021) used the standard k-ε to model the convective heat transfer over narrow side up isothermal flat plates.

k-ω: Like the k-ε model, this model uses two equations. It also aims to obtain the turbulent kinetic energy (k) and the specific dissipation rate (ω). The model was proposed by (Wilcox, 1998). This model accurately predicts the flow near the boundary layer, but it is necessary to refine the mesh near the boundary using an inflation layer, this can increase the time taken to simulate. Research by (Chethan R Patil, 2021) used both the k-ε (CFX) and the k-ω SST (CFD) model to analyse heat transfer around an aircraft engine blade. Both models showed no significant variation in obtaining the heat transfer/temperature results. The k-ω SST (Shear Stress Transport) is a variation of the standard turbulence model which uses the standard k-ω near the wall, which gradually blends into the transformed k-ε model away from the wall. This aims to optimise the benefits of the near wall capabilities of the k-ω model near the boundaries and minimise the limitations which the k-ω model can have in the free stream flow. A paper by (Dawid Taler, 2014) used the k-ω SST model to analyse heat transfer around tubes in a car radiator to compare the Nusselt number values produced with experimental tests, the results differed slightly due to thermal contact resistance between the fins and tubes but this was expected therefore the model could be deemed adequate. Research by (Antar M.M. Abdala, 2013) compared both the k-ε and k-ω models in predicting improvements in film cooling across a plate with a narrow trench. The results were compared with experimental results and at high blowing ratios both models under predicted however at low blowing ratios the k-ω model reigned superior when comparing the results with experimental data. Research by (M Ajmi, 2020) tested four versions of the k-ε and k-ω models in analysing the dynamic and thermal of a heated offset jet. The SST k-ω model was the only model that proved accuracy in resolving the flow.

There are more turbulence models which use a larger number of equations such as The Reynolds stress model however these were not considered for this research due to the already large simulation time which would be excessive for these models.

2.8 Literature Conclusion

As stated, (J.R. Buckle, 2013) used steel as a thermal store due to its high thermal capacity per volume. This research does not intend to use a thermal store; however, steel was chosen as the material of which its temperature would be regulated to keep the hot side of the TEGs stable due to this specific thermal property.

A mesh study was performed in this research in a similar manner as shown by (Ayman Eldesoukey, 2019) to find the ideal number of elements for CFD simulations.

Work by (A. S. Korotkov, 2017) found that using temperature dependence properties of materials makes a 15% correction increase in simulation results, therefore for this work the thermal electric simulation material properties all used temperature dependence properties.

It is clear from the literature that both the k-ε and k-ω model have both been used previously for analysing heat transfer over plates and other surfaces. This research decided to use the k-ω SST model due to papers such as by (Antar M.M. Abdala, 2013) and (M Ajmi, 2020) which compared both k-ε and k-ω and found that the k-ω SST performed superior.

3 Methodology

3.1 Introduction

There are many different calculations, simulations, and experiments performed in this research. Firstly, the hand calculations for both the steady-state thermal analysis and the heat transfer analysis over a flat plate were completed. These give a rough idea of what the values produced from the simulation should look like and make it easier to understand if there are any concerns with the simulation results. So, although these values are not really analysed in the results section, they help understand if early simulation appear to be accurate.

One of the most crucial parts of the research is the physical experiments. These results give data with no assumptions, and the best understanding of how the TEGs would perform in the real world. Before simulating the scaled-up system, it is ideal to simulate replicas of the test rig which performed the physical tests. This was done to see how valid the simulations were compared to data obtained from physical tests.

Finally, once the simulations results were validated by the physical test results, the scaled-up system was simulated in a similar manner to that of the previous simulations for reproducible results.

3.2 Test Rig Layout

3.2.1 Criteria & Reasoning

The main criteria which the test rig was manufactured to is as follows:

- It needed to be possible to control and regulate the temperatures on both the hot and cold side of the experiment to a high level of accuracy.
- The test rig must be structurally sound and strong enough to support the weight not just of itself, but of the water which will be mimicking the sea.
- It is essential that the rig was waterproofed properly, as there was water located directly above electrical components with only a sheet metal acting as a barrier.
- It must be possible to easily change the heat transfer surface between the TEGs and the water, as multiple metals and thickness will be tested.
- There were no gaps between the TEGs and their adjacent interfaces to allow all heat transfer from hot to cold side to take place via conduction.
- Conduction between the hot and cold sides that is not through the TEGs was minimalised.

To maintain the temperature on the hot side of the TEGs, a steel block was chosen to be in contact with the TEGs. The aim was to regulate the temperature of this block at the desired temperature (to simulate the inside of an AUV), steel was chosen as it has a high thermal capacity per volume (≈ 3650kJ/m^{3}K) therefore changes in its temperature were gradual and easy to control.

The cold side of the TEGs was designed to replicate the sea. The walls of the bath containing the water were made of steel to ensure it was strong enough to hold the water. The base of the water container (the heat exchange surface) was changed to test different thicknesses and materials.

To avoid water leaking between the steel walls of the bath and the base material plumbers putty was used to plug and cracks/gaps. Nylon bolts were used for the assembly of the steel

block to the heat exchange surface to ensure nearly all heat transfer occurs via conduction through the TEG modules.

3.2.2 Building Processes

Walls of bath:

The walls of the bath were made from steel sheets of 1.2mm thickness. The thickness of sheet was chosen as it was thin enough to bend without issues, however it was also thick enough that it had the strength to hold the water, and the area to weld the sheets together without issues.

The first step to manufacturing the walls of the bath involved water cutting the sheet metal to the correct dimensions and cut out features such as holes and gaps to allow for the fastenings. Four sections were cut, two longer walls and two shorter walls. The structure had to be cut into multiple parts to make the bending possible.

The next step was the bending to create flanges which will be used for fastening. The method of bending used was wiping.

Finally, the four parts were welded together carefully to make sure the seal is watertight. It was key to make sure the flanges sat level when welding, this was more important that the top of the walls being level for watertightness.

Holes were drilled into the smaller walls near the bottom to add hose tails in. The hose tails used were made of brass to be resistant to corrosion and were 12mm in diameter to fit the same size flexible hose as the chiller. The hose tail was fastened in using brass nuts and a rubber O-ring on each side to seal the fasten watertight.

The walls of the bath were the first part of the rig's assembly manufactured as it is the most difficult to be precise on the locations of the holes for the fasteners, therefore the rest of the parts can be manufactured based off this part.

Rubber Gasket/Sealant:

The rubber chosen for the gasket was made from EPDM (Ethylene Propylene Diene Monomer) sheet with a thickness of 2mm. The sheet of rubber was first cut out to the exact dimensions of the flanges on the walls of the bath by tracing around with a Stanley knife. The holes for fastening were slightly trickier as because it was rubber, drilling was not really an option. A bit of steel pipe was sharpened at the end, this was hammered into the places where the holes were required to cut out the rubber. Finally, the inside section was cut out using a Stanley knife also, leaving a slight overlay of material inside from the walls.

After trialling the rubber gasket, it was not possible for the corners of the water basin to be sealed with it due to the limit which the steel could be welded down. After trialling multiple sealants, it was clear that this would not waterproof the system for the duration of the tests with the water flowing. This was a major concern as the water is flowing directly above live electrical wires from the TEGs, so leakage could be hazardous. It was decided to remove the gasket completely and test sealing the gaps between the bath walls and the heat exchange surface using plumbers putty. This worked perfectly at sealing the system watertight in all conditions and therefore plumbers putty was chosen for the actual tests.

Heat Exchange Surface:

The sheet metals being tested for the heat exchange surface were all purchased in the exact dimensions required. The holes for the fastening bolts were drilled using a 9mm drill bit.

Steel Block:

There were no steel blocks with the required thickness for a reasonable price. To resolve this, a steel flat 20mm thick and 70mm wide was bought at double the desired length of the steel block. The flat was first cut in half, to create two flats of 254mm length. The next step was to extract some material creating grooves on one side of each of the flats, this will create a hole in the final block for the heating element to rest. Once this has been machined, the two flats of steel were welded together, ensuring good thermal contact between the two parts. Holes were then drilled near the top of the block to allow temperature sensors to measure the temperature close to the TEGs.

The block requires some form of flange to allow fastening to the heat exchange surface. To allow this, a section of steel sheet 1.2mm thick is cut out with the same dimensions as the block with flanges on the side and holes in the flanges for fasteners. This was cut using the water cutter. Once this was completed the sheet that was cut was then welded onto the steel block, ensuring good thermal contact between the metals was essential for the temperature readings from the sensors being representative of the temperature near the TEGs. Figure 9 shows the steel block with the TEG modules sat in place on it. The block is insulated in rubber covering almost all of it to minimise heat loss.
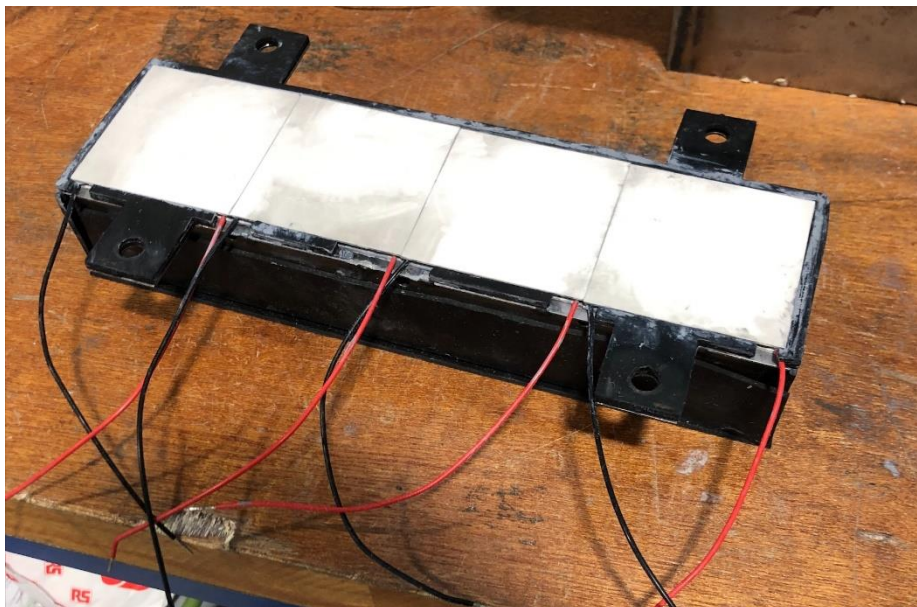
Figure 9: Steel block with the TEG modules arrayed on top

Thermal Insulation:

To insulate around the TEGs so heat is not lost through convection out of their sides, the same rubber used for the gasket was cut the same shape as the steel sheet on top of the blocks using a laser cutter. The only difference being that the sheet is hollowed out by a section of 248mm x 62mm to fit the TEGs in. Two of these sheets are cut out and glued onto the steel stacked on each other. Finally gaps for the TEGs wires were cut out using a Stanley knife.

Heat Transfer Fins:

Segments of aluminium sheet of 2mm thickness were cut to a height of 30mm. A base aluminium piece also of 2mm thickness had holes drilled in using a pillar drill, these were used to fasten the heat transfer fins to the heat exchange surface. Finally, the segments of fin which were cut prior were welded onto the aluminium base with equal distance from each other. Figure 10 shows the finished heat transfer fins welded on to fastening base.

Figure 10: Heat Transfer Fins welded onto Aluminium base (attempt 1)

When the fins were welded onto the base, the heat caused the base by the fins to buckle upwards. This is not ideal as the base requires full thermal contact with the heat exchange surface. To resolve this the areas which had buckled were hammered down with a block of wood and a hammer. The base was the ran on the belt sanding machine to aim to flatten and grooves or ridges. After testing it was apparent that this had not worked, and the base was still not flat enough to obtain suitable results.

To aim to resolve this some heat transfer fins were welded directly onto the 6mm aluminium plate after it had already been tested on its own. This caused slight bending on the plate; however, it was not as extreme as the previous attempt (due to a thicker surface to weld onto). Figure 11 shows the heat transfer fins welded onto the plate using this new method.

Figure 11: Heat Transfer Fins welded onto 6mm thick Aluminium plate

3.2.3 Assembly

Section 3.1.2 described the processes of making the different parts of the test rig, this section aims to show how these parts were assembled for testing. Figure 12 shows a side view of all the parts of the test rig assembled for testing with numbered labels to annotate the location of the parts.
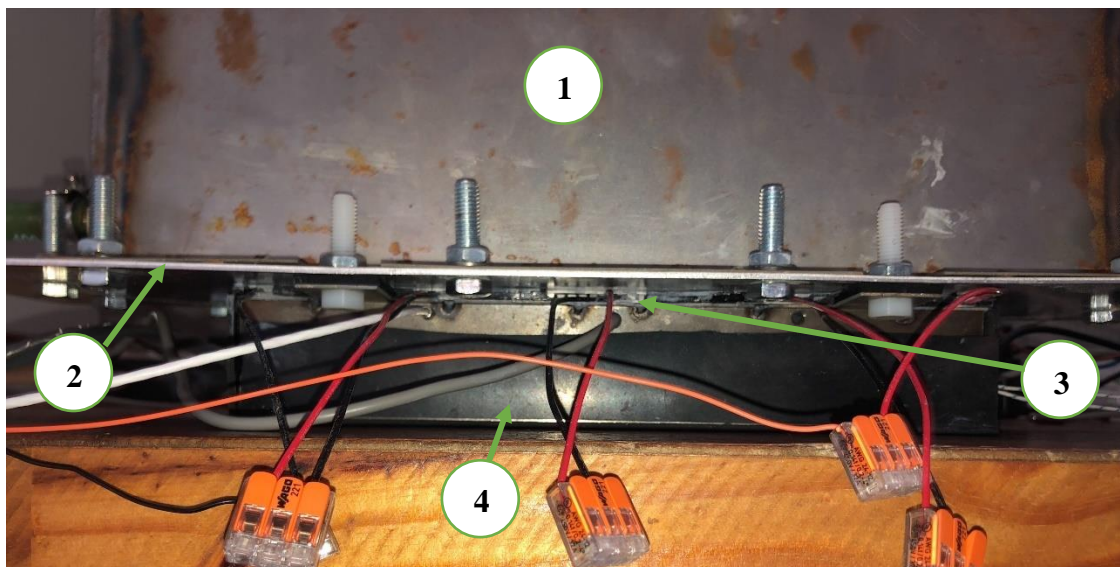
Figure 12: Side view of assembly with 2mm thick heat exchange surface

Label 1 in figure 12 shows the walls of the steel bath and label 2 shows the heat exchange surface, which in this image is 2mm thick aluminium. These two parts are fastened together

with steel bolts and nuts surrounding the walls of the water basin. There is in fact twelve of these bolts to faster these two parts together. Label 3 shows the TEG module layer, consisting of the four TEG modules adjacent to one another. The modules are surrounded by black rubber sheet to thermally insulate the modules. The modules are held in place due to the fastenings between parts 2 and 4 which compress the modules between the heat exchange surface and the steel vessel. A layer of thermal grease sits on the outer surface of both alumina plates of each module. Label 4 shows the steel vessel, which is surrounded by rubber sheet to minimise heat loss and keep the temperature more stable. The steel vessel is bolted onto the heat exchange surface by nylon bolts as shown in the image. The bolts are fastened in the flange of the steel block, the steel and heat exchange surface are separated by rubber sheet with identical thickness to the TEG modules (4mm).

3.3 Electrical Layout

The way that the TEGs are connected in circuit will affect the Voltage/Current produced. If the TEGs are connected in series, then the total voltage produced is calculated by the sum of each individual modules voltage values whilst the current remains the same. On the contrary, If the TEGs are connected in parallel, the sum of each modules current will be the total current produced and the voltage will remain the same as one module. For this research the TEG modules were set out in series to increase to total voltage produced. This is because the TEGs produce a very low voltage which is unusable for most applications therefore it is required to produce as high a voltage as is possible from the modules. Research by (Andrea Montecucco, 2014) aimed to identify experimentally the effect of the orientation (parallel and series) of TEG modules on their performance. It is expected due to resistance through wires that connecting multiple modules in a circuit will cause some power loss, this research aimed to produce comparable data on this. The research found that when the 3 TEG modules were connected in series, they produced 9.22% less power than they would individually. It also found that when connected in parallel, they produced 12.9% less power than they would individually; consequently, according to (Andrea Montecucco, 2014) it is more efficient to connect TEG modules in series rather than parallel.

According to Ohms law, the current 'I' flowing through a circuit can be found using equation 7

$$I = \frac{V}{R} \tag{7}$$

In practice, due to the likelihood of all the modules connected having the exact ΔT being very small, the actual current can be calculated using equation 8 which is sourced from (Andrea Montecucco, 2014).

$$I = \frac{V_1 + V_2 + V_3 + V_4 - V_S}{R_1 + R_2 + R_3 + R_4} \tag{8}$$

Where the voltages subscripted 1 to 4 are the open circuit voltage of each module, V_S is the voltage at the array's terminals, resistances subscripted 1 to 4 are the internal resistance values for each module.

For the experiments in this project the load on the power produced was a variable resistor (potentiometer), with both an ammeter and voltmeter recording the instantaneous power being produced.

The potentiometers (variable resistor) resistance was changed based upon the mean temperature across the TEG to achieve maximum power output. For this experiment, the aim was to satisfy that the load resistance R_L is equal to the internal resistance of the four TEG module combined, R_{int}. According to (Goldsmid, 2017), this load resistance will produce the maximum power output for the TEGs.

The potentiometer chosen had to be of a low resistance as the internal resistance of the TEGs is very low at most temperatures, any product over 100Ω was instantly ruled out as it would be tough to achieve an accurate load resistance.

If the electrical energy produced by the TEGs is to be useful for a particular application, such as charging a battery of reserve power or powering a sub-system in the AUV, then it will need passed through a step-up convertor most likely to produce the voltage required by the battery/system.

The electrical components purchased for this research and their manufacturer/product codes are listed in table 1

Table 1: Electrical Components purchased for this Research

Component Name/Code	Manufacturer
TEG- GM250-127-28-12	European Thermodynamics
4.7Ω Potentiometer-PE60L0FGW4R7MA	Vishay

3.4 Control & Logging Layout

3.4.1 Control

For this research the two main variables of the system that were controlled are the temperature of the water and the temperature of the steel vessel.

The water temperature was regulated/cooled by an aquarium chiller. The chiller chosen for the testing can operate down to 0ºC and can cool both regular water and saltwater. The chiller uses a closed loop control system which can control the water temperature to a high accuracy of 0.5ºC. The chiller does not have a built-in pump therefore a pump was purchased to circulate the water through the system. The pump chosen has options for flow rate options between 750L/hour to 2,500L/hour. The pump uses sine wave control technology. The chiller connects to the system using 12mm diameter flexible tubing which is held on using jubilee clamps. The pump required pipe adapters and connectors to attach a hose tail which would fit the flexible tubing on. Jubilee clamps were also used here. The pump flows the water into the chiller's inlet, through the chiller where it is cooled, out the chiller outlet, though the test rig (over the heat exchange surface), and back to the pump

inlet, as shown by figure 13. The pump operates at max flow rate for the experiments in this paper, which is 2500L/min.

The second temperature which needs to be regulated is that of the steel vessel. A heating element is embedded in the centre of the steel block, which is controlled by a PID based temperature controller, which is taking readings from a PT100 RTD sensor embedded at the top of the steel block, as close to the TEG modules as possible. PT100 RTD sensors were chosen over thermocouples as they are more accurate in reading temperatures, which is the most important feature for the temperature sensors in this study.

Although the voltage and current produced by the TEGs are not being controlled and are rather being measured, their instantaneous readings will be displayed on the control panel to help us see how the TEGs perform whilst the test is underway.

A block diagram to display how the control panel will interface with the rest of the setup is shown in figure 13
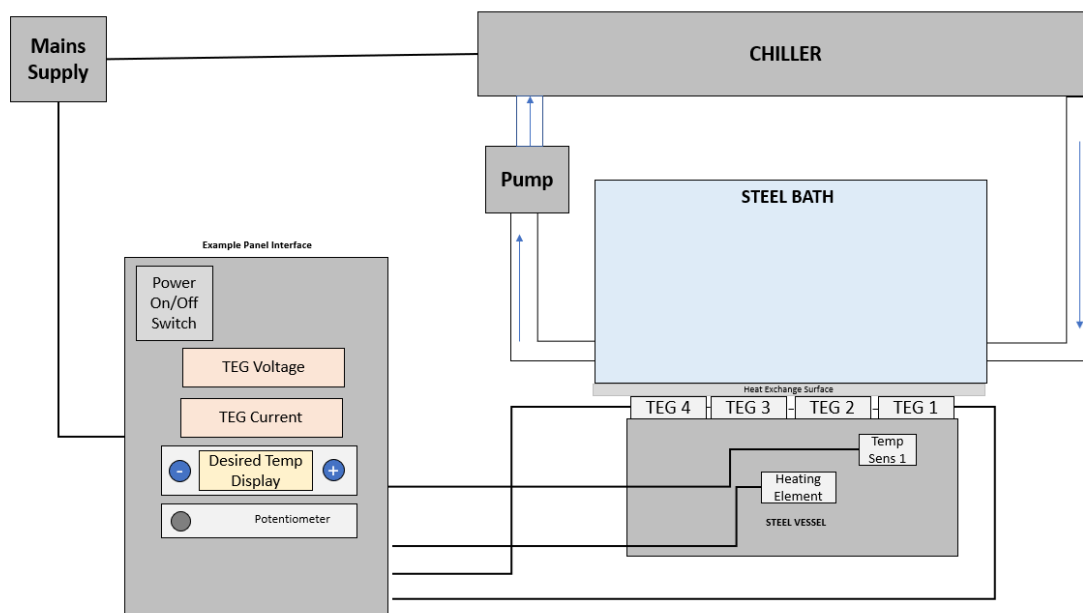
Figure 13: Block Diagram displaying how the control panel links to the test rig and electrical systems (Data Logging Equipment Excluded)

The control panel was built with my industry partner Delkia at their workshops.

Table 2 shows the parts purchased for the control section of the project and their manufacturers.

Table 2: Control Components purchased for this Research

Component Name/Code	Manufacturer
Chiller- TK150	Teco
Pump- DCP-2500	Jecod
PT100 RTD- R14-1B2-4/50T2000	Reckmann
Heating Element- 860-6823	RS Components

Temper Controller- 124-1058	RS Components

3.4.2 Data Logging

To accurately log the exact instantaneous temperature, voltage, and current being produced in the test rig a data logger was used. The data logger chosen was produced by measurement systems limited and contained four ports which allowed the reading of four values at one time. This logger was chosen as for this system exactly four values must be read, these are: The temperature at the top of the steel vessel close to the hot side of the TEGs, the voltage produced by the TEGs, the current produced by the TEGs, and the temperature of the water close to the heat exchange surface.

The data logger works with additional software, which allows graphical representations of the results to be made displaying how the variables affect the electrical output values produced by the TEGs.

Table 3 shows the parts purchased for the data logging section of the project and their manufacturers.

Table 3: Control Components purchased for this Research

Component Name/Code	Manufacturer
Voltmeter- APM-VOLT-APO	Trumeter
Ammeter- APM-AMP-APO	Trumeter
Data Logger- USB-5106	Measurement Systems Limited
Temperature Sensor- TMC6-HD	Measurement Systems Limited

The temperature sensors used for the data logging possessed an accuracy of ±0.25ºC.

3.4.3 Connections/Network

This section shows how the control and data logging elements are connected to each other and the test rig. The figures in this section contain images of the system set up with numbered labels of different parts. The parts which correspond to each number can be found in table 4

Table 4: Section 3.4.3 figure part labels

Label Number	Part
1	Data logger temperature sensor water
2	Data logger temperature sensor steel
3	Temperature controller sensor
4	Ammeter
5	Temperature Controller
6	Voltmeter
7	Data Logger
8	Potentiometer
9	Water chiller
10	Water pump
11	Heating Element

Figure 14 shows the location of the temperature sensors within the system. Part 1 shows that the location of the data logging sensor in the cold side (water) is placed equal distance from the inlet and outlet hose tails and rests with the tip touching the heat exchange surface but the rest of the sensor floating in the water. This was decided to be the best place to get the bulk average temperature of the water flowing across the plate. Part 2 shows the data logging temperature sensor embedded in the steel vessel, approximately 7mm from the TEG modules ceramic surface and located dead centre laterally in the steel vessel to measure the best average across the whole steel, as near the inlet hose tail the steel will get colder than near the outlet. Part 3 is the temperature sensor for the temperature controller, this is located close to the TEG modules but is less centred laterally as this value of temperature is not as critical as the one being logged.
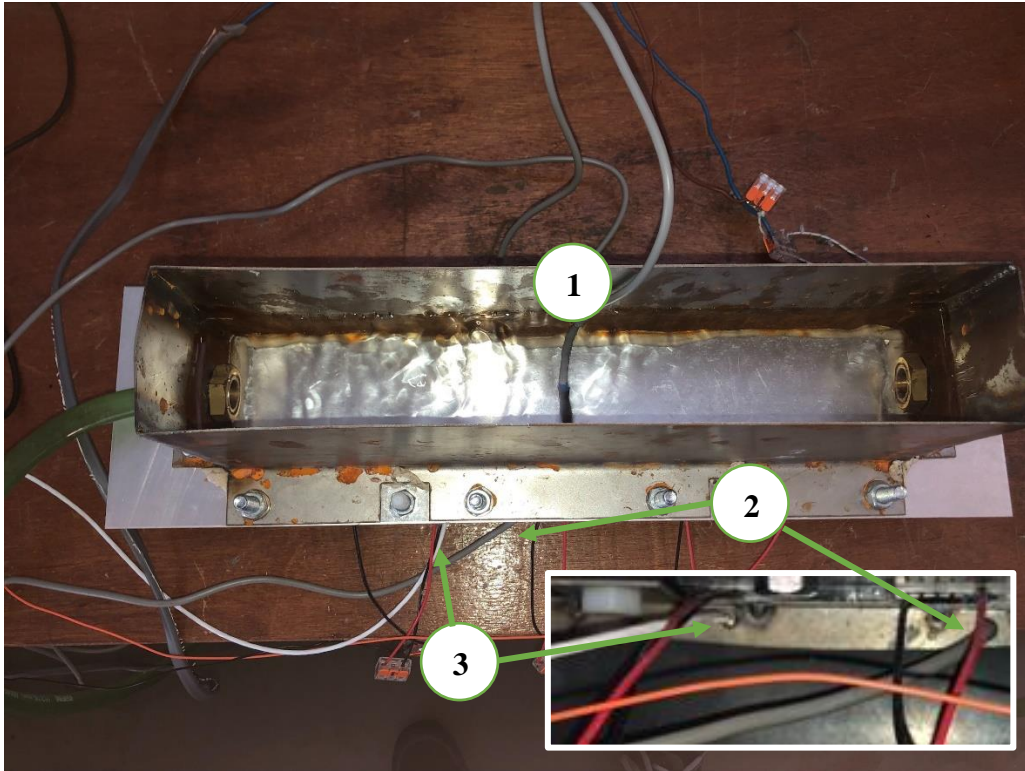
Figure 14: Temperature sensor locations, water & steel vessel, image taken mid test with flowing water

Figure 15 shows the control panel during an experiment. Part 4 and 6 show the ammeter and voltmeter respectively, built into the wall of the control panel. The wires connecting these to the TEGs and potentiometer are hidden behind the door of the control panel. Part 5 shows the temperature controller built into the control panel wall also, this is connected to both a temperature sensor and the heating element. Part 7 shows the data logger which sits on the door of the control panel magnetically. This data logger is connected to the two temperature sensors parts 1 and 2 by cables. The data logger also has a cable connecting it to the laptop with the data logging software downloaded onto it. Part 8 shows the potentiometer built into the door of the control panel. The part visible is the nob which can be twisted to adjust the potentiometers resistance. The wires connecting potentiometer to the TEGs also sit behind the control panel door. All the wires which connect the outside of the control panel to the contents inside leave the panel by glands located on the bottom of the panel. The panel sits on two wooden blocks to allow room for the wires to leave the glands on the bottom.
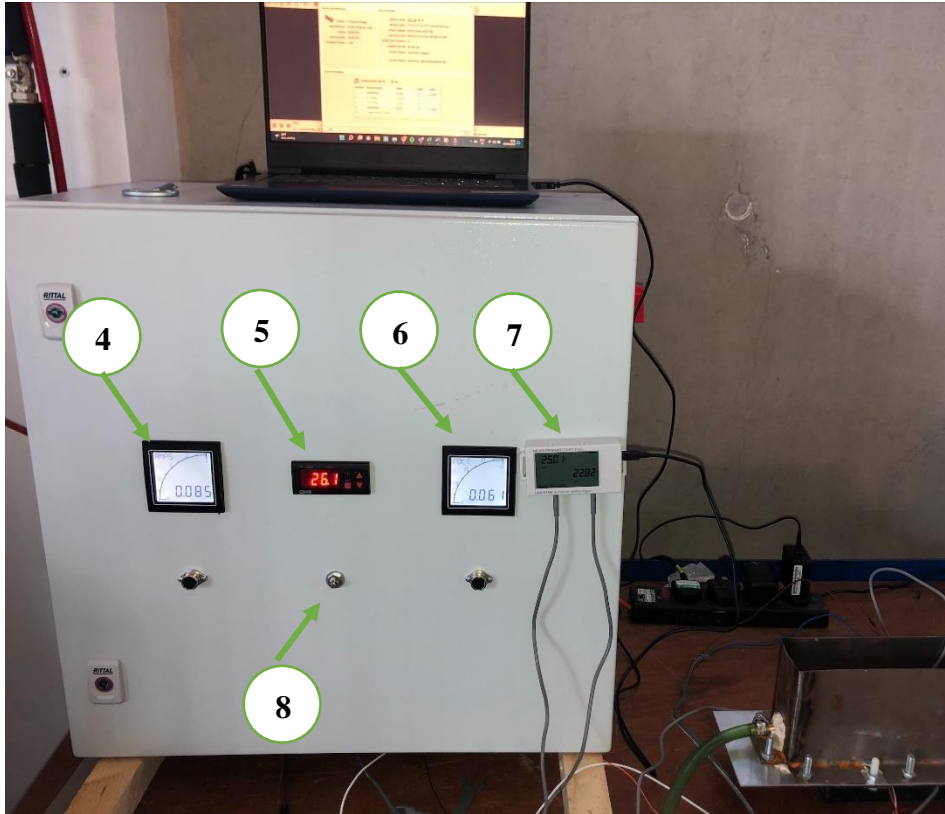
Figure 15: Control Panel & Data logging in action mid experiment

Figure 16 shows the plumbing/water-based control elements of the system. Part 9 is the water chiller, electrically this is connected to the mains, the outlet of the chiller has hose connecting to the inlet of the steel water basin. The inlet of the chiller takes in water through flexible tubing from the pump. The pump is labelled as part 10 and receives water in its inlet through the tubing connected to the outlet of the steel water basin.
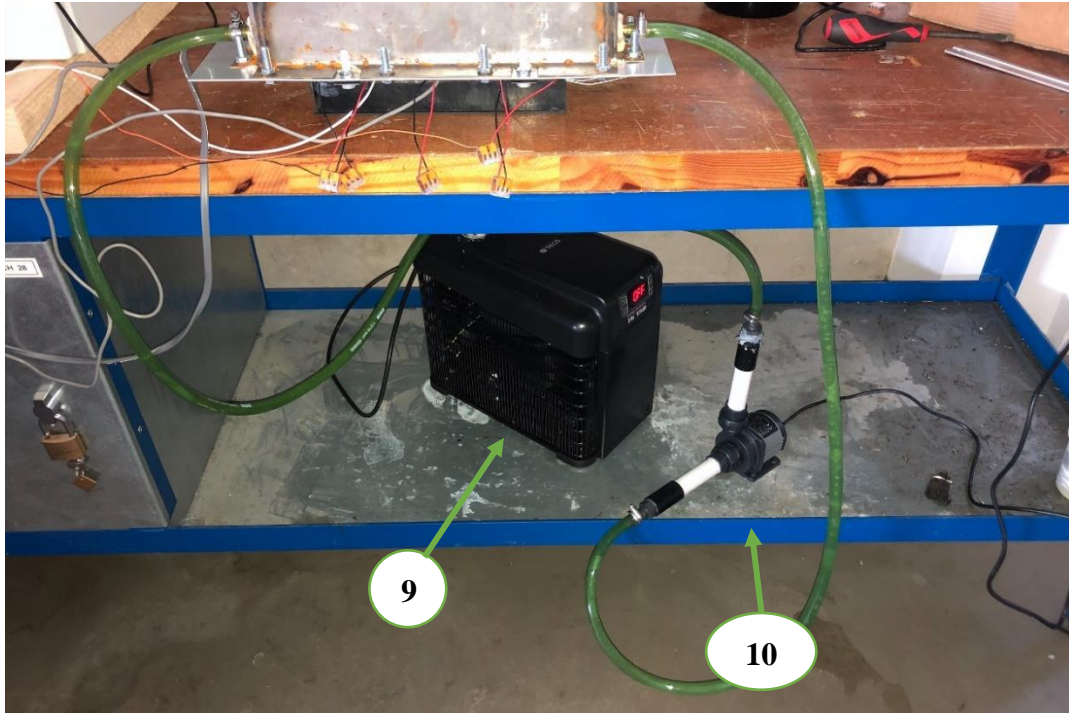
Figure 16: Chiller, Pump, and Plumbing of the system in action mid experiment

Figure 17 shows the frontal view of the system with the heating element location. This is the side of the basin with the outlet hose tail. Part 11 shows the heating element location, the hole is located centrally laterally and vertically in the cross-section of the steel vessel and its wires are connected using Wago clips to wires which lead to the power supply unit and the temperature controller.
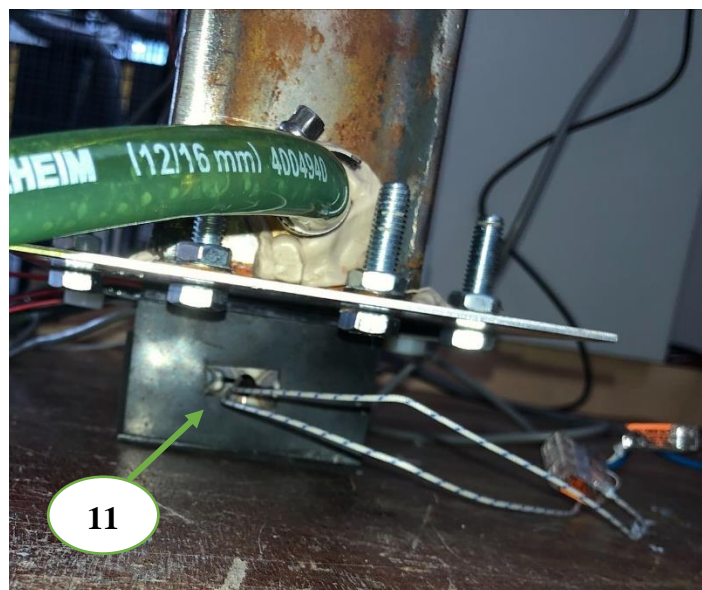
Figure 17: Heating element location in Steel Vessel

3.5 Thermal Analysis

3.5.1 Hand Calculations

The temperature across the TEGs can be calculated if the thermal conductivity of each component is known, and the exact temperate at the water by the wall and the steel block are known. This analysis was undertaken to determine how likely the thickness of the heat transfer surface and its material are to affect the temperature difference across the TEGs. This shows whether many thicknesses/materials need to be tested of just the extremities. The values in this section were assumed for material properties, temperatures, and Si paste thickness, as this was just an estimation.

Figure 18 shows the labels for the positions of the temperatures which can be measured.
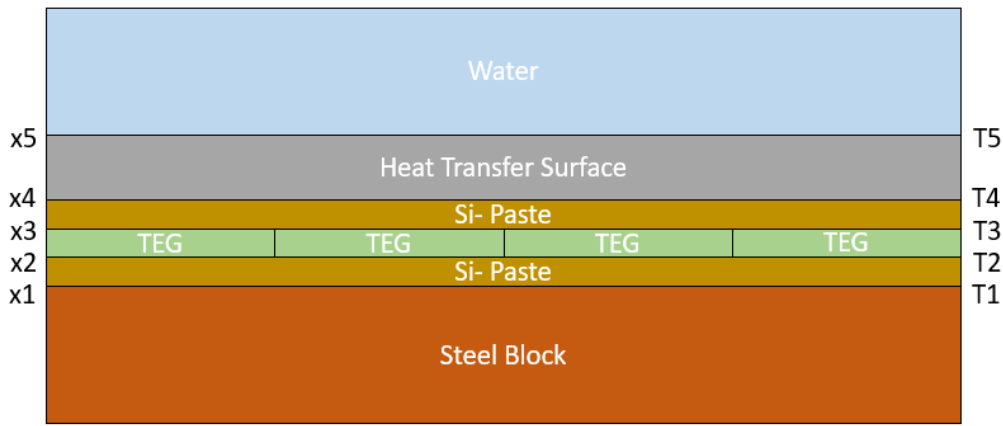
Figure 18: Layers of test setup and the location of temperatures measurable by hand calculations.

If T_1 is known, and we assume T_5 to be the same temperatures as the bulk water temperature, the other temperatures can be calculating using the following method:

The overall heat transfer coefficient can first be calculated using equation 9, where U is the heat transfer coefficient and K is the thermal conductivity of the material between the two points.

$$\frac{1}{U} = \frac{x_{12}}{K_{12}} + \frac{x_{23}}{K_{23}} + \frac{x_{34}}{K_{34}} + \frac{x_{45}}{K_{45}} \tag{9}$$

This heat transfer coefficient can then be used to calculate the overall heat transfer rate '$\dot{q}$' with equation 10.

$$\dot{q} = -U(T_5 - T_1) \tag{10}$$

The heat transfer rate '$\dot{q}$' can then be used with equation 11 in which it is possible to find all the temperatures by inserting the known values.

$$\dot{q} = -K_{12}\frac{T_2 - T_1}{x_{12}} = -K_{23}\frac{T_3 - T_2}{x_{23}} = -K_{34}\frac{T_4 - T_3}{x_{34}} = -K_{45}\frac{T_5 - T_4}{x_{45}} \qquad (11)$$

These equations were sourced from (Mayhew, 1992) and will work no matter how many layers/walls there are if the end two temperatures are known. These equations also assume that all heat transfer occurs via conduction in the direction towards the cold temperature, whereas some heat will be lost to the surrounding air around the steel block.

Using these equations, the thermal conductivity values of each component and setting $T_1=20^{o}C$, $T_5=4^{o}C$, the following temperature differences can be found across the TEGs in table 5 The thickness of the TEGs is 4mm and the thickness of the Si paste was assumed to be 0.2mm. The thermal conductivity of the TEGs is assumed to be 1.643W/mK (this value changes with temperature) and the thermal conductivity of the Si paste is 5W/mK. The thermal conductivity of the aluminium was assumed to be 237.5W/mK.

Table 5: Hand Calculations of Temperature Difference across TEGs when total temperature difference across system is 16ºC for different heat exchange materials with different thicknesses (Celsius)

	Temperature difference across TEGs (T_2-T_3)	
	2mm Thick	6mm Thick
Aluminium 1050	15.44	15.33
Mild Steel CR4	15.21	14.69

It is clear to see from these calculations results that the thickness of the heat exchange surface should not have a major effect on the temperature gradient across the TEG module and therefore there is no need to test any thicknesses between 2mm and 6mm.

3.5.2 Ansys Steady-State Thermal Analysis

It is possible to perform a temperature analysis such as the one done using hand calculations in Ansys using the steady-state thermal package. Like in section 3.4.1, the temperatures were set as $T_1=20^{o}C$ and $T_5=4^{o}C$. The thermal conductivity values for each layer were all set the same as section 3.4.1 except the TEGs. It is possible to plot the thermal conductivity graphically using Ansys, therefore for this simulation the thermal conductivity of the TEGs was set to change with temperature in accordance with the function from their datasheet (ETD, 2022). The simulation was performed with the heat exchange material set as Aluminium of 2mm thickness. The results from Ansys are displayed in figure 19.
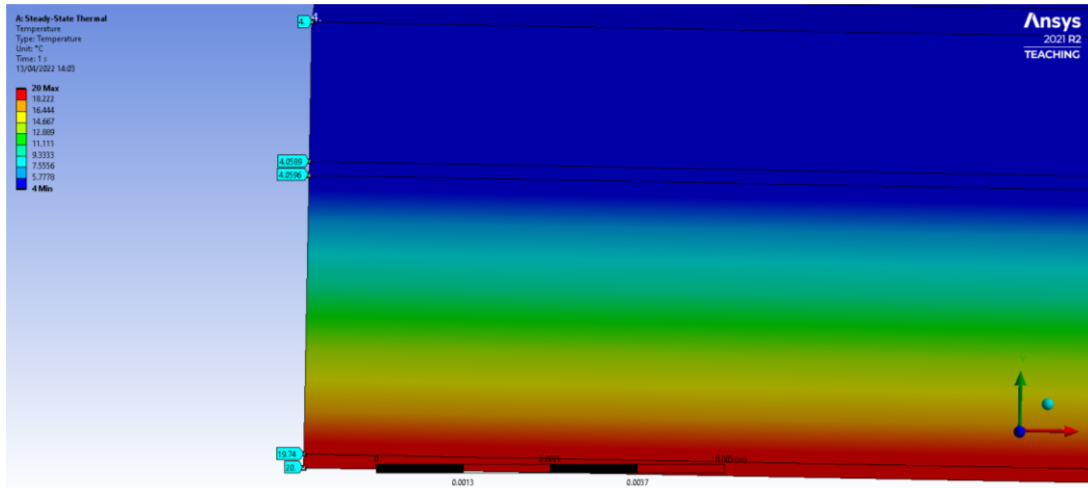
Figure 19: Screen grab from Ansys steady-state thermal analysis on system to find temperatures, heat exchange material- Aluminium 2mm thickness

Figure 19 shows that using Ansys, T_2=19.74⁰C and T_3=4.06⁰C. This is a temperature difference across the TEGs of 15.68⁰C using Ansys, slightly higher than the 15.44⁰C calculated in section 3.4.1. This slight difference will be due to the shifting nature of the TEGs thermal conductivity value.

3.6 Heat Transfer Analysis

3.6.1 Hand Calculations

As discussed in the literature review, the heat transfer coefficient is a complex value to estimate, especially in turbulent flow. One major problem is that all calculations for flow over a flat plate assume that the flow begins laminar and uniform at the start of the plate, when the flow will be coming entering the flat plate from a pipe which will disrupt the uniformity of the flow.

If we assume that the flow begins uniform and laminar at the start of the plate, it is possible to estimate the heat transfer coefficient with relatively simple calculations. These equations can be found in part 2.7 of this document in equations 4 & 5 To use these equations however, the Prandtl number and Reynolds number must be calculated first.

Calculating the Reynolds number also helps us determine whether the flow is laminar, turbulent, or in a transitional phase. It is a measure of the ratio between the inertia forces and viscous forces within a fluid (NASA, 2021). The Reynolds number of a system can be calculated using equation 12

$$Re = \frac{\rho V L}{\mu} \qquad (12)$$

The other value required to calculate the Nusselt number is the Prandtl number. The equation for Prandtl number can be written as shown in equation 13

$$Pr = \frac{C_p \mu}{k} \tag{13}$$

As stated in the literature review, the Prandtl number is hard to predict for calculation, especially in a test which will cover a wide range of fluid temperatures due to both the dynamic viscosity and the thermal conductivity of the fluid being affected by temperature.

The velocity of the fluid is another factor which will make a large difference to the heat transfer by convection away from the plate. AUVs can travel at a range of speeds depending on the specific vehicle. For this case study the data was provided by the partner company for this research Delkia based upon real AUVs.

For the experiments, using the chiller that we are using it is not possible to fully reach the fluid velocity which is likely to be experienced by a cruising AUV. The chiller and pump operate at a flow rate of 2500litres/hour (0.000694m^3/s). The width of the plate which will experience the water flowing over it is approximately 66mm. The shallower the water in the basin, the faster the bulk fluid velocity will be however it is important not to test the water in a basin with water too shallow that it is not deep enough to have sperate boundary layer and bulk flow. The thickness of the boundary layer in laminar flow can be calculated using equation 14, which is derived from the Blasius solution of the flow governing equations (Nuclear Power, 2022).

$$\delta \approx \frac{5}{\sqrt{Re_x}} x \tag{14}$$

The value 'x' is the distance along the flat plate, to find the thickness of the boundary layer at this point. The boundary layer will only get thicker as the distance across the plate increases if the width of the plate stays constant therefore, to find the boundary layer thickness at the thickest point 'x' is equal to the length of the plate.

Calculating the bulk fluid velocity requires the flow rate (m^3/s) and the cross-sectional area which the fluid is flowing through (m^2). Using these values, the bulk fluid velocity is calculated using equation 15

$$U_{bulk} = \frac{Q}{A} \tag{15}$$

If the depth of the water is tested at 52mm, then the bulk fluid velocity will be approximately 0.2m/s.

The fluid used in the tests performed was de-ionised water, the properties of this can be found in table 6, the dynamic viscosity was taken to be 0.007kg/ms at this temperature and the thermal conductivity 0.545W/mK.

Table 6: Properties of Deionised Water, density and specific heat taken from Ansys Fluent database, thermal conductivity and dynamic viscosity taken from (A. Abdullah, 2016)

Property	Value
Density kg/m^3	998.2
Specific Heat Capacity J/kg K	4182
Thermal Conductivity W/m K	0.545 (5ºC) – 0.59 (30ºC)
Dynamic Viscosity kg/m s	0.007 (5ºC) – 0.0056 (30ºC)

Using these properties, the dimensions of the water container, the equations listed, and the bulk flow velocity as 0.2m/s, the following values can be calculated in table 7.

Table 7: Calculated properties of the system with deionised water at a bulk fluid velocity 0.2m/s to find the heat transfer coefficient between the heat exchange surface and the fluid (ΔT=16ºC)

Property	Value
Reynolds Number Re	10,153 (Laminar)
Boundary Layer Thickness δ	17.7mm
Prandtl Number Pr	53.71
Nusselt Number Nu	126
Average Heat Transfer Coefficient h	386.5W/m^2 K
Heat Transfer Rate q̇	149.7W

3.6.2 Ansys FLUENT (CFD) Flat Plate

Even though it is possible to calculate by hand heat transfer for flat plate conditions, it is much more effective to use software as many more parameters can be analysed this way. The software used in this project was Ansys, which offers its FLUENT package for CFD analysis, and a Thermal-Electric package which is used later in this report. As shown in the literature review Ansys is a common tool in engineering for both types of analysis due to its ease of use in doing many simulations quickly and its accuracy, this is the reason it was chosen for this project.

The geometry for the CFD of the flat plate simulations was all designed is Solidworks and imported into Ansys Fluent. All the models were the same geometry except for one part, the heat exchange surface which changed based on which test was being simulated. The fluid was modelled as a solid part in Solidworks with the exact dimensions of the test rig and a depth of 52mm. The geometry of the rig from Solidworks can be seen in figure 20 where the inlet was chosen as the circular face on the end of the pipe. The outlet was located at the exact same location on the other side of the fluid block.
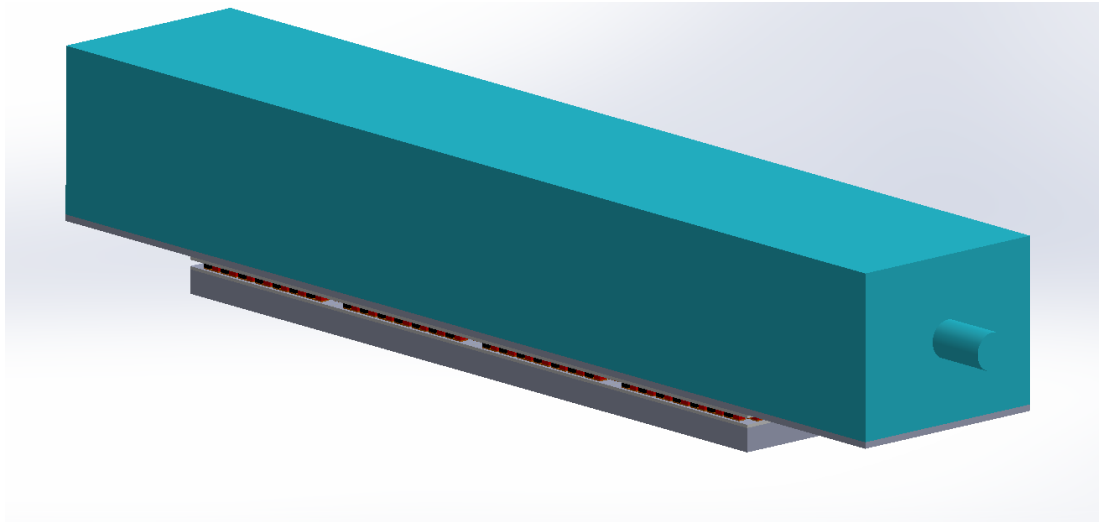
Figure 20: Test Rig model in Solidworks for the 2mm Heat Exchange Plate

Once imported into Ansys, the geometry was edited in Ansys design modeller to allow parts and faces to be named. Firstly, the fluid block was edited to be a fluid rather than a solid (its default). All the individual parts were named to differentiate them to allow material selection in the setup section. The only part not named was the TEG pellets as these were grouped in material selection as an average of both negative and positive pellets at 12ºC which is 1.658W/mk. The faces which parameters were set, and which intend to be analysed must also be named. The inlet and outlet were named on each end of the fluid. Each of the individual outer alumina ceramic plate faces on the TEGs were named to allow analysis of the temperatures on them. The location on the steel where the temperature is measured in the physical test was named as a face to allow the hot side temperature to be inputted as a parameter. The face of the heat exchange surface in contact with the fluid was also named to allow the heat transfer to be analysed. Once all of this was complete the next step was to mesh.

When meshing in Ansys it is crucial to aim for a high-quality mesh to produce the most accurate results possible. Two key measures of mesh quality are mesh skewness and orthogonal quality. For a high-quality mesh ideally the skewness of elements should be as low as possible, and the orthogonal quality of elements should be as high as possible. As stated on (Avraham, 2019): Orthogonal quality is defined as how close adjacent element faces/edges are to optimal angle. Skewness is a measure of element deviation from optimal volume. Calculating an elements skewness is possible using equation 16 (Avraham, 2019).

$$Skewness = \frac{optimal\ cell\ size - cell\ size}{optimal\ cell\ size} \qquad (16)$$

The orthogonal quality can be calculated using equation 17 (Avraham, 2019), the variables in this equation are shown on an element in figure 21

44

$$min\left(\frac{A_i \cdot f_i}{\overrightarrow{|A_i|}\overrightarrow{|f_i|}}, \frac{A_i \cdot c_i}{\overrightarrow{|A_i|}\overrightarrow{|c_i|}}\right) \qquad (17)$$
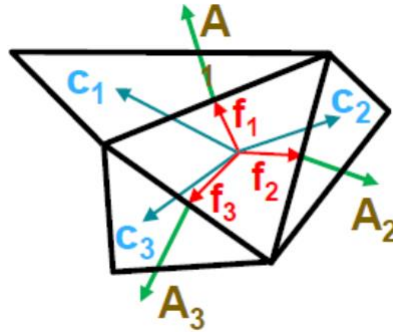
Figure 21 (Avraham, 2019), Orthogonal quality variables on a tetrahedral mesh element

Simulations with the exact same orthogonal quality and skewness values can produce different output values when performed if they have different element sizes and number of elements. A mesh with large elements sizes and therefore a smaller number of elements can be described as coarse. On the other hand, a mesh with small element sizes and a large number of elements can be described as fine. A finer mesh with the same orthogonal quality and skewness values as a coarse mesh will produce more accurate results. Why not just always simulate with as fine of a mesh as possible. The finer the mesh is, the longer the simulation will take as the solver must process a much larger amount of information per iteration. Ideally the mesh should be at a point where it is fine enough to obtain as accurate results as possible, but coarse enough that the simulations can be performed in a suitable time with the hardware available.

As described in section 2.6.2, (Ayman Eldesoukey, 2019) completed a mesh study in which they started with a coarse mesh and gradually refined it to see at what number of elements the results obtained plateaued. The same method was applied in this research but using slightly different results to measure this. For this research the mesh was initial achieved using the default element size settings which were gradually made finer. The results that were analysed in this mesh study were the average temperature difference across the alumina faces on both sides of the TEG modules (ºC). This result was chosen for the mesh study as it is the parameter which will be used in the thermal electric analysis and will directly affect the power produced in the thermal electric simulations. For the initial mesh study, the flat plate test rig test was simulated with a 2mm aluminium heat exchange surface. This initial mesh study is the most thorough as it will give an idea of how many elements are required for the other simulations. The input parameters (fluid velocity, temperatures) chosen for the simulations in this study were taken from the biggest ΔT obtained from the physical test of the 2mm aluminium flat plate. These are shown in table 8.

Table 8: CFD input parameters for mesh study

Parameter	Value
Fluid Velocity	0.18475
Fluid Temperature	6.246
Hot side temperature	25.76

Every simulation in the study had approximately 100% of the elements with an orthogonal quality of 1 (perfect) as this model was simplified to have a rectangular inlet with no pipes. After performing the mesh study, the results for the temperature differences based upon the number of elements is shown in figure 22.
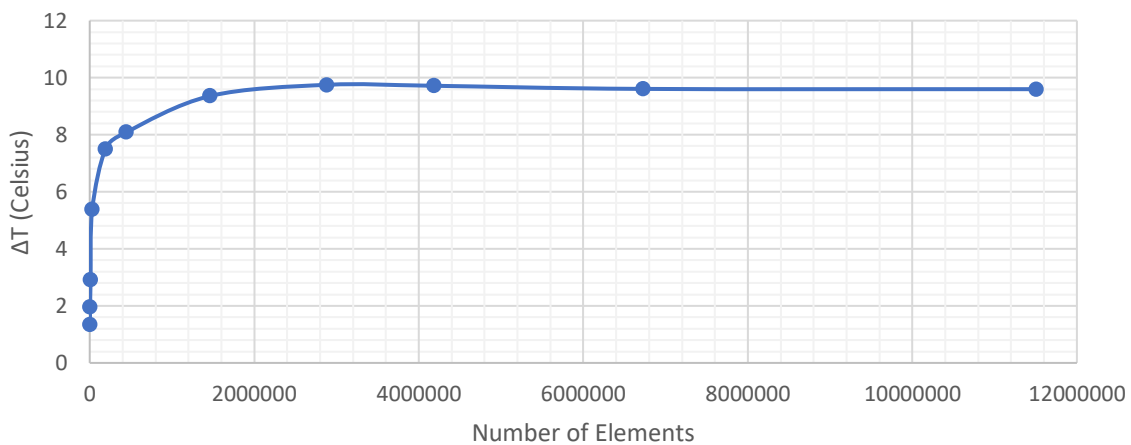
Figure 22: ΔT on Alumina plates in initial mesh study against number of elements. Tests performed for flat plate aluminium heat exchanger 2mm thickness

When decreasing the default element size, the number of elements increases rapidly. Table 9 shows the results from figure 22 plus the default element sizes used.

Table 9: Results from initial mesh study

Default Element Size (m)	Number of Elements	ΔT (ºC)
0.01842	2538	1.349
0.01	4286	1.963
0.006	10556	2.909
0.004	30254	5.378
0.002	193426	7.5
0.0015	448395	8.092
0.001	1462972	9.358
0.0008	2995722	9.75
0.0007	4187110	9.716

0.0006	6730302	9.606
0.0005	11510740	9.597

Based off the results from the mesh study, it was decided that the results plateaued at about an element size of 0.001m. Therefore, all the flat plate CFD simulations were performed with this element size. Furthermore, this element size would be the starting point for the other simulations (rather than the default of 0.01842m).

The k-ω SST model was chosen for reasons supported in section 2.8 of this report. As this model was chosen, the model aimed for a y+ of 1 (Ansys, 2010). As the k-ω model is being used, an inflation layer is required to achieve a first cell height with a y+ of 1. In calculating the first cell height 'y', first the skin friction must first be calculated using equation 18.

$$C_f = 0.058 Re_l^{-0.2} \tag{18}$$

This value is then used in predicting the wall shear stress using equation 19.

$$\tau_W = \frac{1}{2} C_f \rho U_\infty^2 \tag{19}$$

Using the wall shear stress value, the shear velocity can be calculated using equation 20.

$$U_\tau = \sqrt{\frac{\tau_W}{\rho}} \tag{20}$$

Finally, the desired first cell heights can be calculated using equation 21.

$$y = \frac{y^+ \mu}{U_\tau \rho} \tag{21}$$

Using the parameter values for this model and the equations stated, y=9.6805x10^{-5}m, therefore after rounding the aim is to achieve a first cell height of approximately 0.0001m. The inflation option chosen for this research was smooth transition, therefore the growth rate and maximum layers will determine the first cell height. To achieve the desired first

cell height, the growth rate and maximum number of layers should satisfy equation 22 (Uygun, 2020)

$$\frac{Height\ of\ last\ Prism}{Height\ of\ first\ layer} \approx Growth\ Rate^{Number\ of\ layers-1} \qquad (22)$$

The height of the last prism was 0.001m and the height of the first layer was desired to be 0.0001m, therefore the growth rate chosen was 1.259 and the number of layers was chosen to be 11. The transition ratio was chosen to be 0.7.

This initial mesh study was done using approximations of the final model (laminar turbulence model and rectangular inlet instead of a pipe) for simplicity.

For the actual simulations the inlet was pipe shaped to emulate the tubing in the test rig.

The mesh for both the 2mm and 6mm plate systems had minimum orthogonal quality above 0.1 and a maximum skewness below 0.9.

The first part of the setup of interest is the models. Under here the energy equation was turned on as there is heat transfer involved in these simulations. As shown in section 3.1.1 it was expected that the flow would be laminar for the flat plate tests. As stated, the k-ω SST model was selected. The next step is to fill out the material properties to assign to the parts. For the solids, thermal conductivity is the only material property of interest in these simulations. The material properties used in the CFD flat plate simulations are shown in table 10.

Table 10: Thermal Conductivity of Materials used in CFD Simulations

	Thermal Conductivity (W/mK)	Source
Aluminium 1050	121 (121-193)	(Metals4U, 2022)
Mild Steel CR4	25 (25-93)	(MatMatch, 2022)
Thermal Grease	5	(RS Components, 2022)
Alumina	13.739	Ansys Granta
Copper	393.98	Ansys Granta
TEG Pellets	1.658 (Average)	(RS Components, 2022)

The aluminium and steel thermal conductivity on the sources was given as a range as shown in the brackets within the table. The thermal conductivity chosen was based on a value in this range which produced the closest simulation results to the physical tests. The thermal conductivity for the TEG pellets was given as an average of both the positive and negative pellets at 12ºC (a middle temperature for the tests being performed).

The final material of which was inputted was the fluid, which in the case of this experiment was water. More than just the thermal conductivity of the fluid effected the results of the

simulation. The properties of water were taken from the Ansys Fluent materials database and from literature are shown in table 6.

Once all the materials and their properties had been added to the set up, they were assigned to the parts which were named in the design modeller section, this is done in the cell zone conditions part of set up.

After the materials were assigned, the boundary condition section were set up. The first boundary conditions to add are on the inlet of the fluid. The height of the fluid was set to be tested at 52mm as with this height and the pump working at full power the fluid velocity would be 0.2m/s, as stated in section 3.6.1. The inlet velocity in the simulations however was coming through the pipe with a smaller cross-sectional area, the pump was also operating at 21W instead of 23W. Therefore, the flow rate was $6.3406 \times 10^{-4} m^3/s$, this equated to an inlet velocity of 5.6m/s in the pipe. The inlet temperature of the fluid was set as the fluid temperature recorded from the physical test in the simulation being performed. The outlet fluid temperature was also set as this recorded temperature. The final boundary condition set was the temperature on the hot side. For this the face on the bottom of the steel block which is in line with where the temperature sensor was located was set as the recorded temperature from the tests.

Under the methods tab the pressure-velocity scheme was set as coupled and the rest of the setting were left as default, it was tested to see if changing these influenced results and the results stayed identical. The relaxation factors under the controls tab were all left as default.

Aside from the standard residuals monitored, the mass flow rate at the outlet was observed under the report definitions tab as once this value stabilises it gives a good understanding of when the system has also stabilised. All the residual monitors were left as default, when the absolute criteria were made smaller it had no impact on the results obtained therefore default was adequate. The residuals are monitored until they reach the absolute criteria, once this has happened the simulation ends as the residuals have converged to a point which deems the simulation accurate. Essentially, the residuals are a function of the error in the model therefore the lower the value of the residual, the less error at the current iteration. The residuals monitored in this section were: the directional velocities (X, Y, & Z), the continuity which is related to the mass imbalance throughout the model, and the energy as the energy equation is turned on (because there is heat transfer in the model). Finally the k and ω residuals are monitored due to this turbulence model being used.

Once all these steps were completed, the simulation could be initialised and ran to obtain the desired results.

Many methods were tested from using the data from the CFD in the Thermal-Electric simulations to see which yielded the most accurate results in comparison with the physical tests performed. For example, the average heat transfer rate on the heat exchange surface was tested along with trying the average temperature of this surface and other temperatures. The most effective and accurate way of converting the CFD data after trialling was to use the average temperatures on each of the individual ceramic plates of the TEG modules. This would give eight different temperature conditions to use within the Thermal-Electric simulations. The likely reason for this producing the most accurate Thermal-Electric results is down to the use of more conditions rather than one large average, and the location of these conditions being so close to the TEG pellets.

3.6.3 Ansys FLUENT (CFD) Heat Transfer Fins

The hand calculation as shown in section 3.5.1 can be used for a simple example such as flow over a flat plate however, when the geometry is more complicated for example flow across heat transfer fins, hand calculations are not possible. In this situation Computational Fluid Dynamics (CFD) software is required to obtain information such as heat transfer coefficients. The CFD software is used in this case to determine the heat transfer coefficients with different size fins, to determine the optimum size fin for diffusing heat from the system.

This model was like the model simulated in the previous section however the heat exchange surface had heat transfer fins added. Four 30mm high aluminium fins were added as shown by the dimensions in figure 23
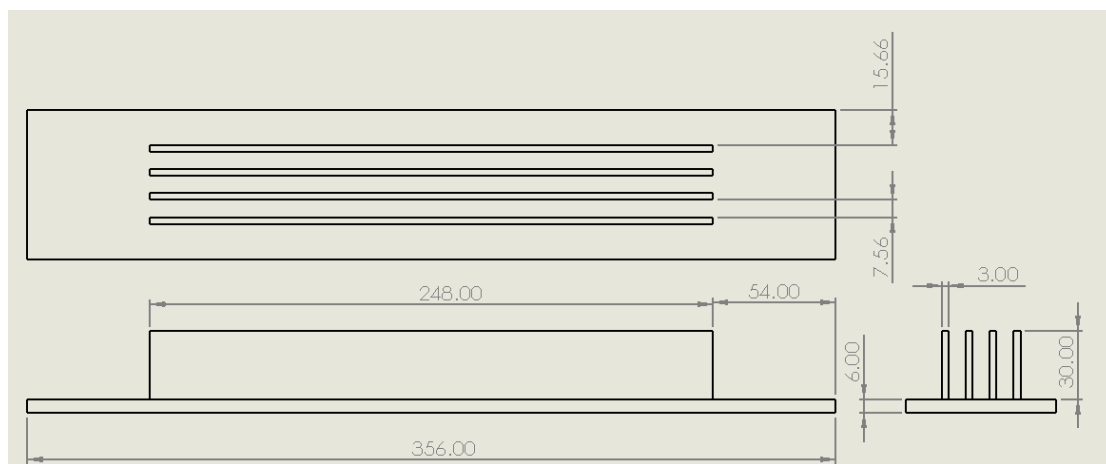
Figure 23: Dimensions of the Heat Transfer Fins which were simulated in Ansys

The fluid region for the CFD study on the heat transfer fins was designed as an object in Solidworks as a block, the area where the heat transfer fins intersect this block was subtracted from the fluid region using the Boolean function in design modeller.

Due to the added complexity of shape from the heat transfer fins, obtaining a good quality mesh was also more complex than the flat plate system. The element sizes for this mesh were chosen to be 1×10^{-3}m like the flat plate models (as the model is the same size). The inflation layer had the same parameters as section 3.6.2 as the element size and most parameters were the same, the only change was the addition of heat transfer fins to the plate.

The mesh generated at no element with an orthogonal quality value less than 0.1 and skewness greater than 0.9.

The set up within fluent was identical to the previous section apart from the fluid temperatures tested.

3.6.4 Ansys FLUENT (CFD) Scaled up Model

The previous results sections show how reliable the Ansys software is at predicting the power output of TEGs, section 4.4 results on the other hand should give us a prediction on how an integrated TEG system could perform in a submarine operating in real world scenarios. Submarines come in many shapes and sizes, but generally they are cylindrical for much of their surface. When modelling the scaled-up system, it was decided that using real

50

world dimensions/geometry of a chosen submarine would give the best representation of how the system would behave. Our business partner Delkia which this project is in collaboration with are involved with the submarine industry, they kindly shared a concept submarine CAD model to use its dimensions for my scaled-up system. Figure 24 shows the CAD model of the concept submarine in Solidworks.
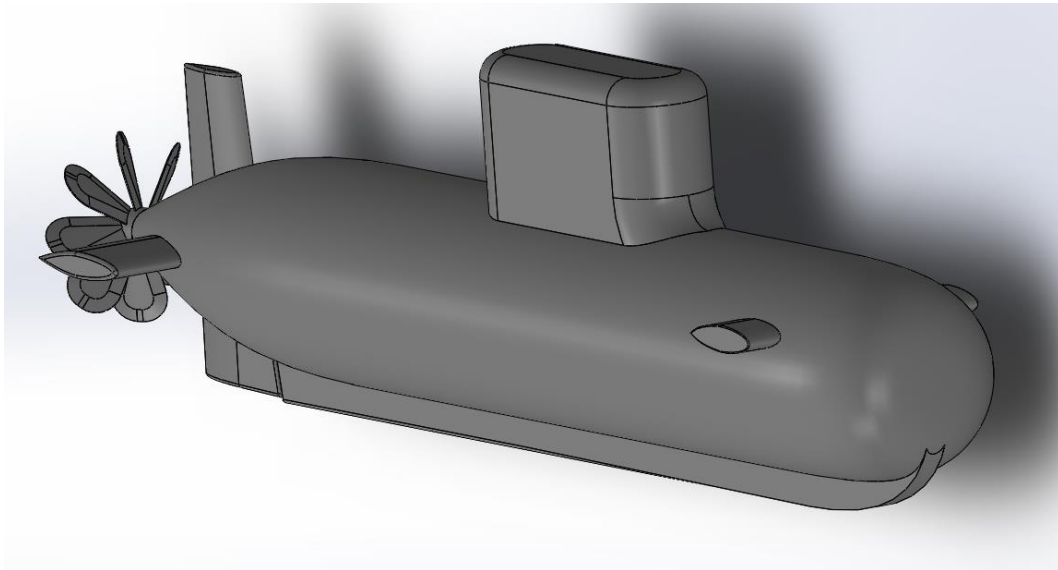
Figure 24: (Delkia, 2022): Concept Submarine CAD model in Solidworks

The simulations performed in this section did not require the full CAD model shown in figure 24, as only the section of the submarine where the TEGs are located will be simulated. The three parameters required were: cross-sectional cylinder radius, wall thickness, and submarine material. The parameters of the submarine are shown in table 11

Table 11: Submarine parameter used for scaled-up simulations

Parameter	Value
Cylinder Radius	2005mm
Wall Thickness	38mm
Wall Material	HY-80 Steel

The scaled-up simulations did not only aim to see how the TEGs would perform in real world scenarios, but also aimed to see what the best configuration is for maximum power output. Four different configurations were tested, each containing the exact same TEG modules as the previous tests for reproducible results. The four models consisted of two models with heat transfer fins and two models without. Each two models consisted of one with the TEG modules in a lateral formation across the cross-section of the submarine and one longitudinal formation down the length of the submarine. The TEGs were positioned near the roof of the submarine as this is the area which is most likely to be impacted by convection from the flowing water. Figure 25 shows the longitudinal model with no heat transfer fins with the fluid region which would be located on the top of the wall hidden.
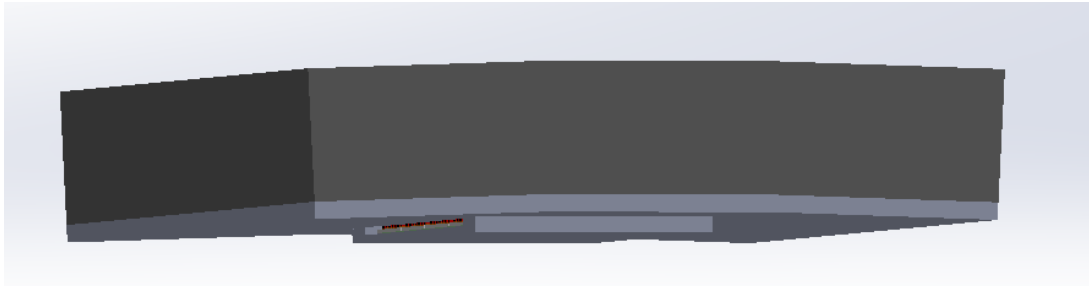
Figure 25: Longitudinal layout model with no heat transfer fins (scaled up model)

The height of the heat transfer fins was determined using equation 24 where the heat transfer coefficient used in the equation was an approximation based upon the heat transfer coefficient contours on the surface of the sub wall for the simulations without fins (water at 10ºC). The ideal lengths were calculated to be 83mm for the longitudinal model and 64mm for the lateral model.

The start of the TEG modules for all the models are exactly 0.2m from the inlet. The fluid flow is expected to become turbulent at approximately 0.1715m from the inlet, 0.2m was chosen to make sure the flow was turbulent at the location of the TEGs and to be consistent across all models tested.

Initially, the element size chosen for meshing was 0.001m. This was chosen as it was seen to be the ideal size for the simulations of the test rig and many of the components are the same as these simulations therefore it is a good starting point. However, it was found that with the hardware used in this research and the size of the model, the computers would not run simulations with mesh elements of this size. An element size of 0.002m was chosen as this was the finest mesh that the hardware was able to simulate with such a large model.

The flow for the scaled-up models was expected to be turbulent, therefore a suitable turbulence model must be chosen. The k-Ω SST model was chosen meaning y+ value of 1 is desired. Using the equations from section 3.6.3 it was possible to calculate that the first cell height of the inflation layer should be approximately 1×10^{-5}m.

Table 12: Inflation layer properties for scaled up models

Model	Growth Rate	Maximum Layers	Transition Ratio
Long	1.303	21	0.7
Long W/ Fin	1.303	21	0.77
Lat	1.303	21	0.7
Lat W/ Fin	1.303	21	0.77

Table 13: Mesh quality values for the scaled-up models (to three significant figures)

Model	Orthogonal Quality			Skewness		
	Min	Max	Average	Min	Max	Average
Long	0.179	1	0.831	0	0.821	0.169
Long W/ Fin	0.0205	1	0.803	0	0.898	0.194
Lat	0.185	1	0.833	0	0.815	0.166
Lat W/ Fin	0.0141	1	0.783	0	0.887	0.214

It was not possible to get all elements to have an orthogonal quality below 0.1 for the models with heat transfer fins however this did not appear to disrupt the results obtained.

The only new solid materials used in this set of simulations were the steel which the submarine was made from and the thermal insulation which was chosen to be expanded polystyrene foam. The hull of the submarine was assumed to be made from HY-80 steel. A paper by (Brad Baker, 2015) stated the thermal properties of this type of steel, table 14 shows the thermal properties for HY-80 steel and expanded polystyrene foam (from Ansys Granta database) at room temperature.

Table 14: Thermal Properties of HY-80 Steel, and Expanded Polystyrene used in Ansys Fluent

Property	Density kg/m^3	Specific Heat J/kgK	Thermal Conductivity W/mK
HY-80 Steel	7750	500	34
Expanded Polystyrene	29.933	1210	0.0329

The properties of the water simulated in the scaled up Ansys simulations were different to that of the previous simulations, as seawater contains salt which causes it to behave differently, which needs to be considered for optimum accuracy. The North Sea has a salinity level of about 34 to 35g/l (New World Encyclopedia, 2018). Because we have data on water properties at 35g/l, we will use this salinity for this research. The properties of saltwater (35g/l salinity) used in these calculations are found in table 15

Table 15: Properties of water with a salinity of 35g/l at 20⁰C (Engineering ToolBox, 2005)

Property	Value
Density ρ	1025 kg/m^3
Dynamic Viscosity μ	0.00109 Ns/m^2
Specific Heat C$_p$	4007 J/kgK
Thermal Conductivity k*	0.6 W/mK

The '*' in table 15 is to indicate that this value was taken from Fluent database and not the source referenced.

The next step in the method of simulating the scaled-up model was to input the boundary conditions. At the inlet the velocity was set to 3.09m/s, this is the velocity which a specific AUV travels when submerged according to data provided by Delkia. The inlet and outlet water temperatures were tested at 5, 10, & 15ºC which are a range of temperatures experienced at different depths in the North Sea. Lastly the temperature for the inside of the submarine must be set. The face on the bottom of the insulation and the bottom of the steel holding the TEGs are both set to 20ºC (room temperature).

Like the CFD simulations completed in the previous sections, the same residuals were monitored with the same absolute criteria of convergence. The mass flow rate at the outlet was also monitored for the same reason as stated previously.

3.7 Ansys Thermal-Electric Set-Up

3.7.1 Materials & Geometry

To simulate the TEG modules, a replica to the exact dimensions had to be designed in CAD software. The software chosen for this was Solidworks and the TEG module designed is shown in figure 26 with the red pellets being positive and the black ones being negative.
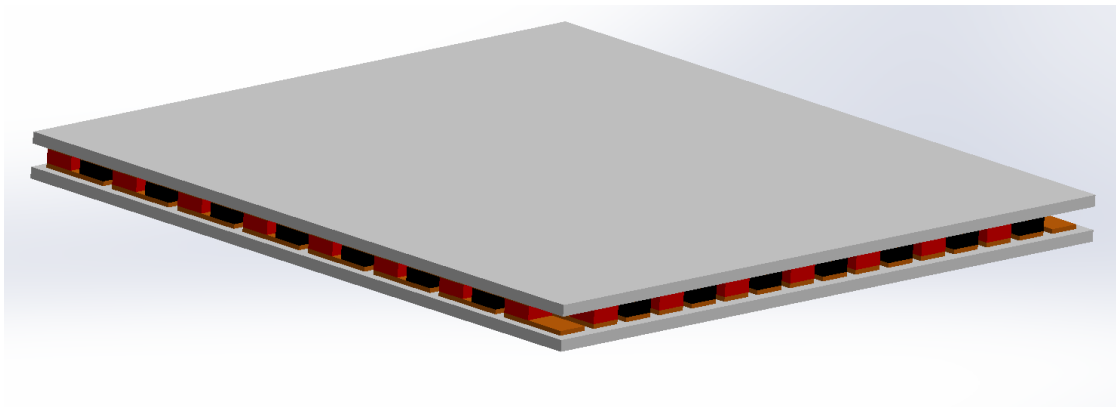
Figure 26: TEG Module GM250-127-28-12 designed using Solidworks

The dimensions drawing of the module from a side view are shown in figure 27.
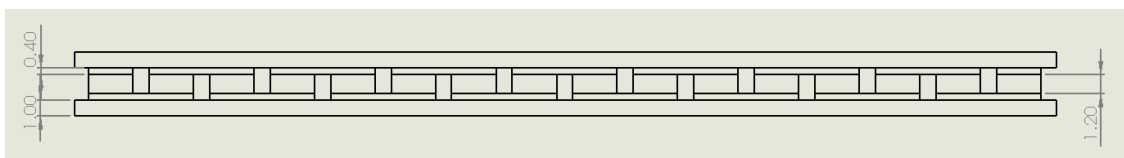
Figure 27: Dimensions of TEG Module GM250-127-28-12 from Solidworks Drawings, values in mm.

Ansys workbench 2021 R2 software was used for simulating the system, specifically the Thermal-Electric section within the software. The first section to complete for the simulations to be accurate is the engineering data section. In this part the materials being simulates and their properties were added.

The ceramic heat transfer plates sandwiching the contents of the module are made of Alumina, and the contact pads electrically connecting the pellets are made of copper. The properties of both these materials as inputted in Ansys can be found in table 16 and are the properties for the materials as used in Ansys Granta database, which is a large databased of material properties.

Table 16: Properties of TEG module parts as inputted in Ansys

Property	Alumina	Copper
Thermal Conductivity W/mK	13.74	393.8
Electrical Resistivity Ohm.m	10^{12}	1.68×10^{-8}

The properties of the TEG pellets are temperature dependent, the equations governing the properties of both the positive and negative pellets can be found it table 17, with the temperature being values being inputted in Kelvin. These properties are from the modules datasheet (Eauropean Thermodynamics, 2022).

Table 17 (ETD, 2022): Temperature (T-Kelvin) Dependent Properties of the Pellets within the TEG module

Property	P-Type	N-Type
Thermal Conductivity W/mK	$0.0000361558 \times T^2 - 0.026351342 \times T + 6.22162$	$0.0000334545 \times T^2 - 0.023350303 \times T + 5.606333$
Seebeck Coefficient 10^{-6}V/K	$-0.003638095 \times T^2 + 2.74380952 \times T - 296.214286$	$0.001530736 \times T^2 - 1.08058874 \times T - 28.338095$
Electrical Conductivity 10^2S/m	$0.015601732 \times T^2 - 15.708052 \times T + 4466.38095$	$0.01057143 \times T^2 - 10.16048 \times T + 3113.71429$

These properties were inputted into the Ansys data sheet to be applied to the pellets on the model of the module. The resistivity was calculated as 1/Electrical conductivity, as the values in Ansys use electrical resistivity as opposed to conductivity.

As stated previously in section 3.3, for the power output of the module to be at its maximum the internal TEG resistance should be equal to the resistance of the load. Based upon data from (ETD, 2022), the expected internal resistance of one TEG module was expected to be 0.575Ω at 12ºC. Using equation 23 it was possible to create a length of material with a chosen resistivity to produce the desired load resistance. The load resistance desired for the simulations was approximately 2.3Ω.

$$\rho = \frac{RA}{L} \quad \quad (23)$$

The length of the resistor built in Ansys was 0.24194m, the cross-sectional area was 5.625×10^{-7}m^2, therefore the resistivity of the material was set to be 5.3474×10^{-6}ohm m.

The next section which is required is the geometry. The module designed in Solidworks and shown in figure 26 was imported into Ansys Spaceclaim four times and the modules were lined up adjacently, as they would be in the real test rig. The rest of the geometry was built around these using Ansys Spaceclaim. The final geometry is shown in figure 28 built into a larger assembly within Solidworks. This consisted of the four modules lines up adjacent to one another and connected in series via wires of copper. The modules were also connected to the resistor with the dimensions stated previously. The rest of the system, including the thermal grease, steel, and heat exchange surface were assembled around the modules. The steel was modelled to have a height of 7mm, the distance from the PT100 sensor which is logging the data to the steel in which the TEGs rest upon. The rubber insulation surrounded the TEGs was not modelled in Ansys, as the thermal conductivity is so low it is believed it would make very little difference if simulation.
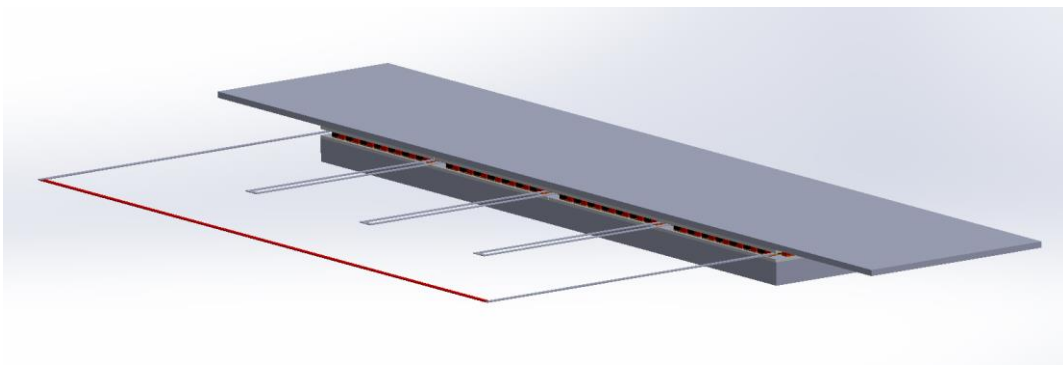
Figure 28: Assembly of flat plate 2mm heat exchange surface thickness system from Solidworks

3.7.2 Set-up within Ansys- Meshing & Analysis

As stated previously, the maximum power produced by the TEGs will occur when the load resistance is equal to the internal resistance of the TEGs. The internal resistance of the TEGs will change mildly with the changing temperature throughout the experiments/simulations; for simplicity, a resistor of 2.3Ω was simulated which is the expected TEG internal resistance across the 4 modules at 12ºC, the average temperature across the TEGs at the last step of the simulations.

There are three main conditions which must be added in the set up for this simulation to work. These are: the temperature on the hot side, the temperature on the cold side, and a voltage condition.

The temperature conditions (eight in total) are split, four on the hot side ceramic plates, and four on the cold side ceramic plates. The values for these temperatures were calculated from CFD simulations using Ansys Fluent and are shown in section 4.2.1. The temperature values used as the conditions are averages from the CFD simulations.

Because the temperature conditions were all chosen to be on the ceramic Alumina plate surfaces, the heat exchange surface, steel, and thermal grease parts of the model could be

supressed. When tested with these unsuppressed, the difference between the results produced was negligible.

The voltage is set at 0V on the negative wire from the end TEG near the resistor. This will allow us to clearly see the voltage distribution across the TEGs and the resistor.

A convection condition was also set on the load resistor to avoid it getting too hot in simulations and allow easier analysis of the temperature post simulation of the TEGs without a skewed scale.

3.8 Test Conditions

3.8.1 Materials & Conditions

The focus of this project is on the potential use of TEGs in Submarine/AUVs; therefore, the test conditions must replicate the potential conditions experienced in the Ocean water on one side, and on the inside of an AUV for the other side. The main conditions here which were to be focused on was the temperatures, as this is what determined the power outage of the TEGs.

Data for the temperatures experienced in the North Sea are cited in the literature review, the North Sea was chosen as it is local to where this project is being carried out. The data from (Carl Freitas, 2021) suggests highs of around 20ºC at the surface (in warmer seasons) and lows of about 4ºC.

As stated in the literature review, simulations on TEGs in AUVs using MATLAB & Simulink have been performed by both (J.R. Buckle, 2013) & (J. Falcão Carneiro, 2018). These two papers simulated with the temperature of the water ranging between 20ºC→5ºC & 27ºC→4ºC respectively.

The temperature on this inside of the AUV/Submarine is believed to stay relatively constant, which is the reason for the steel block with a high thermal capacity being used as it should keep the temperature on this side relatively constant. For the tests the temperature on this side of the system was aimed to be kept constant at approximately 25ºC.

The tests were done covering all potential temperatures and the data was logged to see how this affects the power output from the TEGs. The max temperature seen in the North Sea from (Carl Freitas, 2021) shows that it can reach 20ºC at the surface in summer therefore this was the maximum water temperature tested. The temperature was gradually decreased for each test to as low as possible for a large range of data, but the data was always collected up to 6ºC as this is the minimum which the chiller can realistically stay stable at during tests and is close to the minimum temperature experience in the North Sea.

The materials selected for testing were chosen for the following reasons: Aluminium is being tested as due to its high thermal conductivity making it an ideal material for conducting heat away from the TEGs at the cold side. Steel is being tested as it is the most common material for Submarines/AUVs to be made from due to its mechanical properties, however steel does not have as ideal thermal properties as aluminium.

The heat transfer material between the TEGs and the water is not the only variable which was tested. (J. Falcão Carneiro, 2018) previously stated that heat transfer fins would be necessary due to high thermal convective resistance caused by a small heat transfer area. With both materials, Aluminium heat transfer fins were to be manufactured to bolt on and

test whether they make an improvement on the power produced by the TEGs; Aluminium was chosen due to its high thermal conductivity. The length of heat transfer fins makes a great difference on how they will perform, for the purpose of this research the ideal length of the heat transfer fins was calculated using equations from (Michael Freunek, 2009). These equations were as follows.

$$L_{fin} = \frac{2.3}{\eta} \tag{24}$$

Where 'δ' can be calculated using equation 25

$$\eta = \sqrt{\frac{h_{H2Ofin} \cdot (2 \times e_{fin} + 2 \times w_{fin})}{k_{fin} \times e_{fin} \times w_{fin}}} \tag{25}$$

The heat transfer fins will be welded onto an aluminium plate of 2mm thickness, which was designed in such a manner that it could easily be bolted onto the heat exchange surface.

The length of the heat transfer fins were chosen to be 30mm and we also 2mm thickness. Four fins were welded to the plate with equal distance between them.

3.8.2 Test Procedure

Both the physical test and the simulations will aim to mimic conditions which would be experienced for an AUV which is gradually descending into deep water by gradually decreasing the temperature of the water.

Each test will be set up using the following order:

1. The rig was assembled by bolting on the heat transfer surface which is being tested to the steel bath walls, with the plumbers putty in place to waterproof.
2. The tank is then filled with water to ensure there are no leaks with the hose tails at either side covered, if there is a leak gasket sealant or more putty may be required, dependent on leak location.
3. The tank is emptied for the rest of the assembly.
4. Next, the Silicone paste should be evenly spread as a thin layer on each side of the TEG modules which are then placed on the steel block adjacent to one another, with the wires all facing the same direction between the gaps of rubber insulation. The TEGs should all have the same face in contact with the same surface, so that the power all flows the same direction. The paste needs to be applied aiming not to let it get inside the TEGs as the will decrease their power output.
5. The block holding the TEGs is then bolted to the heat transfer surface (nylon bolts).
6. The heating element and temperature probes are then inserted into the steel block, and the TEGs are connected to the potentiometer, voltmeter, and ammeter.
7. The potentiometer resistance is set using a multi-meter to achieve desired resistance.

8. The temperature probe is also secured in the desired location of the water tank.
9. The tank is then be filled up with de-ionised water, with the chiller and pump connected.
10. The control panel is switched on to allow the heating element and temperature controller to help the steel block achieve the desired temperature.
11. Next the pump is switched on and off a few times till all air bubbles are forced out of the pipeline.
12. Once all bubbles are gone, the water depth is measured and adjusted by slowly filling the water till the desired depth is reached, before turning the pump back on.
13. As the pump is flowing, not before, the chiller is then turned on with the desired temperature set at 20ºC
14. The system is allowed time to reach a steady state on both sides of the TEGs.
15. Once at a steady state, the data logger is switched on.
16. The chiller temperature is set to decrease by 2ºC every time the system has stabilised, and the results being produced are relatively constant. All whilst the data is being logged from the TEGs and temperature sensors. The hot side temperature must be within 24-26ºC when data is being logged for reproducibility.
17. Once complete, all electrics are turned off and the TEGs wires are separated from the rest of the system to remove risk of electrical fire.
18. Finally, the water is emptied and the assembly is unscrewed and cleaned, ready for the next tests to be completed.

4 Results

4.1 Experimental Results

4.1.1 Aluminium 2mm Flat Plate Exchanger

The results from the experiment consisted of the voltage and current produced by the TEGs at instantaneous temperature differences. For these tests the heat exchange surface was made of Aluminium and had no heat transfer fins. Figure 29 shows the instantaneous voltage and current produced by the TEGs when the data was recorded.
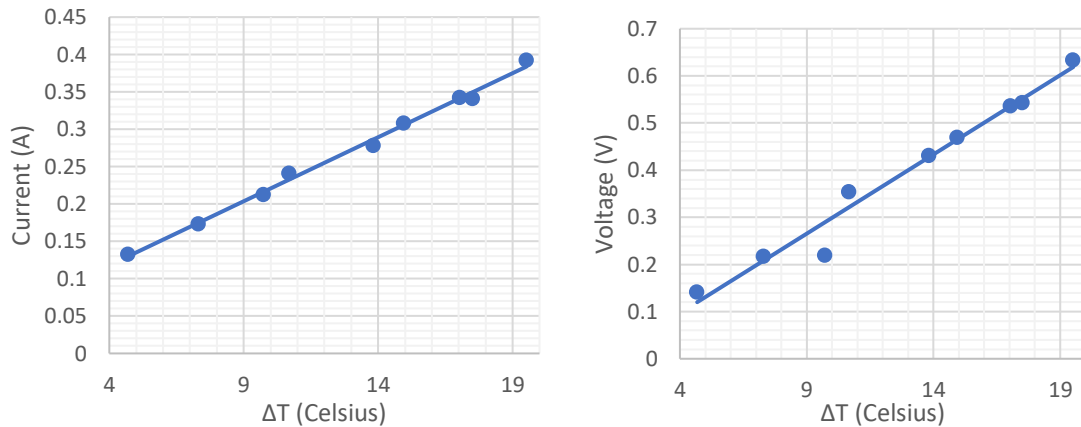
Figure 29: Current and Voltage produced by TEGs in experiment with 2mm thick Aluminium heat exchanger

Figure 29 shows a positive correlation with both the current and voltage produced as the temperature difference increases. Both graphs show a linear trendline, this is as expected based off the manufacturer datasheets. There is only one potentially anomaly in this data is the voltage at the temperature difference of 9.73⁰C.

Figure 30 shows the power produced by the TEGs against the temperature difference in the system. The power is calculated as the product of the Voltage and the Current.

Figure 30 also shows a positive correlation however this graph is not linear in the data trendline. This is expected as it is a product of the voltage and current which are both linear graphs. Excel allows trendlines for power graphs to be produced automatically, which is what was used for the power results in this report.

4.1.2 Aluminium 6mm Flat Plate Exchanger

The results in this section were recorded in the same manner as section 4.1.1, the difference for these results was that the heat exchange surface was 6mm thick rather than 2mm. Figure 31 shows the instantaneous voltage and current produced by the TEGs when the data was recorded.
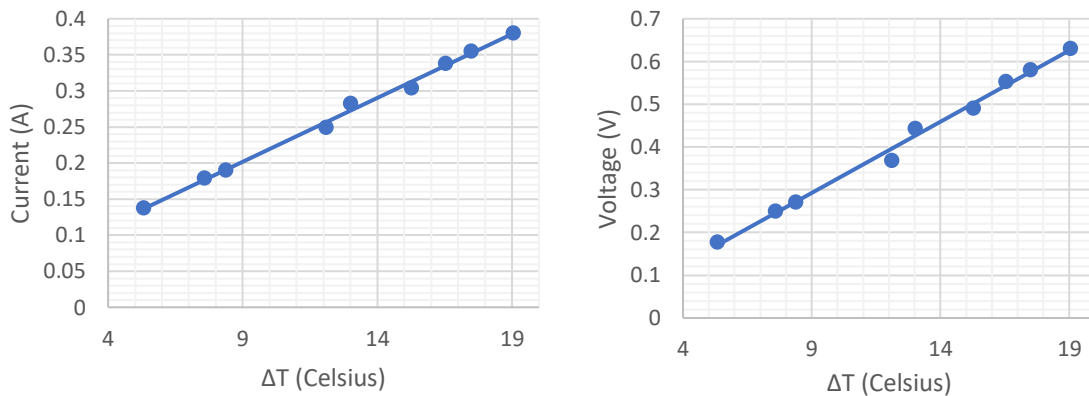
Figure 31: Current and Voltage produced by TEGs in experiment with 6mm thick Aluminium heat exchanger

Both graphs in figure 31 show a positive correlation as temperature difference increases which is expected. No anomalies are shown away from the trendlines.

Figure 32 shows the power produced from these tests calculated with the current and voltage from the tests.

61

Figure 32 shows a positive correlation, and all the points are close enough to the trendline that the data can be said to have no anomalies.

4.1.3 Steel 2mm Flat Plate Exchanger

The results displayed in this section differ from the prior two in the manner that the heat exchange surface material used is steel. Figure 33 shows the instantaneous voltage and current produced by the TEGs when the data was recorded.
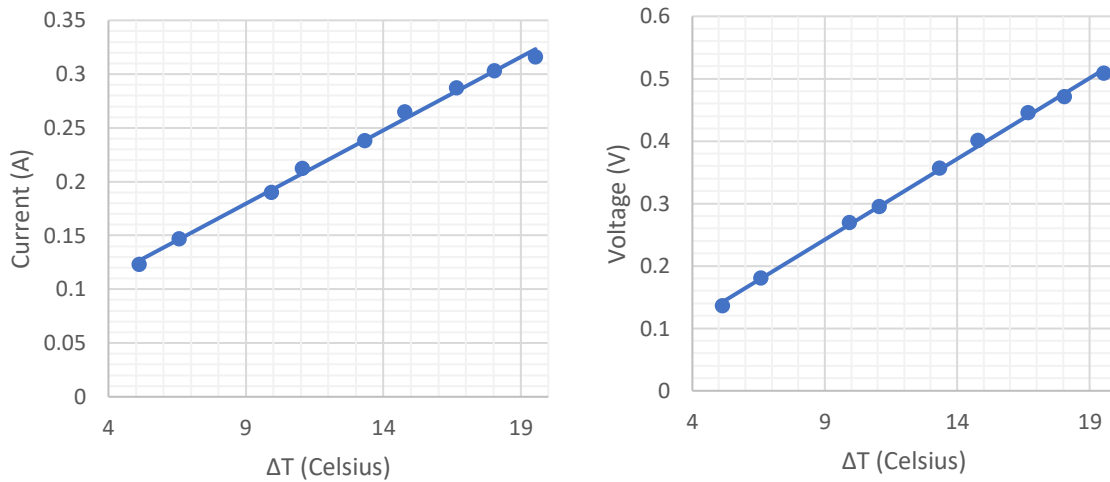
Figure 33: Current and Voltage produced by TEGs in experiment with 2mm thick Steel heat exchanger

Both graphs in figure 33 show a positive correlation and all the points fit almost perfectly on a linear trendline which on initial viewing implies accurate results.

Figure 34 shows the power produced from these tests calculated with the current and voltage from the tests.

62

Figure 34 shows a positive correlation as expected, all the points fit almost perfect to the trendline.

4.1.4 Steel 6mm Flat Plate Exchanger

The results in this section are similarly obtained to the ones in section 4.1.3 however these tests used a 6mm thick steel heat exchanger as opposed to 2mm. Figure 35 shows the instantaneous voltage and current produced by the TEGs when the data was recorded.
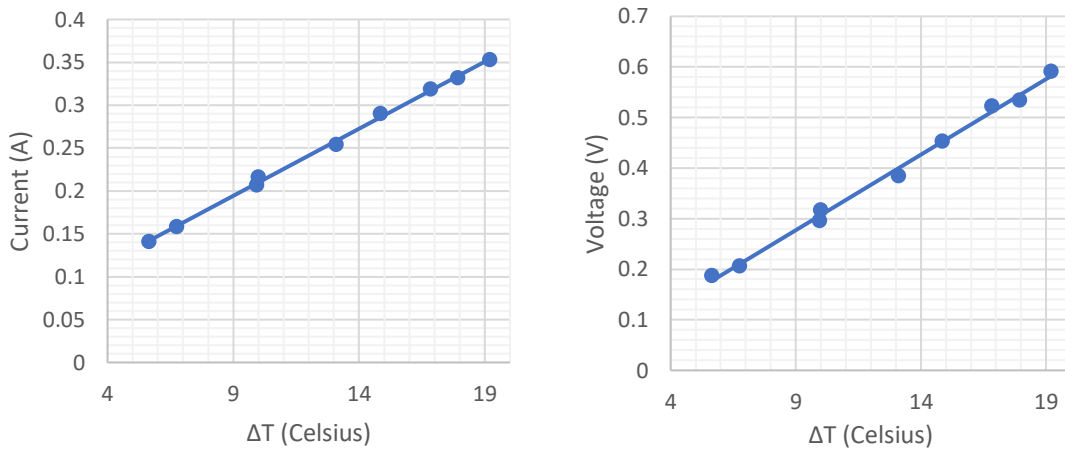
Figure 35: Current and Voltage produced by TEGs in experiment with 6mm thick Steel heat exchanger

Both graphs in figure 35 show a positive correlation as temperature difference increases which is expected. No anomalies are shown away from the trendlines.

Figure 36 shows the power produced from these tests calculated with the current and voltage from the tests.
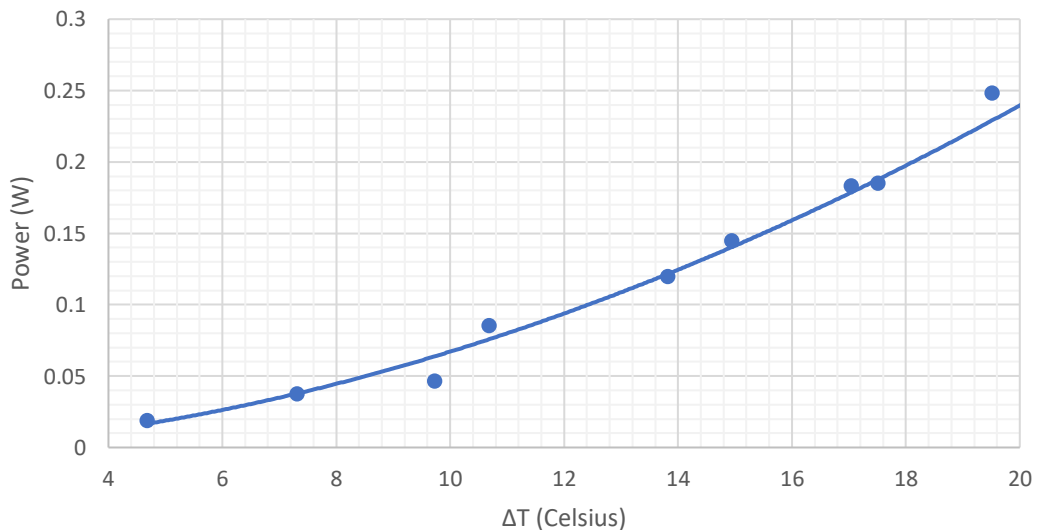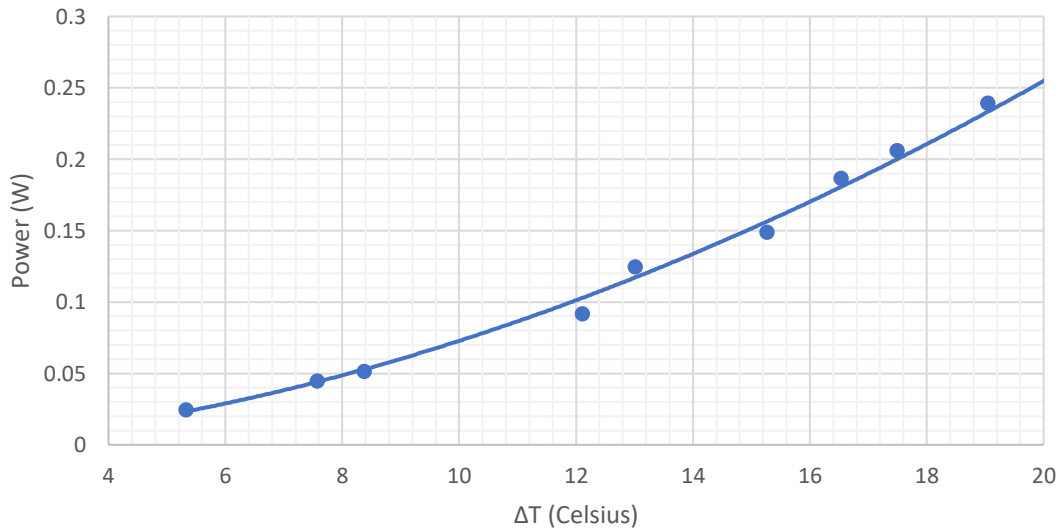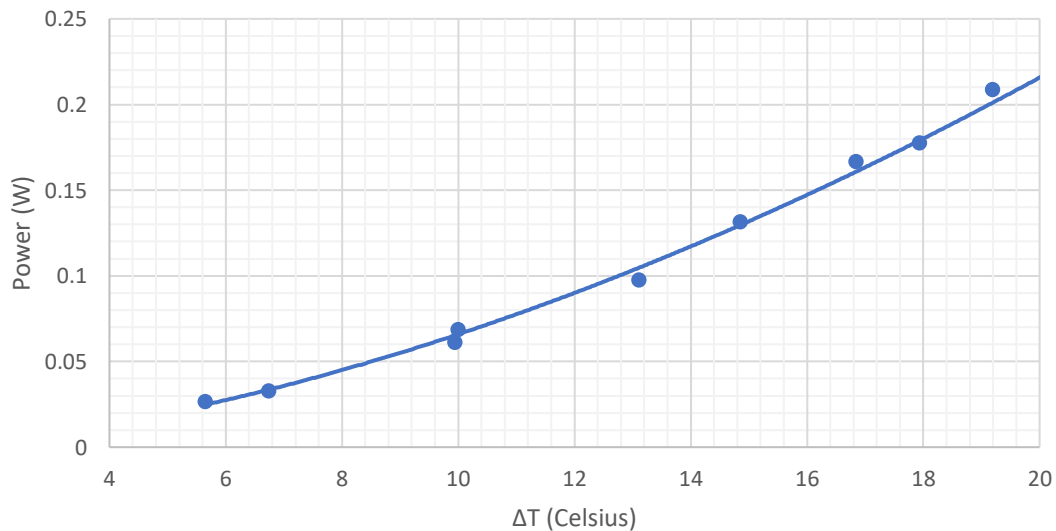

Figure 36: Power produced by TEGs in experiment with 6mm thick Steel heat exchanger

Figure 36 shows a positive correlation, and all the points are close enough to the trendline that the data can be said to have no anomalies.

4.1.5 Flat Plate Comparisons

The results one their own give an idea of how much power can be produced by the TEGs, comparing the results allows understanding of how the thickness and material used as the heat exchanger affects the outputs of the system. Figure 37 shows a comparison of the trendlines for the current produced by each of the flat plate tests.
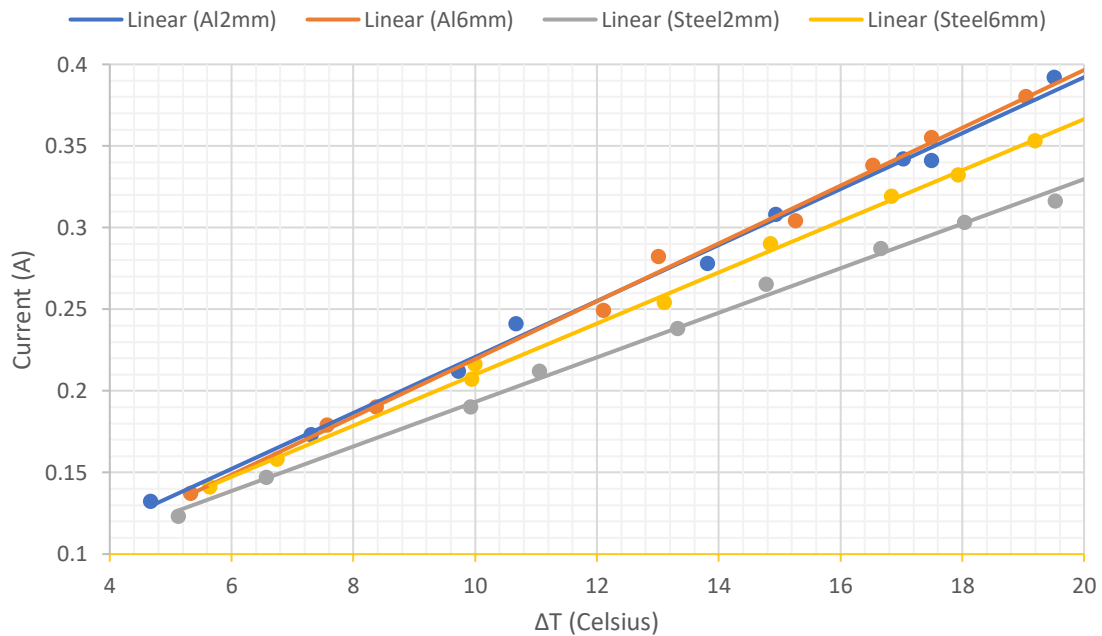
Figure 37: Comparison of the Current produced by the tests of the different thickness and material flat plates (no heat transfer fins)

The aluminium heat exchange surfaces clearly produce a greater current than that of the steel heat exchange surface. The thicker heat exchange surface appears to perform better than that of the thin one when comparing the tests using steel. The thickness of the heat exchange surface seems to have very little impact on the aluminium tests.

Figure 38 compares the voltage produced by each of the flat plate tests.
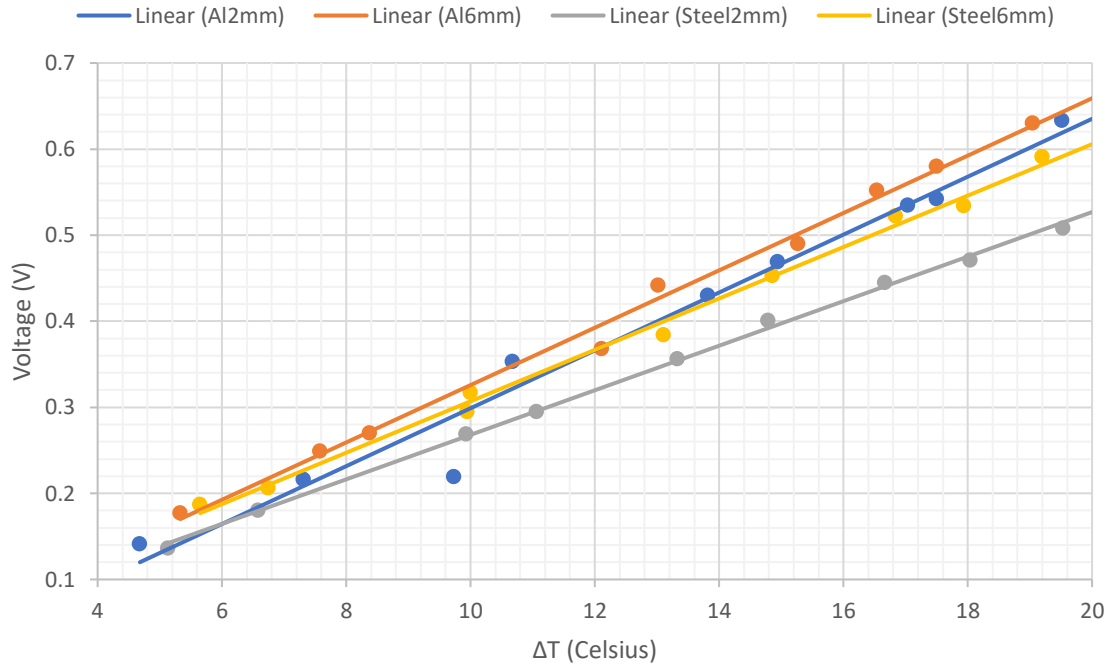
Figure 38: Comparison of the Voltage produced by the tests of the different thickness and material flat plates (no heat transfer fins)

It is clear to see that all the tests follow the expected linear trend of as ΔT increase, so does the voltage. As with the current, the aluminium heat exchange surface produced a larger voltage than the tests with the steel heat exchanger. When comparing the thickness of the exchangers, the 6mm (thick) plates produced a higher voltage than the 2mm (thin) plates of the same material.

The power output of the system was clearly affected by the change in heat exchange system, however not as initially expected as shown in figure 39.
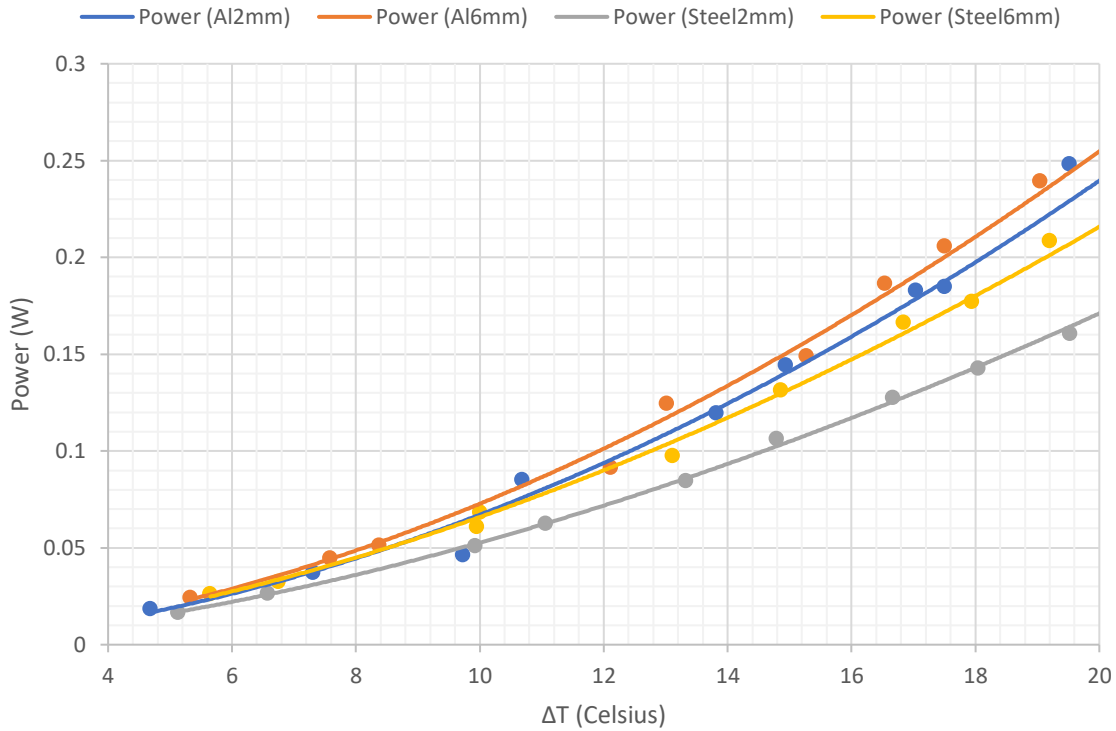
Figure 39: Comparison of the Power produced by the tests of the different thickness and material flat plates (no heat transfer fins)

As is clear to see from figure 39 all four of the different tests produced trendlines with a positive correlation and the expected increasing gradient as ΔT increases. Also, as expected the aluminium tests produced a higher power output than that of the steel. What was not expected is that the thicker heat exchange tests (6mm) had a higher power output than that of the thinner tests (2mm). The thinner exchange surfaces should hypothetically produce the most power due to less distance for the heat to travel through to the convective surface.

4.1.6 Heat Transfer Fin Tests

The initial method for testing the plates with heat transfer fins which involved bolting on an aluminium base with heat transfer fins welded onto it was unsuccessful. The results obtained produced less power than without the heat transfer fins, this was due to lack of contact between the base for the fins and the plate it was bolted onto. The lack of contact was due to the 2mm thick aluminium base buckling when it was welded. To aim to gather a more accurate representation of how heat transfer fins may affect power produced, they were welded directly onto the 6mm aluminium plate, in the hope that the thicker base would stay flat during welding. The plate still bent in the welding process causing poor contact on one side of the plate with the TEGs, however the results obtained were better than the initial method of fins used.

All the results in this section compare the 6mm flat plate tests with the heat transfer fin tests with the fins welded directly onto the 6mm aluminium plate. Figure 40 compares the current produced in both tests.
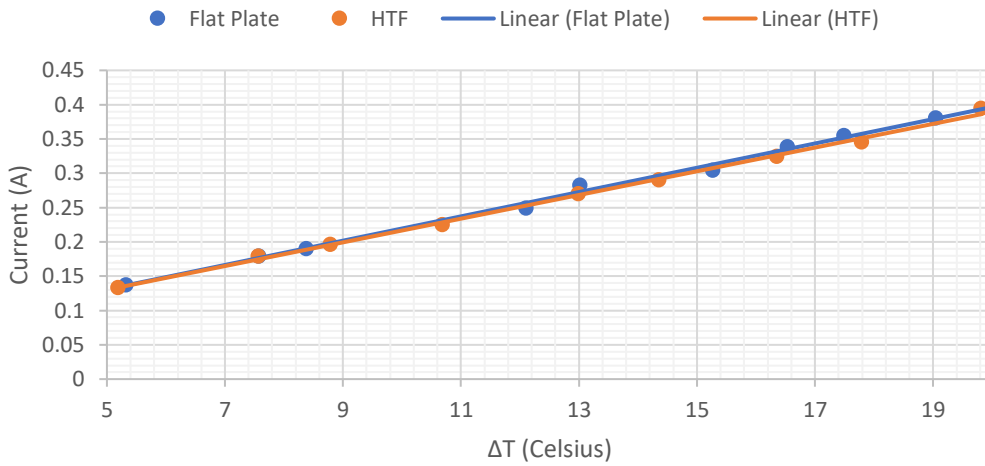
Figure 40: Comparison of the Current produced in the tests with a 6mm thick aluminium heat exchange plate with and without heat transfer fins

The trendline for current is almost identical throughout all cases of ΔT, with the flat plate tests being only slightly higher at larger ΔT.

Figure 41 compares the voltages produced from both tests.
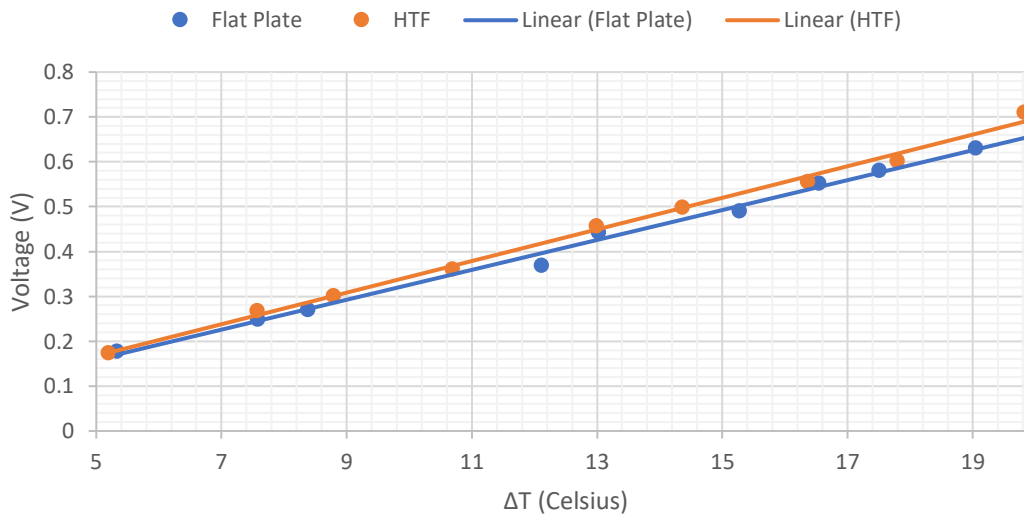
Figure 41: Comparison of the Voltage produced in the tests with a 6mm thick aluminium heat exchange plate with and without heat transfer fins.

The voltage produced is increasing at a faster rate as ΔT increase with the heat transfer fins in comparison to the flat plate test. It is clear to see that at higher ΔT values the voltage produced in the heat transfer fin tests is higher, although not by a considerable amount.

Figure 42 compares the power produced in both the tests.
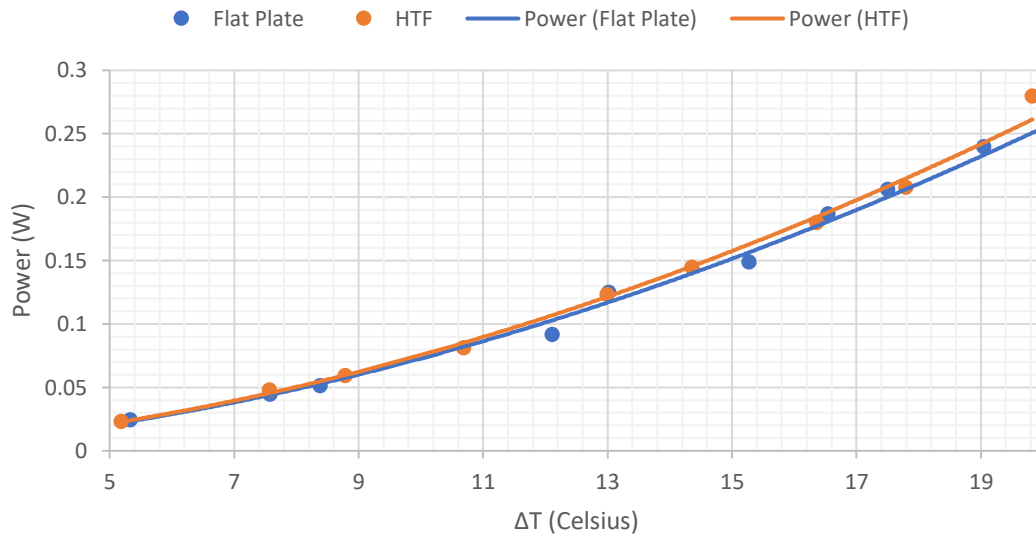
Figure 42: Comparison of the Power produced in the tests with a 6mm thick aluminium heat exchange plate with and without heat transfer fins.

The power produced in the heat transfer fin tests increases at a slightly faster rate as ΔT increases in comparison to the flat plate tests. It was expected that the heat transfer fins would increase the power produced, although for these tests it was expected to have a greater impact if the heat exchange surface had better contact with the TEGs in the heat transfer fin tests.

4.2 Ansys Simulations of Test Rig- Flat Plate

4.2.1 CFD Results

The method for obtaining the results from the CFD can be found in section 3.5.2. As stated in that section the aim of the CFD simulations was to obtain average temperatures of each Alumina plate on the TEGs which will be used as input parameters on the Thermal-Electric simulations. The temperature values are taken from the outer faces of the Alumina plates on the TEGs.

The CFD simulations were performed using Ansys FLUENT, the results for the system with an Aluminium flat plate heat exchanger 2mm thickness are shown in table 18.

Table 18: Alumina plate temperature results obtained from the CFD Simulations for the Aluminium heat exchange surface 2mm thickness, all results in ⁰C

ΔT (⁰C)		Front	Second	Third	Rear
19.51	Hot	21.732	22.063	22.855	23.958
	Cold	11.399	12.586	15.393	19.325
13.82	Hot	22.885	23.099	23.843	24.667
	Cold	15.703	16.47	19.108	22.063
7.31	Hot	24.152	24.282	24.722	24.965
	Cold	21.221	21.689	23.279	24.128

It is clear from table 18 that the plates at the front of the system which experience the water flow first experience colder temperatures based upon the simulations due to it experiencing the coldest flow of water. The water warms as it travels through the system. The rest of the CFD simulations for the other thickness/materials of heat exchange surface are shown in the tables 19, 20, & 21.

Table 19: Alumina plate temperature results obtained from the CFD Simulations for the Aluminium heat exchange surface 6mm thickness, all results in ⁰C

ΔT (⁰C)		Front	Second	Third	Rear
19.05	Hot	21.639	22.116	23.014	23.892
	Cold	11.658	13.352	16.549	19.683
13.02	Hot	22.487	22.712	23.308	23.905
	Cold	15.856	16.66	18.777	20.912
7.58	Hot	24.366	24.573	25.042	25.382
	Cold	20.935	21.665	23.343	24.564

Table 20: Alumina plate temperature results obtained from the CFD Simulations for the Steel heat exchange surface 2mm thickness, all results in ⁰C

ΔT (⁰C)		Front	Second	Third	Rear
19.53	Hot	21.732	22.067	22.784	23.814
	Cold	11.642	12.862	15.415	19.089
13.33	Hot	22.675	22.855	23.597	24.387
	Cold	16.009	16.54	19.302	22.132
6.58	Hot	23.818	23.948	24.241	24.371
	Cold	21.78	22.248	23.321	23.786

ΔT (°C)		Front	Second	Third	Rear
19.2	Hot	21.717	22.003	22.83	24.025
	Cold	12.172	13.192	16.127	20.377
13.11	Hot	22.793	22.985	23.53	24.092
	Cold	16.658	17.351	19.288	21.302
6.75	Hot	23.797	23.981	24.275	24.491
	Cold	21.62	22.281	23.336	24.109

The rest of these results all show the same pattern as table 18

Looking at figure 43 it is clear to see that the temperature of the boundary layer of the fluid warms as it approaches the outlet of the system which causes the alumina plates at the rear of the system to be warmer.
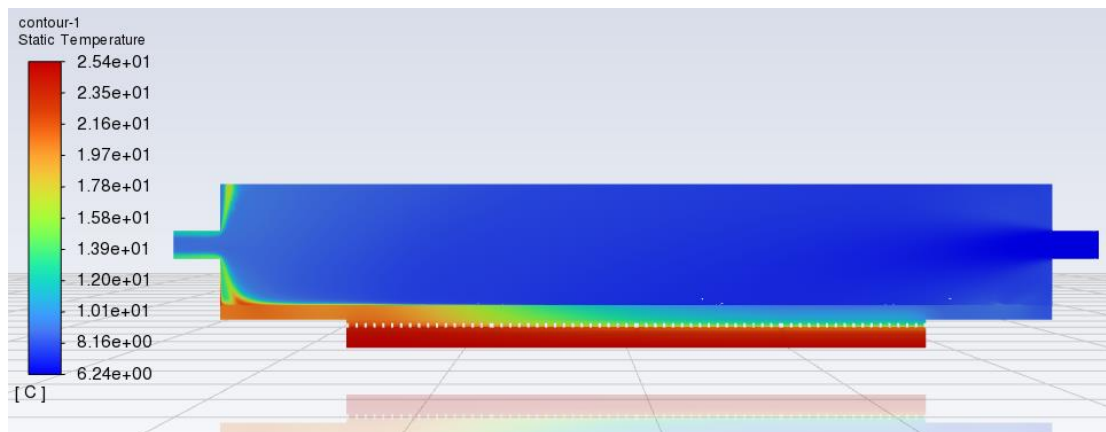
Figure 43: Steel 6mm Flat Plate high ΔT simulation, temperature contour plane

Figure 44 shows the velocity contours for the same system with a 6mm thick steel heat exchanger. The highest fluid velocities are seen at the inlet and outlet pipes of the system. The slower speeds near the surface of the heat exchange plate are likely to decrease the heat exchange rate which shows as the velocity of the fluid is lower near the

Figure 44: Steel 6mm Flat Plate high ΔT simulation, velocity contour plane

4.2.2 Simulation Results

For the simulation there were three results which were of interest to us: Temperature, Total Current Density, and Electric Voltage, but specifically the latter two.

When reading the voltage, it is key that we always probe the value from the same point for reproducible results. The location which is probed is at the end of the wire touching the resistor for the high voltage end of the circuit (positive end wire). Figure 45 shows the voltage contour of the simulations in Ansys Thermal Electric for the data from the test rig simulations with the Aluminium heat exchange surface (6mm thickness). This figure shows the location of the probe in which the voltage is being taken from the simulations.
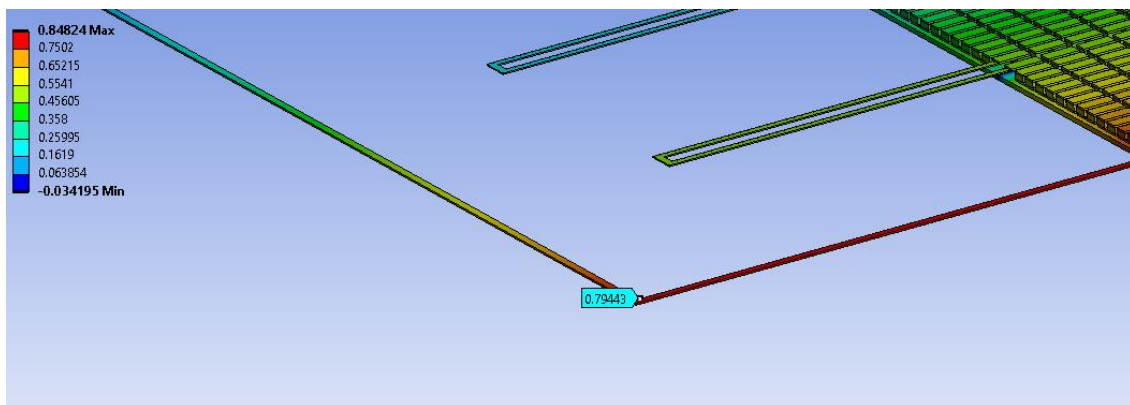
Figure 45: Thermal Electric Analysis of test rig with Aluminium Heat Exchange Plate (6mm), Voltage Probe Location

The voltage produced in this simulation as shown by figure 45 is 0.79443V.

The current values given as results within Ansys Thermal-Electric are given as total current densities with the units A/m^2. To find the value for current flowing through the resistor in Amperes the current density must be probed and then multiplied by the cross-sectional area of the resistor, which is as stated previously $5.625 \times 10^{-7} m^2$. Figure 46 shows the location of the total current density probe reading.
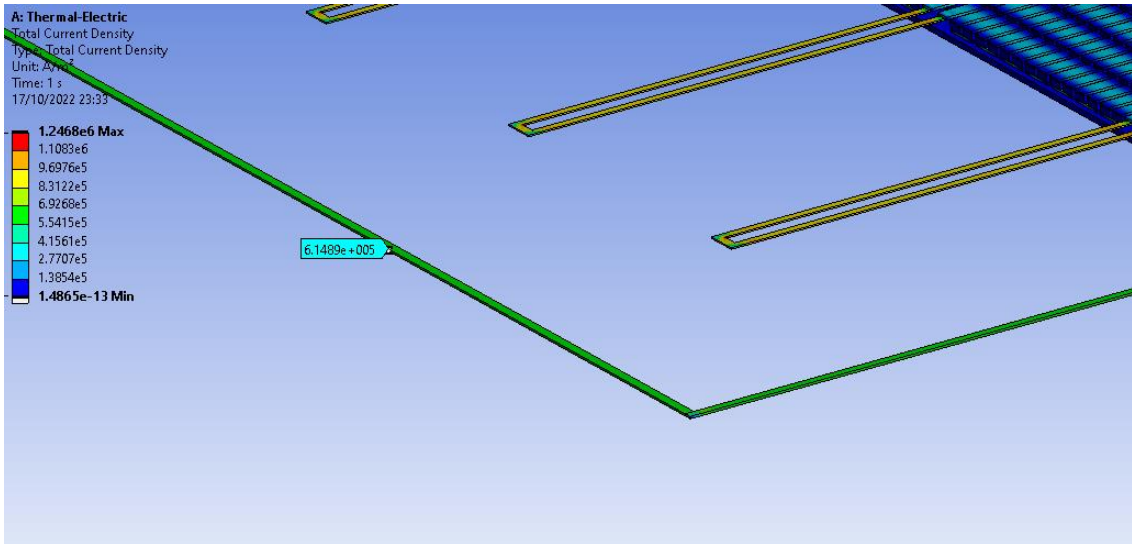
Figure 46: Thermal Electric Analysis of test rig with Aluminium Heat Exchange Plate (6mm), Current Probe Location
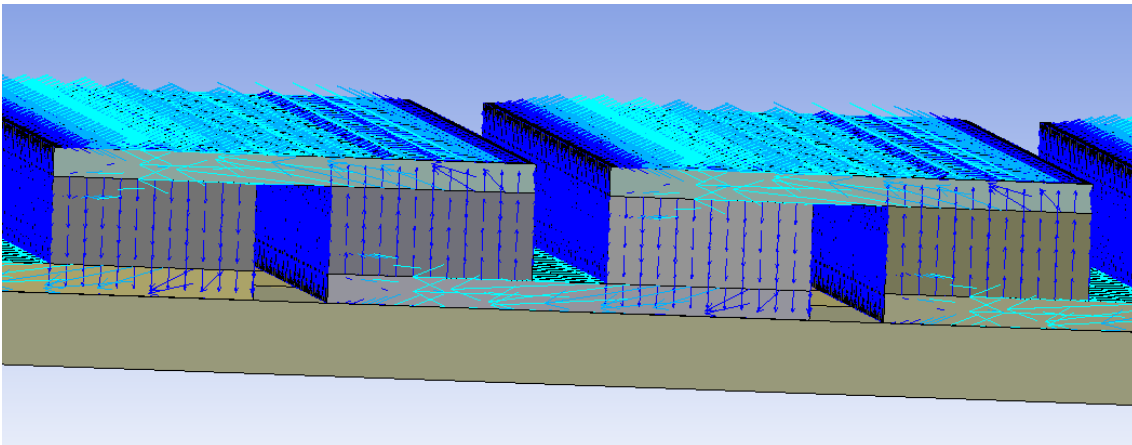
Figure 47: Thermal Electric Analysis of test rig Total Current Density Vectors of TEG pellets

As shown by the CFD results, for each of the heat exchange plates there were three temperature differences simulated, the highest, lowest, and middle from the physical tests. This was done so that it was possible to get trendlines to analyse for the power output of each of the flat plate scenarios. The first of these was the current produced in the simulations, figure 48 compares the current trendlines for all four heat exchange plates.

72
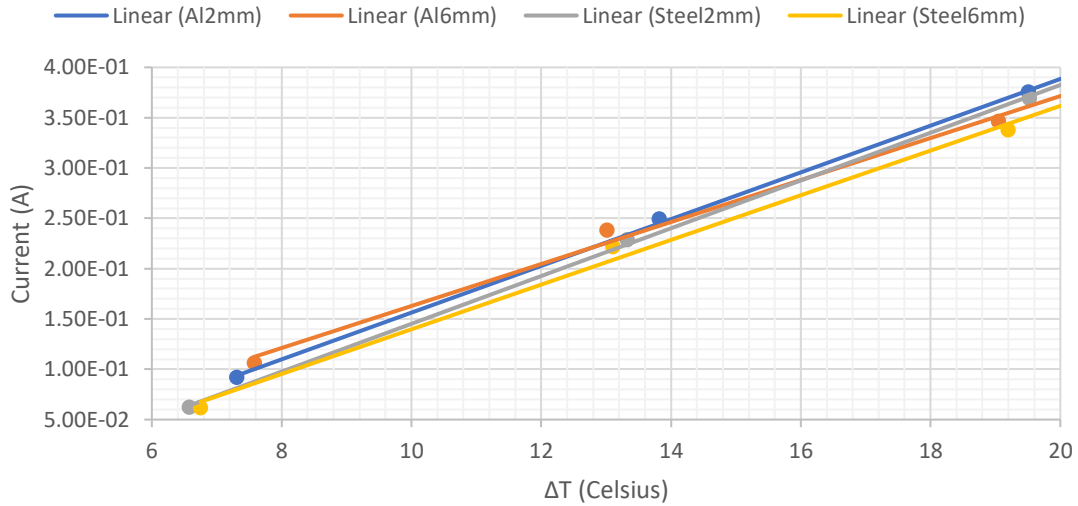
Figure 48: Current trendlines for Simulations of flat plate heat exchangers

All the simulations results for current produced fit a linear trendline with a positive correlation against an increase in ΔT as expected. Generally, there was not a large difference in the current production expected between the plates, generally as expected aluminium is expected to produce greater current as a heat exchange plate and the thinner plates should produce a larger current.

Figure 49 shows how the voltage was affected by the different heat exchange plates in the Ansys simulations.
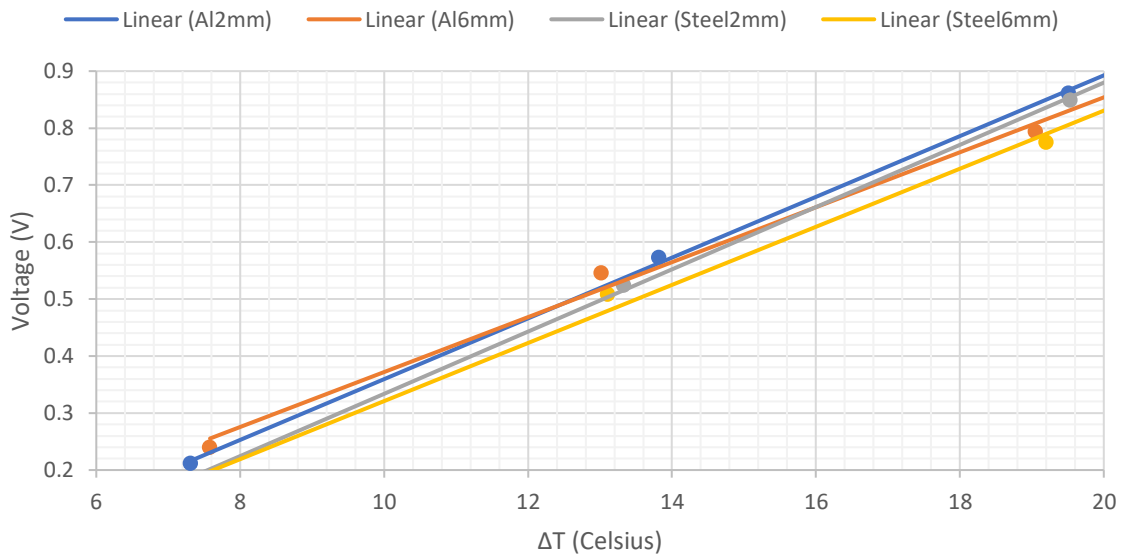
Figure 49: Voltage trendlines for Simulations of flat plate heat exchangers

As with the results for current output, all voltage trendlines show a linear, positive correlation as ΔT increases. The same trends are apparent with the voltage as aluminium and 2mm thick plates reign superior at producing higher voltages.

Figure 50 shows the calculated power trendlines for the flat plate simulations using the voltage and current output data.
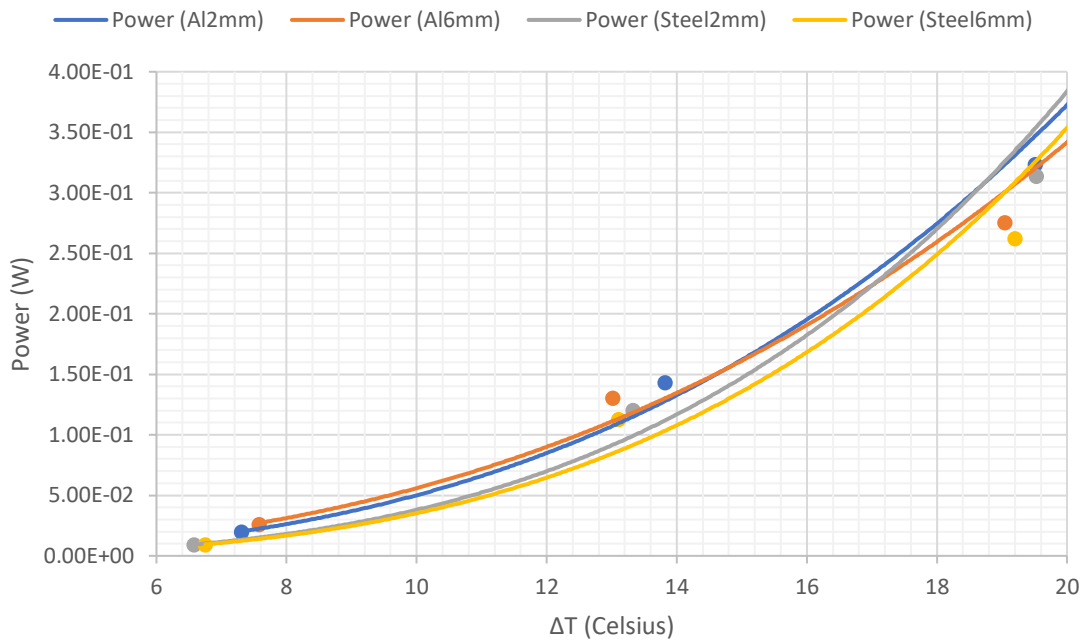
Figure 50: Power trendlines for Simulations of flat plate heat exchangers

This data shows that the thinner plates should produce a larger power than the thicker ones, and for the most part that aluminium heat exchangers should produce higher power outputs than steel. The gradients of the curves are slightly skewed against each other which may be due to different ΔT values being tested to match the physical data.

4.3 Ansys Simulations of Test Rig- Heat Transfer Fins

4.3.1 CFD Results

The methodology for calculating the CFD results was outlined in section 3.6.3. Like the flat plate CFD simulations, the main results of interest were the average temperatures on the surface of the ceramic plates of the TEG modules. This meant 8 temperatures were obtained per simulation. The maximum, minimum, and median ΔT tested in the physical tests were simulated. The results obtained using Ansys FLUENT are shown in table 22

Table 22: Alumina plate temperature results obtained from the CFD Simulations for the Aluminium heat exchange surface 6mm thickness with Heat Transfer Fins, all results in ºC

ΔT (ºC)		Front	Second	Third	Rear
19.97	Hot	21.671	21.942	21.992	21.651
	Cold	11.478	12.443	12.625	11.389
11.9	Hot	22.372	22.586	22.593	22.331
	Cold	15.93	16.688	16.711	15.763
7.57	Hot	24.321	24.478	24.501	24.32
	Cold	21.317	21.875	21.955	21.31

The values in table 22 show that the temperatures are more distributed and there is not a steep increase like there is with the flat plates. The fins allow better heat transfer across the whole plate rather than just the part closest to the inlet. This is supported by figure 51 which shows the temperature contours on the heat transfer fins at the largest ΔT tested.
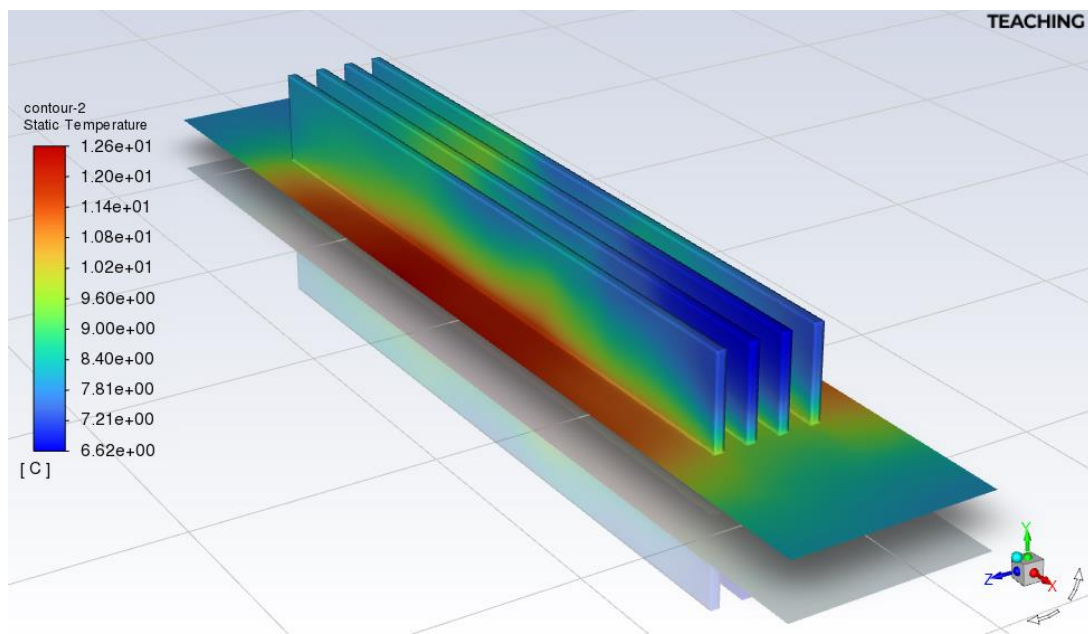
Figure 51: Heat Transfer Fin Temperature contours for maximum ΔT simulated

4.3.2 Simulation Results

The three temperature differences were simulated to allow the development of trendlines for voltage, current, and power to compare with the flat plate simulations. As stated previously, the heat transfer fins were welded directly onto the 6mm thick aluminium plate, therefore all these results for the heat transfer fins will be compared with the simulations for the 6mm aluminium flat plate. Figure 52 shows the trendlines for the current produced in the simulations with and without the heat transfer fins.
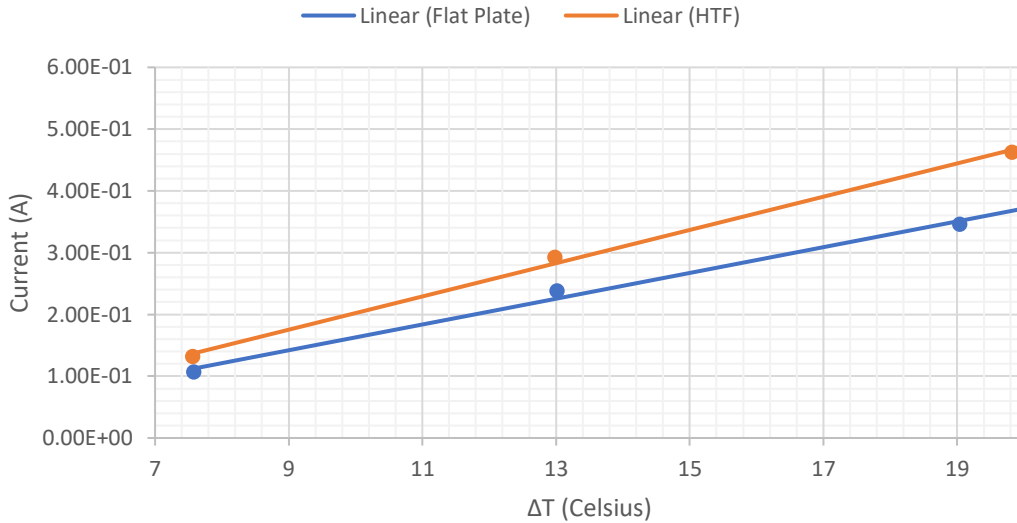
Figure 52: Current produced from Ansys simulations for the test rig with 6mm aluminium heat exchange plate, comparing with and without heat transfer fins

It is clear to see from figure 52 that it should be expected the addition of heat transfer fins would increase the current produced and the rate current increases as ΔT increases.

Figure 53 compares the voltage produced between the two models.
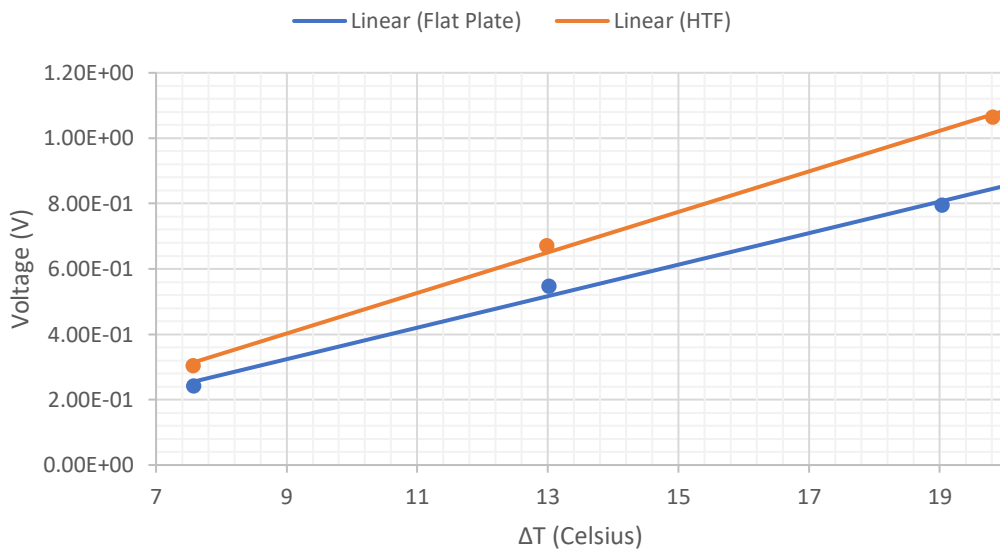
Figure 53: Voltage produced from Ansys simulations for the test rig with 6mm aluminium heat exchange plate, comparing with and without heat transfer fins

The addition of heat transfer fins according to the simulations should increase the voltage produced and increase the rate at which the output voltage increases as ΔT increases. It appears from the trendlines that at $\Delta T=20^{\circ}C$ the voltage produced form the heat transfer fin model should be approximately 0.24V higher than the flat plate.

Figure 54 shows how the addition of heat transfer fins affects the power produced in the simulations.
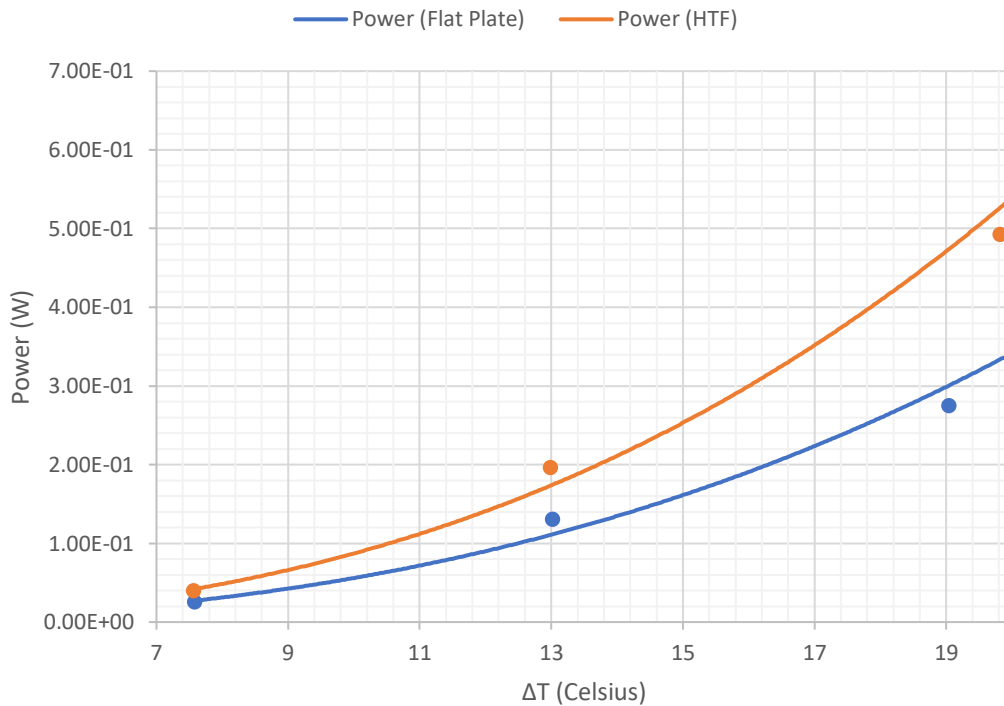
Figure 54: Power produced from Ansys simulations for the test rig with 6mm aluminium heat exchange plate, comparing with and without heat transfer fins

The addition of heat transfer fins would expect an increase in power produced across all ΔT values tested, according to the Ansys simulations. The difference in the amount of power produced between the simulations increases with an increase in ΔT, with at $\Delta T = 20°C$ the power from the heat transfer fin simulations being approximately 0.54W, whereas the simulations without expect about 0.34W. These simulations expect that the addition of heat transfer fins increase power produced by 58% for $\Delta T = 20°C$.

4.4 Physical Test & Simulation Comparison

4.4.1 Aluminium 2mm Flat Plate

As stated previously in this thesis, the reason behind completing both physical tests and simulations was to compare both sets of results to understand how simulations in Ansys reflect results obtained in real life. The three results compared are current, voltage, and power produced by the TEGs. The first scenario tested was the flat plate heat exchanger of 2mm thickness made of aluminium. Figure 55 shows a comparison of the current produced between the physical tests and the simulations.

Figure 55: Comparison of Current produced by TEGs in physical tests and simulations, heat exchange surface aluminium 2mm thickness (Flat)

It is clear to see that the current from the physical tests is greater than the simulations throughout, however the gradient of the linear trendlines show that the current from the simulations is increasing at a faster rate as ΔT increases.

Figure 56 shows a comparison of the voltage produced in the physical tests and the simulations.

Figure 56: Comparison of Voltage produced by TEGs in physical tests and simulations, heat exchange surface aluminium 2mm thickness (Flat)

The voltage from the simulations is higher for all ΔT values greater that 7 in the simulations and appears to be increasing at a steeper gradient.

Figure 57 compares the power produced by the physical tests and the simulations.

78

Figure 57: Comparison of Power produced by TEGs in physical tests and simulations, heat exchange surface aluminium 2mm thickness (Flat)

At the lower ΔT the power produced is larger in the physical tests than the simulations however the simulation power curve is increasing at a steeper gradient and at approximately $\Delta T=13°C$ the simulation power overtakes that of the physical tests. At the largest ΔT tested (19.51°C), the difference between the power values recorded is 0.075W. The physical test value at this point is producing 77% power of the simulations.

4.4.2 Aluminium 6mm Flat Plate

For this section the 6mm thick aluminium heat exchanger tests, both physical and simulation, are compared. Figure 58 compares the current produced in both forms of testing.

The current produced in the physical tests is greater than the simulations for all the physical tests in comparison to the simulations. However, the current in the simulations is increasing at a faster gradient as ΔT increases.

Figure 59 compares the voltage produced from the physical tests and simulations.

Figure 59: Comparison of Voltage produced by TEGs in physical tests and simulations, heat exchange surface aluminium 6mm thickness (Flat)

The voltage obtained from the simulations is higher than that of the physical tests across nearly all the temperature differences tested. The gradient of the simulation's voltages trendline obtained appears to be slightly steeper than the physical tests.

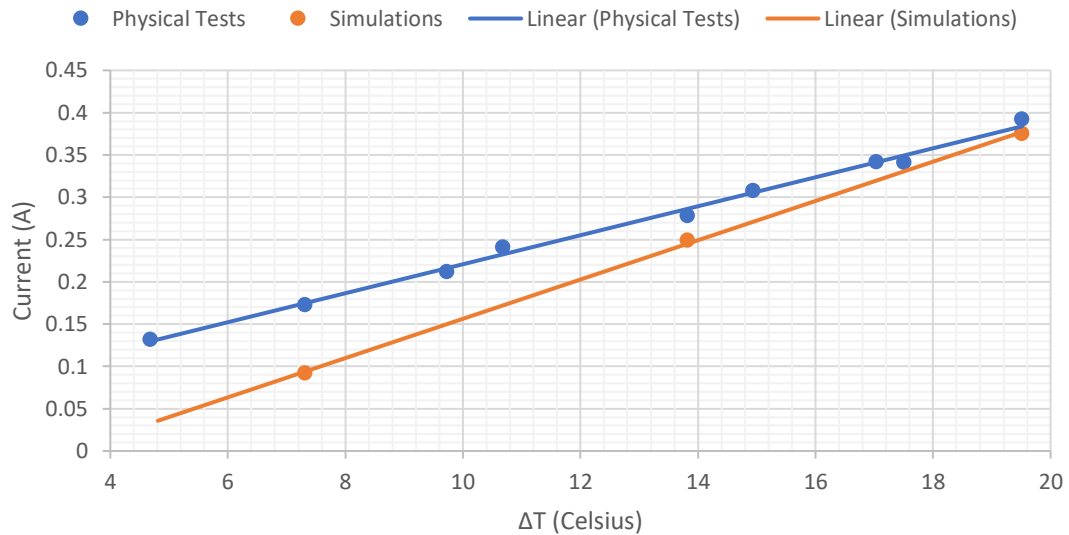Figure 60 shows a comparison of the power produced by both methods of testing.

Figure 60: Comparison of Power produced by TEGs in physical tests and simulations, heat exchange surface aluminium 6mm thickness (Flat)

The power produced at the lower ΔT values tested is larger in the physical tests, however the simulation curve is increasing at a faster rate and overtakes the physical test trendline at approximately ΔT=14ºC. At the largest ΔT tested the difference between the power produced in both tests is 0.036W. The physical tests are producing 87% of the power generated from simulations at this point.

4.4.3 Steel 2mm Flat Plate

The tests and simulations compared in this section are both using a steel flat plate heat exchanger with a thickness of 2mm. Figure 61 compares the current produced between the physical tests and the simulations.
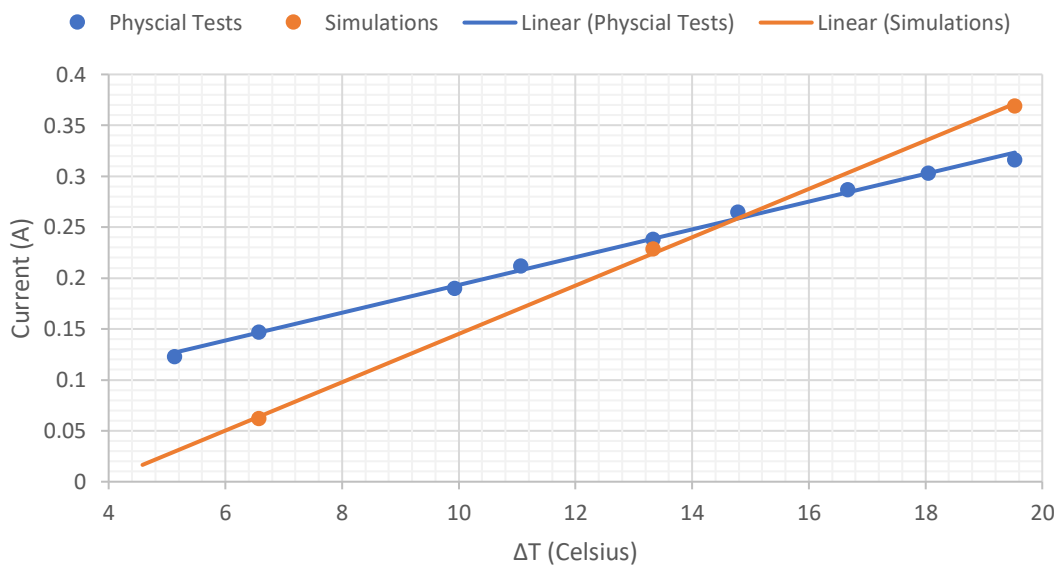
Initially at the lowest ΔT tested, the physical tests produce a larger current than the simulations. However, the results show that at around ΔT=15⁰C the trendline of the simulation surpasses the physical tests and any temperature difference greater than this the simulations produce a higher current than the physical tests.

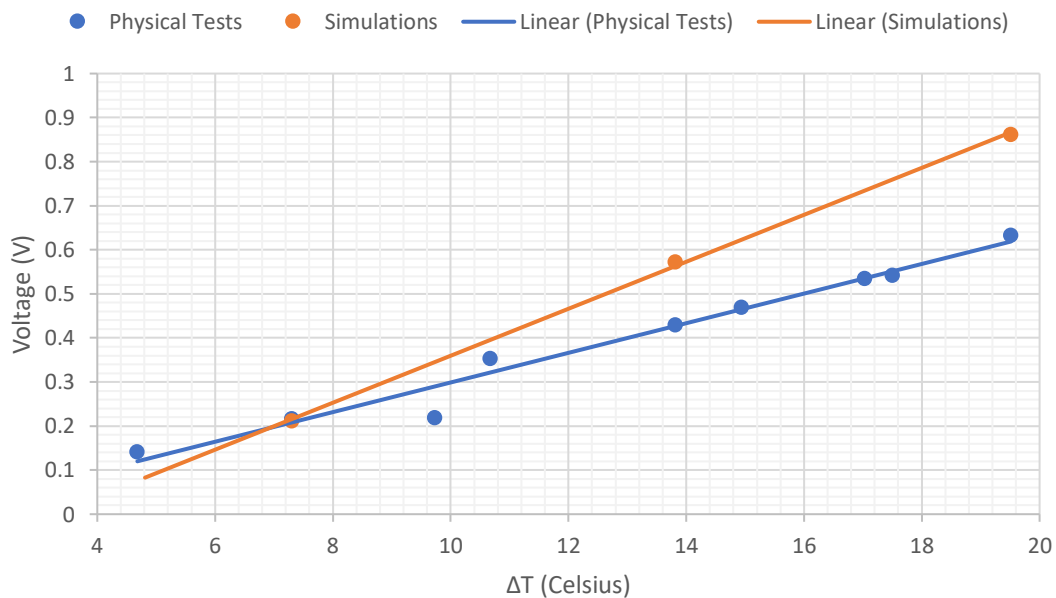Figure 62 compares the voltage produced in the two methods of testing.
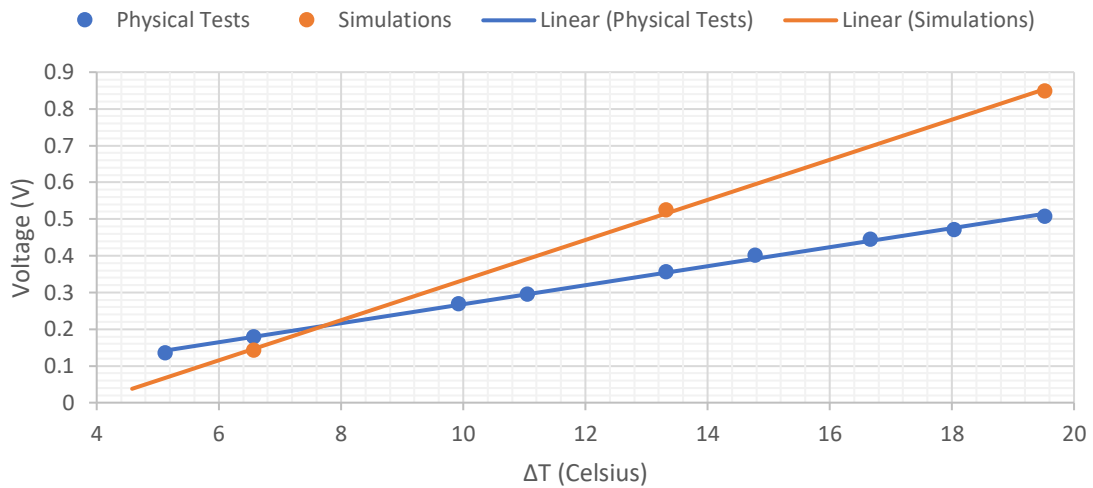
Figure 62: Comparison of Voltage produced by TEGs in physical tests and simulations, heat exchange surface steel 2mm thickness (Flat)

The voltage produced in the simulations is higher than the physical tests for all temperature differences tested above 8⁰C. The voltage trendline in the simulations appears to be increasing at a faster rate than the physical tests as ΔT increases.

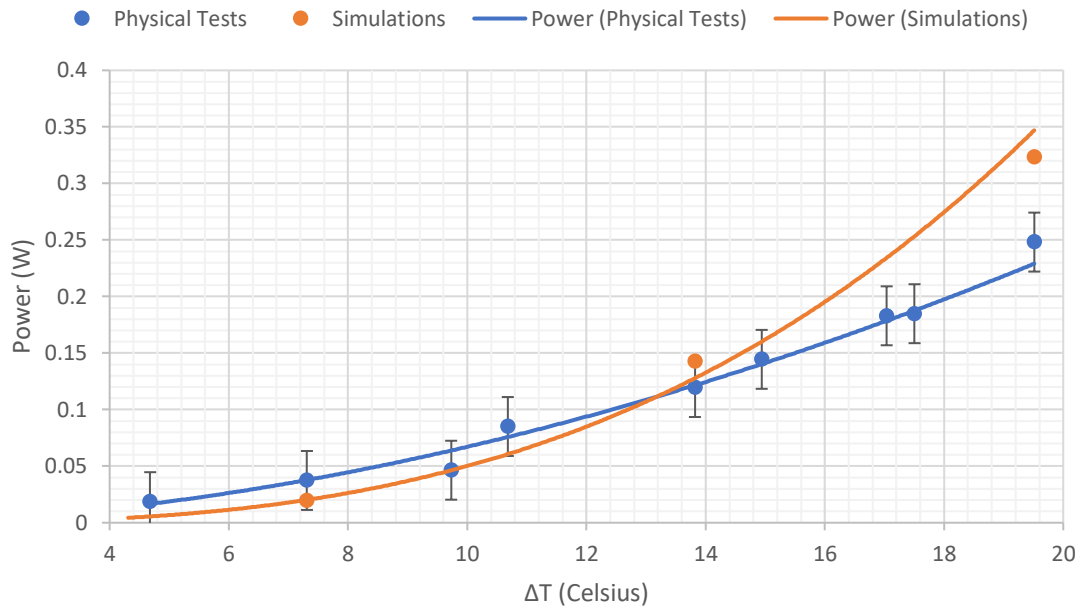Figure 63 compares the power output of the simulations and physical tests.
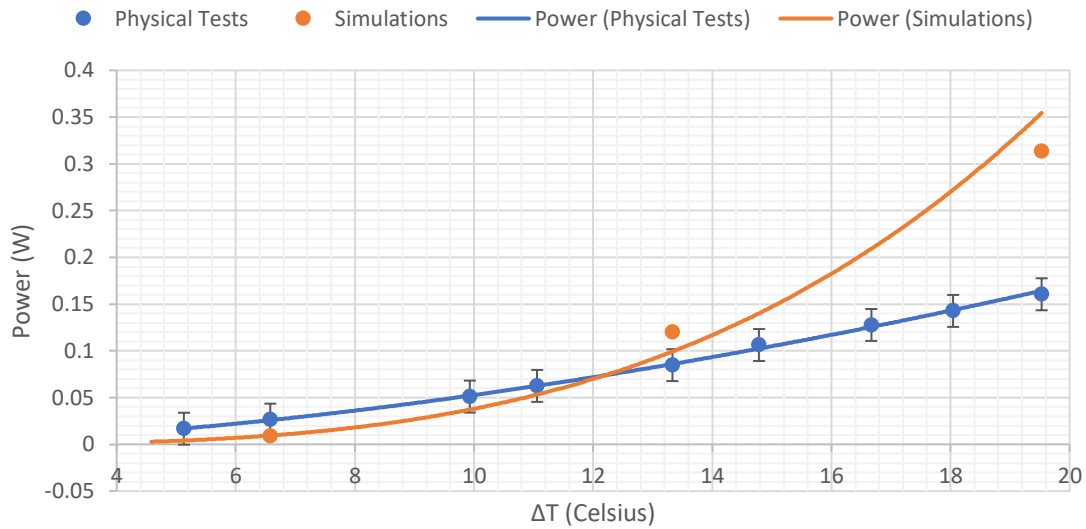
Figure 63: Comparison of Power produced by TEGs in physical tests and simulations, heat exchange surface steel 2mm thickness (Flat)

At the lowest ΔT value tested the power produced is slightly higher in the physical tests. When we look at the largest ΔT tested this difference is drastically bigger as the simulation trendline increases in gradient much faster than the physical tests. The difference in power at the largest ΔT is 0.153W. The physical tests produced just 51% of the power compared to the simulations at this point.

4.4.4 Steel 6mm Flat Plate

The comparisons in this section are between the physical tests and simulations of the flat plate system using a 6mm thick steel heat exchanger. Figure 64 shows a comparison of the results for the current produced between the two methods.
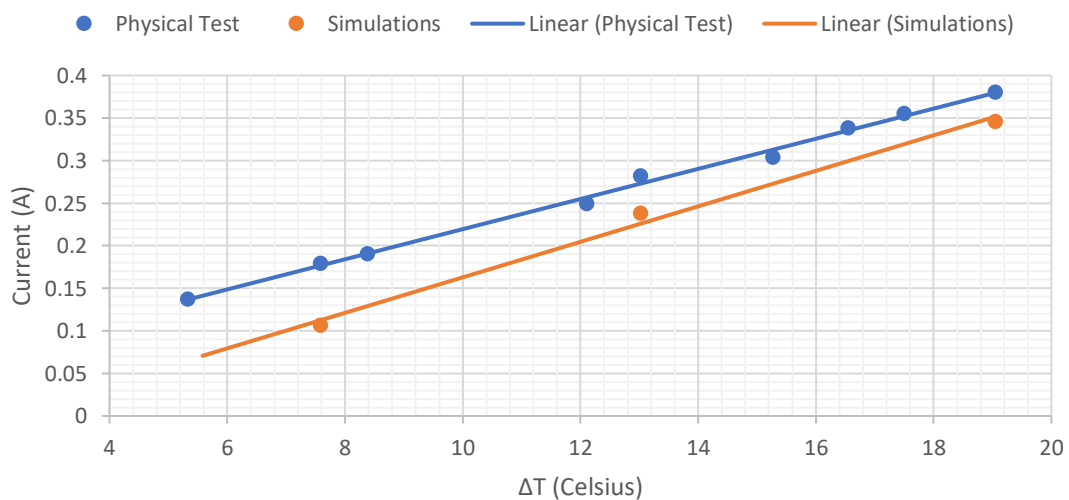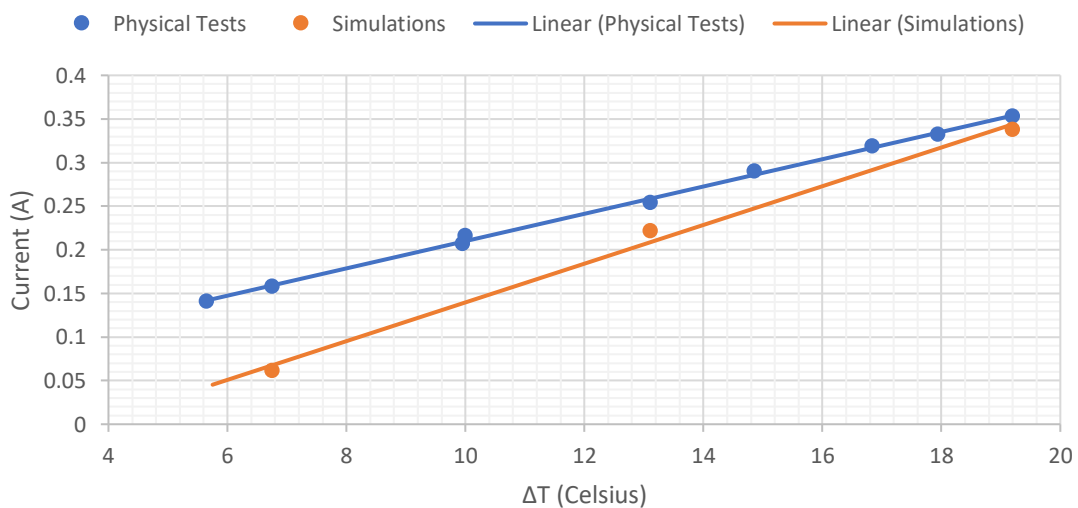

Figure 64: Comparison of Current produced by TEGs in physical tests and simulations, heat exchange surface steel 6mm thickness (Flat)

The current produced in the physical tests is higher for every ΔT tested. It can be assumed that for any value after what was tested based upon the gradients, the simulation would be higher.

Figure 65 compares the voltage produced between the two methods.
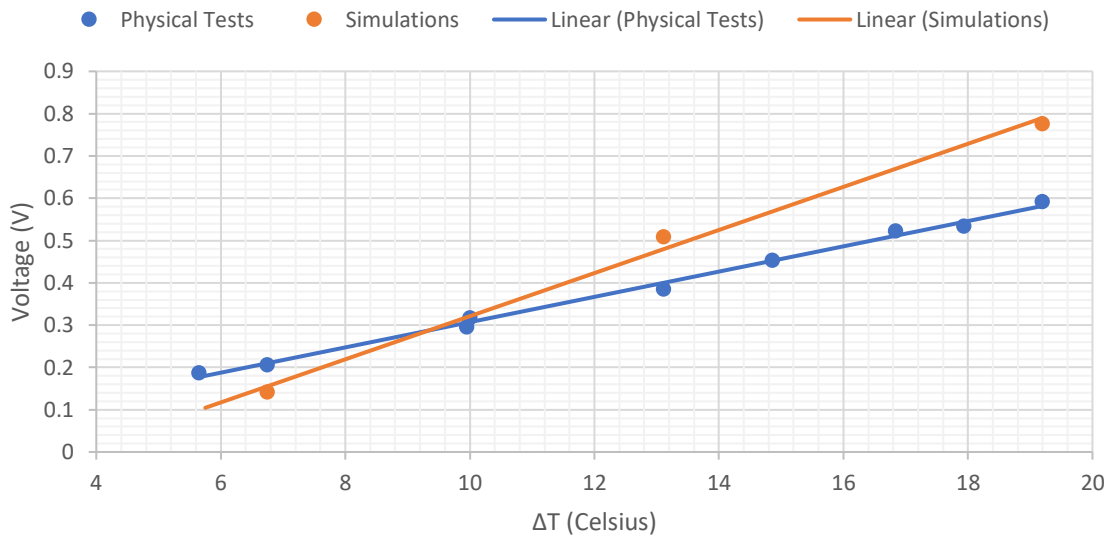
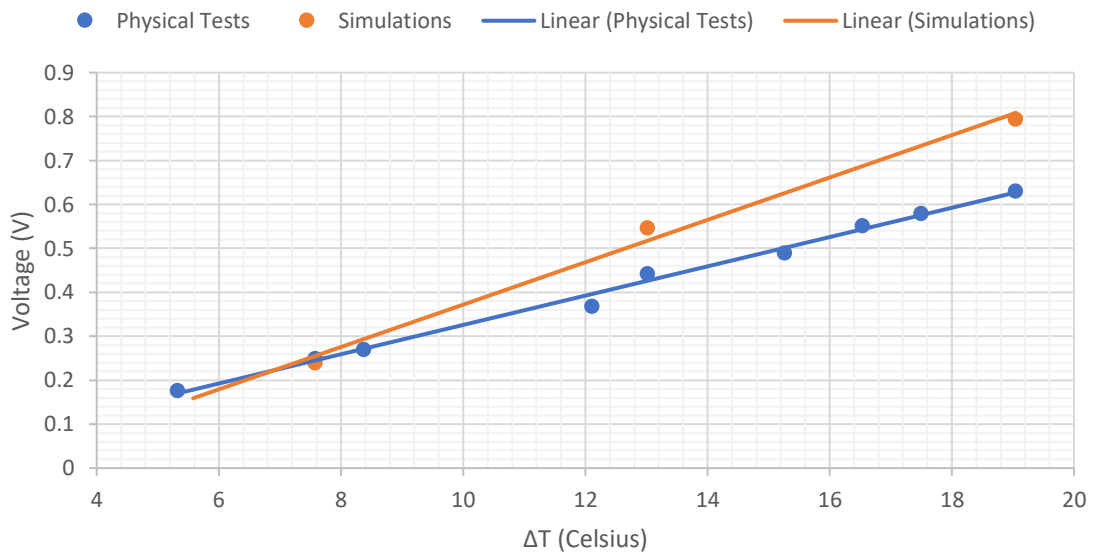*Figure 65: Comparison of Voltage produced by TEGs in physical tests and simulations, heat exchange surface steel 6mm thickness (Flat)*

The voltage from the simulations is higher for every ΔT > 10ºC tested in comparison to the physical tests. The gradient of the linear trendline for the simulations is steeper than the physical tests.

Figure 66 compares the power produced by both methods of testing.
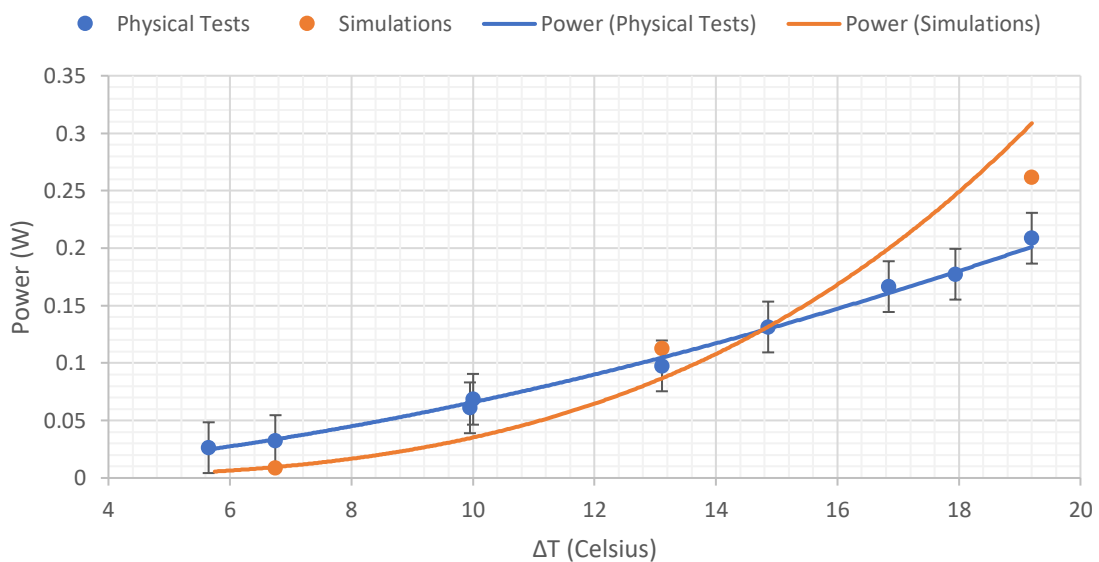
Figure 66: Comparison of Power produced by TEGs in physical tests and simulations, heat exchange surface steel 6mm thickness (Flat)

The power for the physical tests is initially higher however the simulation trendline overtakes and for any value after ΔT=15 the simulation power is higher. The difference in power produced at the largest temperature difference is 0.053W. The physical test value at this point is producing 80% of the power expected from the simulations.

4.4.5 Aluminium 6mm Heat Transfer Fins

The comparisons in this section are between the physical tests and simulations for the test rig with the 6mm aluminium heat exchange surface plus heat transfer fins. Figure 67 compares the current produced by both the physical tests and the simulations.
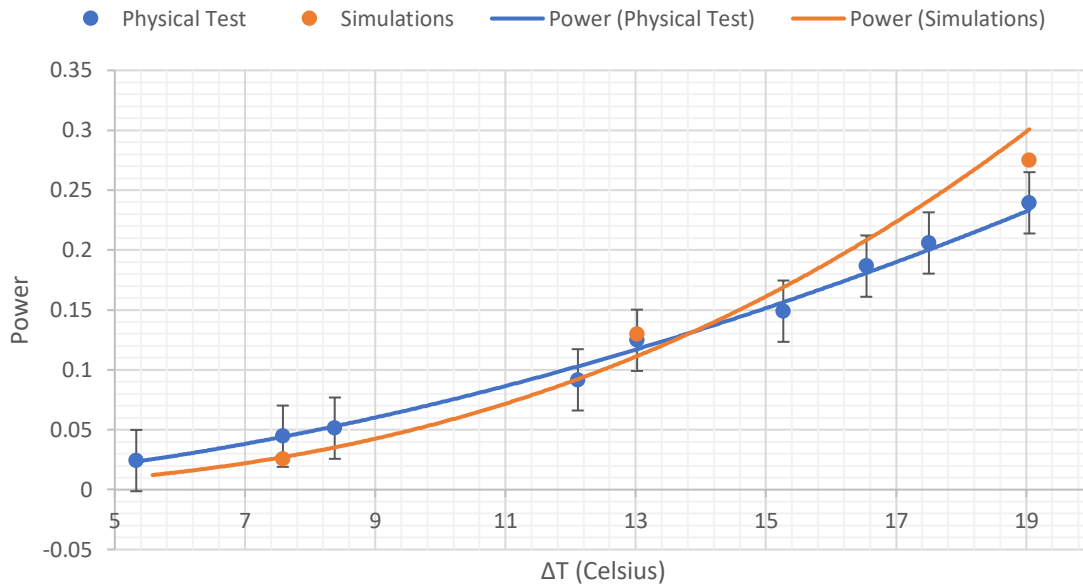

Figure 67: Comparison of Current produced by TEGs in physical tests and simulations, heat exchange surface aluminium 6mm thickness with heat transfer fins

The current produced in the simulations is higher for every value of ΔT greater than 12⁰C in comparison with the physical tests.

Figure 68 compares the voltages produced from both methods of testing.
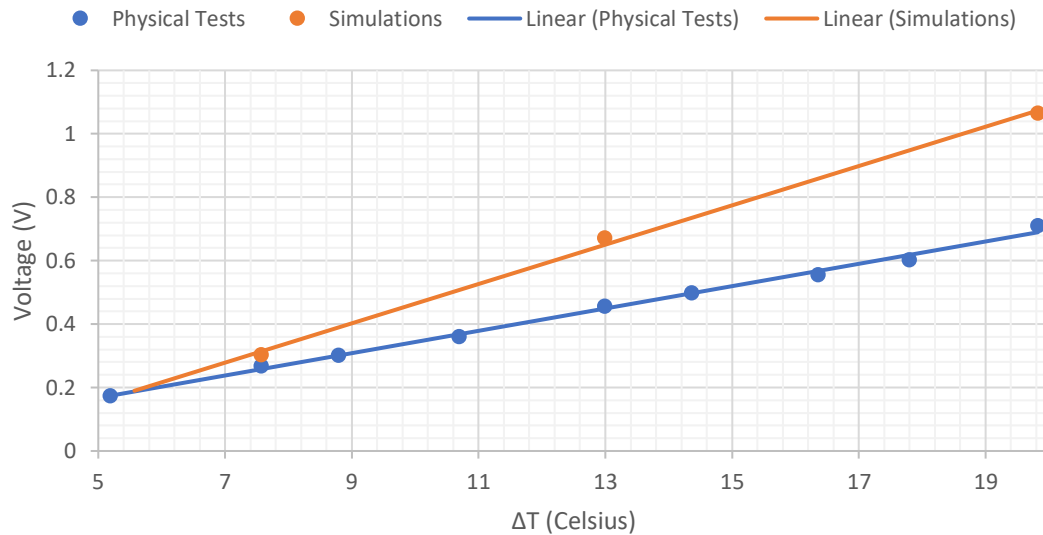
Figure 68: Comparison of Voltage produced by TEGs in physical tests and simulations, heat exchange surface aluminium 6mm thickness with heat transfer fins

The voltage produced in the simulations is higher than the physical tests for all values of ΔT tested.

Figure 69 compares the power produced by both methods of testing for a range of temperature differences.
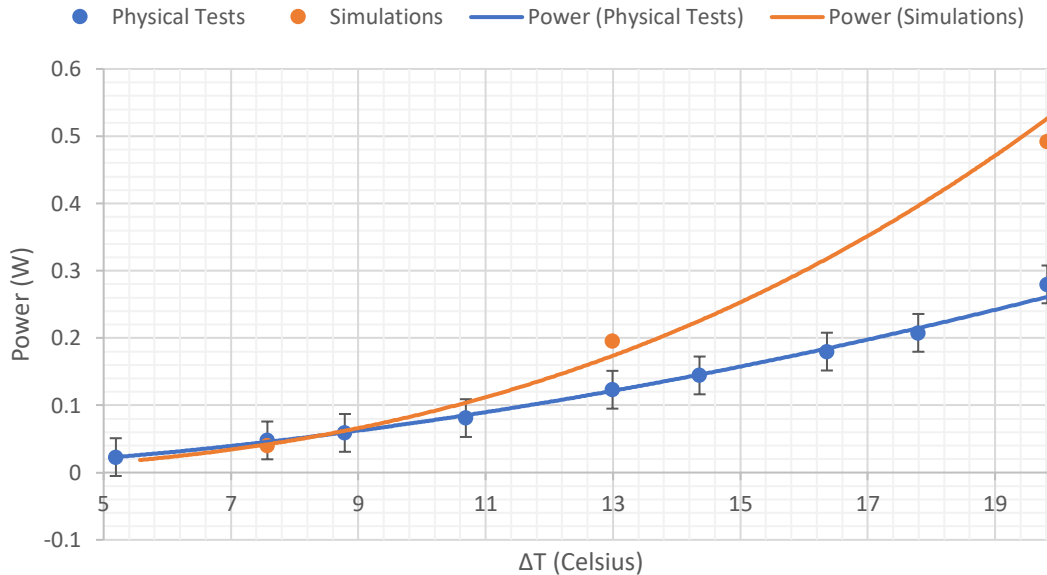
Figure 69: Comparison of Power produced by TEGs in physical tests and simulations, heat exchange surface aluminium 6mm thickness with heat transfer fins

The power produced from the simulations is similar at lower values of ΔT however as the temperature difference increases, the power produced in the simulations increases much faster than the physical tests. At $\Delta T=19.82$ (the largest tested), the difference in power

produced between both methods is 0.212W. The physical tests at this point are only producing approximately 57% of the power expected from the simulations.

4.4.6 Summary

The flat plate tests using the Aluminium 2mm, 6mm and the steel 6mm heat exchange plates all produced relatively similar results the simulations (77%, 87%, & 80% of the simulation power at maximum ΔT). The steel 2mm plate however produced only 51% of the power from the simulations at the highest ΔT, this could be due to the rusting which had begun on the surface of the steel causing a thermal resistance.

The heat transfer fins physical tests produced 57% of the power produced in the simulations in the largest ΔT tested. This underperformance was likely due to the buckling caused to the plate in manufacturing which will have reduced the thermal contact between the TEGs and the heat exchange plate.

4.5 Scaled up Ansys Simulations

4.5.1 CFD Results

The methodology for obtaining the temperature parameters to input in the Ansys thermal electric model was outline in section 3.6.4. Tables 23, 24, 25, & 25 shows the temperature parameters obtained through the Ansys Fluent simulations for the different scaled up models. For all the CFD simulations performed in this section the residuals converged to the absolute criteria.

Table 23: Alumina plate temperature results obtained from the CFD Simulations for scaled up longitudinal layout with no fins, all results in ⁰C

ΔT (⁰C)		Front	Second	Third	Rear
15	Hot	18.84	18.874	18.878	18.834
	Cold	10.396	10.851	10.885	10.502
10	Hot	19.227	19.249	19.252	19.224
	Cold	13.597	13.901	13.923	13.668
5	Hot	19.613	19.625	19.626	19.612
	Cold	16.613	16.951	16.962	16.834

Table 24: Alumina plate temperature results obtained from the CFD Simulations for scaled up lateral layout with no fins, all results in ⁰C

ΔT (⁰C)		Right	Second	Third	Left
15	Hot	18.864	18.96	18.96	18.886
	Cold	10.72	11.536	11.535	10.773
10	Hot	19.245	19.307	19.31	19.26
	Cold	13.829	14.359	14.381	13.871
5	Hot	19.626	19.649	19.658	19.638
	Cold	16.94	17.151	17.21	16.995

Table 25: Alumina plate temperature results obtained from the CFD Simulations for scaled up longitudinal layout with heat transfer fins, all results in ⁰C

ΔT (⁰C)		Front	Second	Third	Rear
15	Hot	18.203	18.305	18.306	18.209
	Cold	10.665	11.213	11.221	10.705
10	Hot	18.802	18.87	18.871	18.806
	Cold	13.777	14.142	14.147	13.803
5	Hot	19.401	19.435	19.435	19.403
	Cold	16.888	17.071	17.074	16.902

Table 26: Alumina plate temperature results obtained from the CFD Simulations for scaled up lateral layout with heat transfer fins, all results in ⁰C

ΔT (⁰C)		Right	Second	Third	Left
15	Hot	18.954	19.033	19.032	18.932
	Cold	11.345	12.135	12.122	11.271
10	Hot	19.303	19.355	19.354	19.288
	Cold	14.23	14.756	14.748	14.181
5	Hot	19.651	19.678	19.677	19.644
	Cold	17.115	17.378	17.374	17.091

These tables show numerically the data which is needed to be inputted as parameters into the thermal electric simulations, however looking at the tables does not show a picture of how the whole system performed, just the TEGs plates. Figure 70 shows a plane of the temperature contours for the longitudinal layout with no fins.
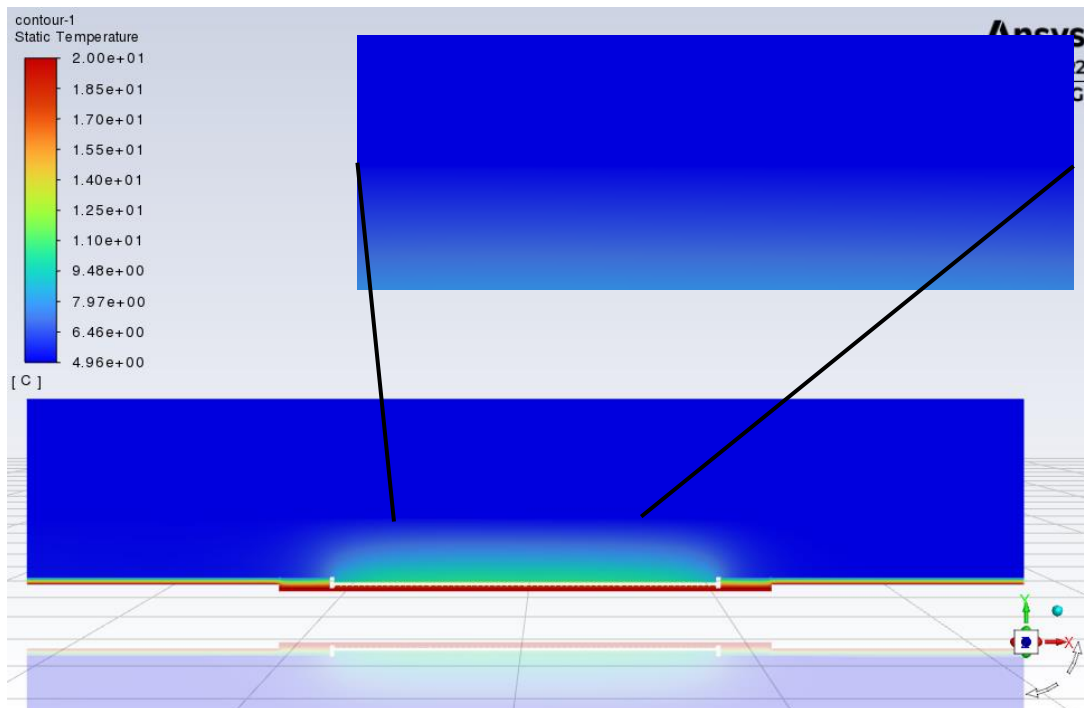
Figure 70: Temperature Contours for the longitudinal layout with no fins. The enlarged section shows the boundary between the sub wall and fluid with the black lines highlighting this surface location.

The black line in the figure connects the sub wall surface in contact with the water in both the figure and it enlarged section. It is clear to see that there is not a drastic temperature drop between the submarine wall and the fluid, this is likely due to the high fluid speed and thick submarine wall. The expanded polystyrene (insulation) clearly works successfully as base upon the temperatures in the sub wall it is clear to see that the heat from the inside is mainly travelling through the TEGs as this area above them of the wall is warmer.

4.5.2 Simulation Results- Comparison of Layouts

Four layouts were simulated for comparison. The TEGs were tested laid both longitudinally and laterally, with and without fins. All results in this section, like the previous tests, all use a load with a resistance of 2.3Ω. Figure 71 compares the current produced by the TEGs in each layout.
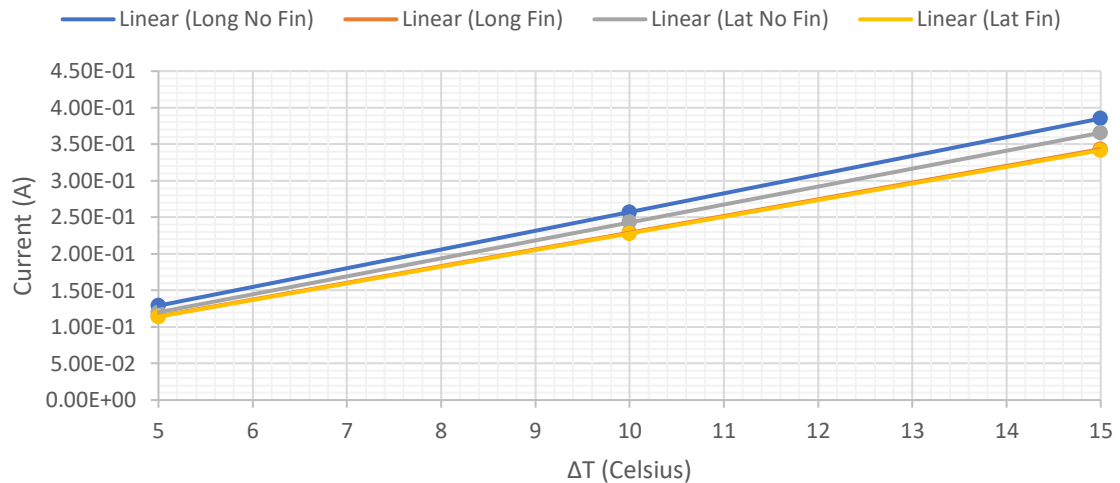
Figure 71: Comparison of Current output from the scaled-up models Ansys results

From the simulations, the layouts with the heat transfer fins produce an almost identical current trend which is the lowest recorded. The highest current produced was by the TEGs with no heat transfer fins in the longitudinal layout.

Figure 72 compares the voltage outputs produced by the four models.
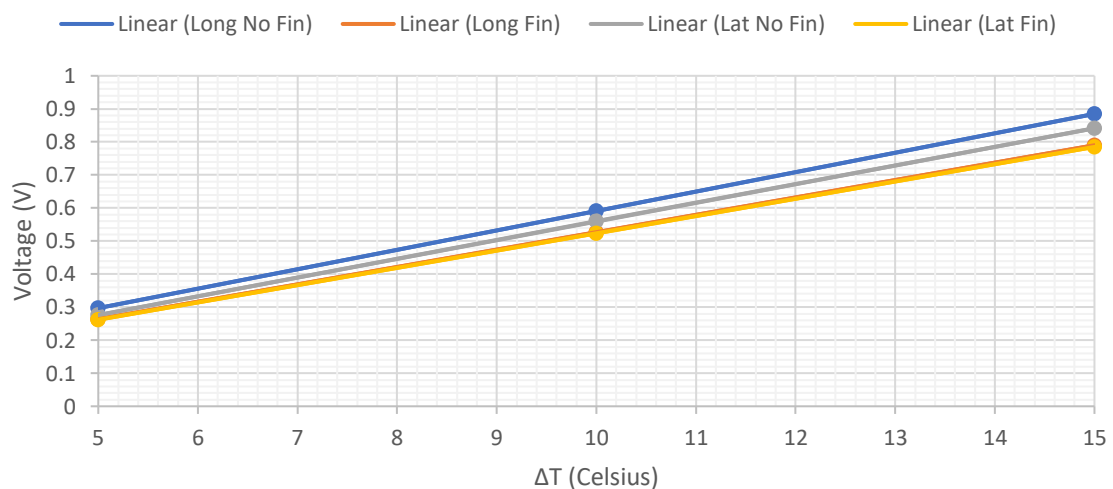
Figure 72: Comparison of Voltage output from the scaled-up models Ansys results

The trendlines for the voltage show an almost identical pattern as the current outputs, the models with fins produce the lowest voltages whilst the longitudinal model without fins produces the highest voltage.

Figure 73 compares the power produced from all four of the models simulation results.
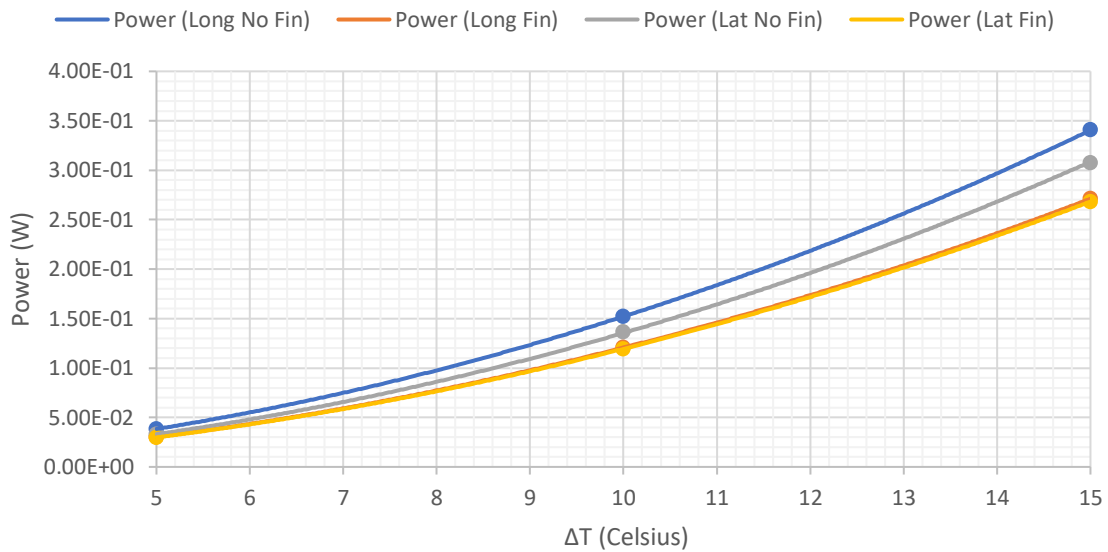
Figure 73: Comparison of Power output from the scaled-up models Ansys results

It is clear to see that the power produced in the longitudinal layout without fins is superior across all values of ΔT simulated. The lateral layout without fins followed closely behind and the two models with fins interestingly produced the least power.

4.5.4 Chosen System & Optimisation

As is shown in the previous section, the superior layout was the TEGs in a longitudinal formation with no heat transfer fins. This system produced a greater power output than the others across all ΔT simulated, making it a clear winner.

All the simulations in the previous section were carried out with a load resistance of 2.3Ω as this was approximately the expected internal load resistance of the four modules. Now that it is clear which layout performs best, it is possible to see what load resistance produces the maximum power point at each temperature and what the maximum power point is. To do this, the thermal electric simulations for the longitudinal layout parameters are done whilst adjusting the load resistance to analyse its effect on the power output. Figure 74 shows the results for all three temperature differences simulated with load resistance values ranging between 1.1Ω - 2.3Ω.
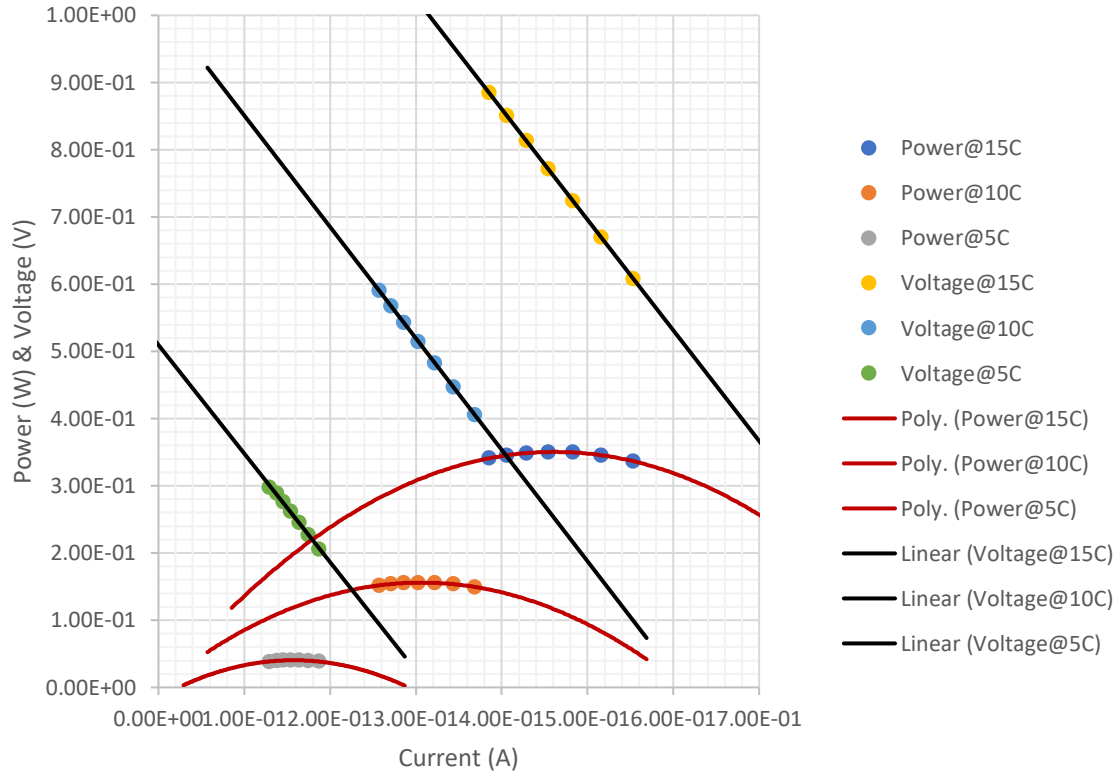
Figure 74: MPP for the longitudinal scale up model with no fins. Temperature differences of 5,10, & 15ºC

The maximum power point for all three ΔT values simulated all occurred with a load resistance of 1.7Ω. Table 27 shows all the output values when the load resistance is set to 1.7Ω.

Table 27: Output result from thermal electric simulation of longitudinal scaled-up model with load resistance set at 1.7Ω

ΔT (ºC)	Current (A)	Voltage (V)	Power (W)
5	0.154	0.262	0.0403
10	0.303	0.514	0.156
15	0.454	0.771	0.35

Looking at this table, when the ΔT value triples from 5ºC to 15ºC, the Power output increases by a multiplication factor of 8.7. This shows just how important it is to try to increase the temperature difference across the TEGs as much as possible. The power output compared with the temperature differences for this table can be seen in figure 75.

92
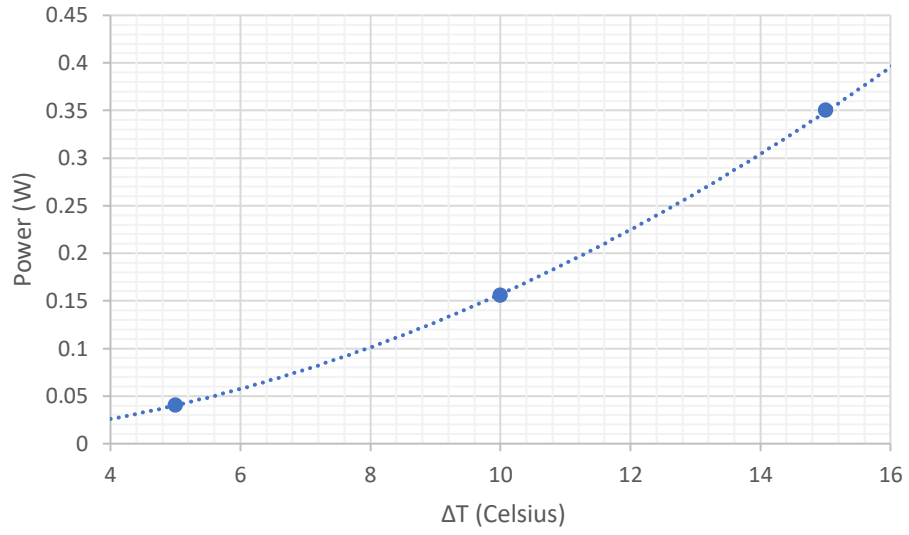
Figure 75: Power Output for the scaled up longitudinal model with no fins when the load resistance is 1.7Ω

5 Discussion

5.1 Assumptions & Limitations

The simulations are not expected to produce the exact same results as the physical tests number for number due to assumptions made in simulations and limitations of physical testing. Some of the assumptions and limitations include:

- There are potential discrepancies in the testing apparatus such as the voltmeter, ammeter, temperature probes and multi-meter used in the tests. To aim to minimise the risk of this happening the voltmeter and ammeter were cross checked with a power supply unit.
- Another issue with testing was one of the TEG modules ceramic plates became damaged in clamping as a small corner broke off (please see figure 76).
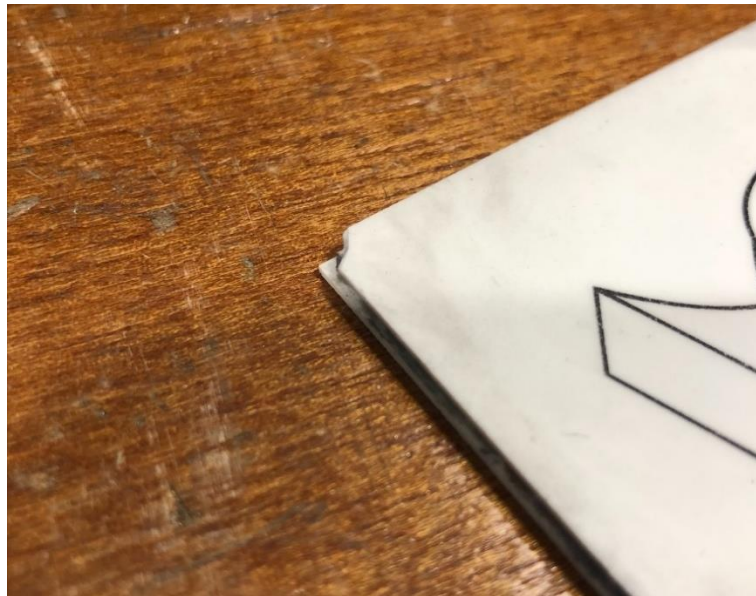
Figure 76: Broken ceramic on one of the TEGs, potentially from excessive clamping.

It was decided that the damage was not enough to cause concern as it had not broken deep enough to affect the semiconductor pellets.
- Another limitation from the physical tests was the corrosion of the surface of the steel 2mm plate which was used to modify the test rig. The numerous tests performed with this plate caused it to corrode, this rust was sanded off with wet and dry paper however it is hard to achieve the smoothness of the original plate once this damage has occurred.
- The heat transfer fins produced had buckling at the base when they were welded as the material used was aluminium and the base was too thin. In future, if heat transfer fins were to be tested they should be produced by either die casting or CNC machining.
- Finally, a jet effect was produced at the inlet of the system

Assumptions within Ansys which have potential to produce skewed results include:

- It was not possible to know the exact material properties used for every material in the simulations.
- The contact between all surfaces was assumed to be perfect which is unlikely to be the case.
- It was assumed that there was not heat loss through convection to the air, this was minimised by insulating the physical test rig with rubber sheeting.

- It was also assumed that the temperature of the water at the inlet and outlet on the simulations was the same as the recorded temperature which was recorded in the centre of the equidistant from the inlet and outlet in the physical tests.
- The temperature of the steel was assumed constant across the surface at the hot end of the system, which was likely not the case for the physical tests.

5.2 Physical Test Results

5.2.1 Flat Plate Results

The flat plate tests in theory, and in practice were the easier of the tests to perform. Initially there was issues with the insulating rubber surrounding the TEGs being too thick reducing the contact on between the TEGs and the heat exchange surface however this was quickly resolved by using thinner rubber sheet. After that all tests were easily performed.

As shown in section 4.1 all the current, voltage, and power trendlines for the physical tests show a positive correlation with increase in ΔT and follow the expected gradients. It was expected that the tests with aluminium as the heat exchange surface would produce higher output values (current, voltage, power) than the tests with steel due to the higher thermal conductivity of aluminium as a material. It was also expected that the thinner heat exchange materials would produce higher output values as section 3.5 of this report predicted that this would create a larger ΔT across the TEG modules. This was not the case; the thicker plate tests produced higher output values with both materials. The reason for this cannot be known for certain, however it is possible to hypothesise on potential reasons for this unexpected result. One key reason which could have contributed to this could be that the thinner material experience slight bending when clamped which would reduce the contact in places between the TEG modules and the heat exchange surface. The thick plates will be less malleable and stiffer, therefore when they were clamped, they experienced less bending than the thinner ones, to resolve this issue for future experiment it would be ideal to have more clamping points spread around the areas of the TEG modules. Another potential cause for this unexpected result could be that both the thinner plates were used multiple times in tests trying to perfect the test rig and testing methods. This will have caused erosion from the times which water had passed over the heat exchange surfaces. The plates were sanded with wet and dry paper to try to minimise this effect however this may not have got them to the same condition as the unused thicker plates. In particular, the aluminium plate had a near perfect shiny surface when new which was not possible to obtain from the sanding performed. The final potential reason which could have affected these results was that it appears the steel plates sent by the supplier were not of the exact same mild steel. Although both were mild steel, the thicker plate was slightly darker in colour and did not rust quite as fast as the thinner plate, this steel may have had slightly different and potentially more beneficial properties for this system.

5.2.2 Heat Transfer Fin Results

Trying to test the plates with heat transfer fins caused a few more problems than the tests discussed in section 5.1.1. The initial plan desired to test all four of the flat plates with aluminium heat transfer fins to see how it affected each heat exchange test for greater comparison. To do this the heat transfer fins were welded onto an aluminium base which was intended to be bolted onto each heat exchange surface to be tested. The welding of the

fins onto the base however caused some issues, as it caused the areas of the base in contact with the fins to buckle upward, making the base not flat and reducing the contact possible with the heat transfer plates in the most crucial areas. To attempt to resolve this issue, a block of wood was placed on the fins and a hammer was used to spread an even force which would push the malleable aluminium base back to a flatter shape. This helped but there was still much to be desired in terms of the flatness of the base. To further try to resolve this the base was placed on a belt sander in the aim of removing material which was blocking the contact of the concave areas. The base was finally sanded using wet and dry paper to create as smooth a surface as possible. The base was then bolted onto the 2mm thick aluminium plate with thermal grease between the surfaces to aim to increase thermal contact area. The test was performed and unfortunately this method was deemed unsuccessful as even with these adjustments the power output was lower than the test of the flat plate 2mm aluminium heat exchange surface. In an ideal scenario, to perform this method of bolt on heat transfer fins, a block of aluminium should have been CNC machined into the desired shape of the fins and base. Another method which would have worked better would be to die cast the heat transfer fins from molten aluminium. However, these methods would have put large economical strain on the project which was deemed unnecessary at the time of planning.

With the time and resources available, it was decided to weld some heat transfer fins directly onto the 6mm thick aluminium plate for testing to see how they may perform. The 6mm plate was chosen to reduce the risk of the plate buckling or bending during the welding process.

5.3 Validation of the Tests

5.3.1 Ansys Simulations

Two methods were used to model the test rig in Ansys. The results from the physical tests were modelled in Ansys using a rectangular inlet in the dimensions of the cross-section of the fluid domain with a laminar flow for simplicity. The second method used a circular inlet and outlet to emulate the pipes used in the real tests. The method which has been heavily documented through the report was using the pipe inlet and outlet with the k-ω turbulence model as this way these simulations are set up as like the scaled-up models as possible.

With all the simulations completed, the residuals converged to the absolute criteria and the other monitors showed no sign of error therefore there was no worry about the accuracy of simulations on initial sight. After analysing the results from the simulations of the test rig they all followed the patterns expected generally but some of the results are slightly skewed because the ΔT values simulated were different for each model. This was to allow comparison between physical tests and simulations however as the lowest ΔT simulated for the aluminium 6mm flat plate was higher than the rest of the plates, it appeared to decrease the gradient of the power curve slightly. In general, all the flat plate tests produced similar results to one another which was expected as the thickness and material should have only made a small difference with the thicknesses tested.

5.3.2 Comparisons & Validation

As stated in the objectives of this report, the results will be deemed valid if the simulation results lie within the standard error of the physical tests. The results graphs in section 4.4 for the power comparisons show the standard error bars for the physical tests.

For the 2mm Aluminium flat heat exchange plate, the data shows that the simulations are within the standard error of the physical tests for 67% of the points tested. The simulation results are within the standard error values of the physical tests for ΔT values under approximately 16⁰C.

For the simulations involving the 6mm flat aluminium plate as the heat exchange surface 78% of the simulation results can be deemed valid as they fit within the standard error of the physical tests. Upon looking at figure 60 it appears that all temperature differences below approximately 17⁰C are within tolerance.

The tests for the 2mm thick steel heat exchange plate did not shows as accurate results as the aluminium plates. Only 56% of the physical test points had a simulation power within the standard error tolerance range. It showed that all the points below approximately 14⁰C were within tolerance.

For the 6mm steel flat plate scenario, only 44% of the test points had simulation power within the tolerance. This appears much worse than it is due to two points near $\Delta T \approx 10$⁰C just having the simulation results fall outside the tolerance. The rest of the values stay within tolerance up to approximately a ΔT of 16⁰C.

For the simulations with the heat transfer fins on the 6mm aluminium plate only 44% of the simulation results can be deemed valid. Any ΔT higher than 11⁰C had simulation results out of tolerance.

5.3.3 Validation Decision

As stated, there were limitations such as bending which may have resulted in some of the physical results being lower than expected. With the knowledge of the limitations of some of the plates, the aluminium 6mm plate was the one which appeared to have the least issues as the steel plates had issues with corrosion and the thinner plates had potential issues with bending. Therefore, the results from the aluminium 6mm plate will be used to validate the scaled-up model. This is that all results ≤17⁰C will be deemed valid. At $\Delta T \approx 20$⁰C, the power produced is likely to be approximately 87% of what is shown in the simulations.

5.4 Scaled-Up Model

5.4.1 Ansys Simulations

As described four models were simulated to analyse how the TEGs may perform once scaled-up into a submarine. The TEG modules were positioned longitudinally in line with the submarine, with and without a heat transfer fin, and laterally across the cross section of the submarine, with and without heat transfer fins. What may come as a surprise on first sight of the results is that both the models with heat transfer fins produced less power than the models without. Heat transfer fins are usually added to increase the rate of forced convection, so why in this case does it decrease the amount of power produced? To understand this, we look at figure 70 which shows a cross sectional view of the temperature contours in the longitudinal layout with no fins. Due to the thickness of the submarine hull and the speed at which it is travelling, there is no large temperature drop from the surface of the submarine wall to the fluid in the boundary layer. In fact, the temperature near the surface of the hull is nearly the same as the free stream fluid temperature. The recommendation by (J. Falcão Carneiro, 2018) that an AUV using TEGs would require heat transfer fins was likely based upon a slower moving AUV with a much thinner wall. The

heat transfer fins added in this research appear to just increase the distance in which the heat must travel to reach the forced convection rather than adding any benefit. This can be looked at as good news as the installation of this system would not require the addition of any external features to the submarine which would cause additional drag and potentially upset the handling of the submarine. Four modules were simulated in the system, however if more power was desired then the number of modules could be increased, if a higher voltage was desired then these could be connected in series in addition to the original modules. This will likely be required if the system is to charge a backup battery as at the maximum power point for $\Delta T=15^{\circ}C$ the voltage produced is 0.771V which is unlikely to be enough to charge a useful battery.

5.3.2 Implementation of the system

Looking at the power, voltage, and current values being produced by the system there are two clear methods for utilising the electricity generated, it could either power a subsystem within the submarine/AUV or charge up a backup battery to be used however is required. In both cases, some form of DC-DC conversion would likely be necessary to convert the voltage to a usable form. In a similar manner to (Jensak Eakburanawat, 2005), it would be possible to utilise the energy to charge a 6V battery and store the power as useful electrical energy. To optimise the power produced by the TEGs when charging the battery, the correct number of modules should be chosen based upon where the submarine will operate.

For the sake of this report, it is presumed that the submarine in question will operate at a depth which creates a ΔT of $15^{\circ}C$ between the submarine interior and the water. To achieve maximum power output the system described in this report should be laid out eight time connected in series electrically. This should create a voltage of approximately 6.2V which would be suitable for charging the battery. It is unlikely the temperature difference will stay the same throughout the journey therefore a SEPIC convertor like the one described in to (Jensak Eakburanawat, 2005) should be used to keep the voltage at a suitable level to charge the battery.

6 Conclusions

6.1 Current Research

This research aimed to determine whether the use of TEGs in submarines/AUVs was logistically and economically viable. The system logistically is definitely viable as it would be relatively easy to implement. All that would be required to be made would be a steel holding base for the TEGs and an aluminium heat transfer surface which can transfer the heat from the TEGs to the submarine wall. These could be CNC machined or die cast. Thermal insulation would also have to be used on the submarine wall in the vicinity of the system. Economically, the system would be relatively expensive at first, as if the scenario described in section 5.3.2 is used, ideally 32 TEG modules should be used. This would cost approximately £3,200 for just the TEGs. However, this would be an investment for the future as the modules require no maintenance and will produce a passive energy source for a massive amount of time. The TEG modules will not need replacing unless they are damaged, giving them an advantage over many other sources of power.

This thesis has developed a method of analysing how TEGs will perform in a system with forced convection using water to maintain a temperature difference across TEGs for power generation. The results from simulations were deemed viable for the temperature ranges which would be found in the scenarios analysed in this research, therefore the scaled-up models simulating how the system would perform in a submarine can judged to be an accurate representation.

This thesis also confirmed that the use of heat transfer fins is not necessary for a submarine with a hull thickness like the one studied in this report (38mm). The research also showed that the TEGs being line longitudinally down the submarine is superior to laterally across the cross section of the hull.

The results obtained from this research show that Ansys Fluent and Thermal Electric are can both be used to obtain accurate predictions of how TEG modules may perform in a system with forced convection to increase heat transfer. The research not only showed that this is possible but has displayed a method which clearly works when analysing systems with a low temperature difference ($\Delta T \leq 17^{\circ}C$).

6.2 Future Recommendations

If a project like this was to be carried out, a few recommendations on improving the accuracy of the results include:

- More temperature sensors should be used in the water. If temperature sensors in the water at both the inlet and outlet were used, then the simulation input values in Ansys for temperatures of the water could have been more accurate. A further temperature sensor could also be used in the middle of the flow as was used in this, for an average temperature at the mid-point of the flow.
- Like the previous point, more temperature sensors would be advised for used in the steel on the hot side of the system. It is suggested by the author that in future, a temperature sensor under each TEG module would be ideal; this would allow for four different input temperatures when simulating in Ansys rather than one average. This will produce more accurate results.

- As stated in section 5.1, if heat transfer fins are to be manufactured out of aluminium, die casting or CNC machining is recommended to avoid welding induced buckling of the material.
- For future work, the transitions from the hose to the area of water being simulated should be made more gradual by using a funnel shaped design to gradually increase the cross-sectional area. This may reduce the complexity of the flow which the simulations must calculate whilst also producing a more similar flow to that which would be experienced in a system on a real submarine.

The simulations in this research give a good estimate of how TEGs should perform when implemented into a system such as a submarine/AUV. For future work it is recommended that a system like the one designed in this research is built and implemented into a submarine to be tested in a mission to understand exactly how much power it could produce in the real world. This research has shown how based upon simulations, heat transfer fins should not be necessary for submarine due to the thickness of the hull. This makes a system much easier to build and implement for testing in a real submarine mission.

Further research into specific sub-systems within a submarine which the system could power would be beneficial for implementing the system in the real world.

Bibliography

A. Abdullah, e. a. (2016). Thermal conductivity and viscosity of deionised water and ethylene glycol-based nanofluids. *Journal of Mechanical Engineering and Sciences*, 2249-2261.

A. Agarwal, R. M. (2021). Numerical analysis of tube flow with helical insert using nano fluid to enhance heat transfer. *Materials Today: Preceedings*, 5093-5097.

A. S. Korotkov, V. V. (2017). Modeling thermoelectric generators using the ANSYS software platform: Methodology, practical applications, and prospects. *Russian Microelectronics, 46*, 131-138.

Abolhasan Khajepoura, F. R. (2017). An approach to design a 90Sr radioisotope thermoelectric generator using analytical and Monte Carlo methods with ANSYS, COMSOL, and MCNP. *Applied Radiation and Isotopes*, 51-59.

Alexander Korotkov, V. L. (2017). *Simulation of thermoelectric generators and its results experimental verification.* Iasi: IEEE.

Andrea Montecucco, J. S. (2014). The effect of temperature mismatch on thermoelectric generators electrically connected in series and parallel. *Applied Energy*, 47-54.

Ansys. (2009, September 1). *Guide to a Successful Simulation Using ANSYS FLUENT*. Retrieved from AFS: https://www.afs.enea.it/project/neptunius/docs/fluent/html/gs/node17.htm

Ansys. (2010). *Fluent Lecture 6 Turbulence*. Retrieved from Ansys: https://imechanica.org/files/fluent_13.0_lecture06-turbulence.pdf

Antar M.M. Abdala, Q. Z. (2013). A two-equation k-omega turbulence model simulation to narrow trench on flat plate. *International Journal of Energy and Environment*, 699-712.

Artur Wodołazski, N. H. (2021). CFD Numerical Modelling of a PV–TEG Hybrid System Cooled by Air Heat Sink Coupled with a Single-Phase Inverter. *MDPI: Materials, 14*(19).

Avraham, T. (2019, February 1). *Know Thy Mesh- Mesh Quality*. Retrieved from CFD Israel: https://cfdisrael.blog/2019/02/01/know-thy-mesh-mesh-quality-part-i/

Ayman Eldesoukey, H. H. (2019). 3D model of thermoelectric generator (TEG) case study: Effect offlowregime on the TEG performance. *Energy Conversion and Management, 180*, 231-239.

Bass, & C., J. (1993). *United States of America Patent No. US5625245*.

Benchmark Minerals. (2021, April 13). *Lithium Prices.* Retrieved from Benchmark Minerals: https://www.benchmarkminerals.com/lithium-prices/

Brad Baker, M. J. (2015). *Use of High-Power Diode Laser Array for Pre- and Post- Weld Heating During Friction Stir Welding of Steels.* Research Gate.

Carl Freitas, D. V.-R. (2021). Sea temperature effects on depth use and habitat selection in a marine fish community. *Journal of Animal Ecology, 90*(7), 1787-1800.

Cheng Jin An, Y. H. (2017). High-performance flexible thermoelectric generator by control of electronic structure of directly spun carbon nanotube webs with various molecular dopants. *Journal of Materials Chemistry A, 30*.

Chethan R Patil, D. D. (2021). NUMERICAL INVESTIGATION OF HEAT TRANSFER IN AIRCRAFT ENGINE BLADE USING K-EPSILON AND SST K-OMEGA MODEL. *IOP Conference Series: Materials Science and Engineering 1013 012027*.

Cong Jiang, e. a. (2021). Ultrahigh performance polyvinylpyrrolidone/Ag2Se composite thermoelectric film for flexible energy harvesting. *Nano Energy, 80*.

D. Samson, M. K. (2011). Wireless sensor node powered by aircraft specific thermoelectric energy harvesting. *Sensors and Actuators A: Physical, 172*(1), 240-244.

D. Samson, M. K. (2012). Flight Test Results of a Thermoelectric Energy Harvester. *Electronic Materials, 41*(6), 1134-1137.

D. Samson, T. O. (2010). Aircraft-Specific Thermoelectric Generator Module. *Electronic Materials, 39*(9), 2092-2095.

Davide Beretta, e. a. (2019). Thermoelectrics: From history, a window to the future. *Materials Science & Engineering, 138*, 210-255.

Dawid Taler, P. O. (2014). Determination of heat transfer formulas for gas flow in fin-and-tube heat exchanger with oval tubes using CFD simulations. *Chemical Engineering and Processing: Process Intensification*, 1-11.

Dehua Hu, X. C. (2020). Thermoelectric Materials: High Thermoelectric Performance in n-Type Perylene Bisimide Induced by the Soret Effect . *Advanced Materials, 32*(45).

Delkia. (2022). Concept Submarine CAD model. Cumbria, England.

Douglas C. Webb, P. J. (2001). SLOCUM: An Underwater Glider Propelled by Environmental Energy. *IEEE JOURNAL OF OCEANIC ENGINEERING, 26*(4), 447-452.

Dresselhaus, L. D. (1993). Thermoelectric figure of merit of a one-dimensional conductor. *Phys. Rev. B, 47*(24).

Eauropean Thermodynamics. (2022). *GM250-127-28-12 Datasheet.* Retrieved from https://docs.rs-online.com/40a2/0900766b81110d9c.pdf

Engineering ToolBox. (2005). *Seawater Properties*. Retrieved from Engineering ToolBox: https://www.engineeringtoolbox.com/sea-water-properties-d_840.html

ETD. (2022). *GM250-127-28-12 Datasheet.* Retrieved from European Thermodynamics: https://docs.rs-online.com/40a2/0900766b81110d9c.pdf

G. Constantinescu, J. C. (2013). New promising Co-free thermoelectric ceramic based on Ba–Fe–oxide. *Journal of Materials Science: Materials in Electronics, 24*, 1832-1836.

Gabriel Constantinescu, S. R. (2021). Exploring the High-Temperature Electrical Performance of Ca3−xLaxCo4O9 Thermoelectric Ceramics for Moderate and Low Substitution Levels. *Symmetry, 13*(5).

Geppert, A. F. (2014). A High-Temperature Thermoelectric Generator Based on Oxides. *Energy Harvesting and Systems, 1*(1-2).

Gökhan Canbolat, A. Y. (2018). Numerical Investigation of Transitional Flow over a Flat Plate under Constant Heat Fluxes. *Academic Prospective Procedia*, 187-195.

Goldsmid, H. J. (2017). *The Physics of Thermoelctric Energy Conversion.* New South Wales: Morgan & Claypool Publishers.

Guohui Wang, Y. Y. (2020). Ocean thermal energy application technologies for unmanned underwater vehicles: A comprehensive review. *Applied Energy, 278*, 1-26.

Hyeongdo Choia, Y. J. (2018). Enhancement of reproducibility and reliability in a high-performance flexible thermoelectric generator using screen-printed materials. *Nano Energy, 46*, 39-44.

J. Falcão Carneiro, F. G. (2018). Model and simulation of the energy retrieved by thermoelectric generators in an underwater glider. *Energy Conversion and Management, 163*, 38-49.

J.R. Buckle, A. K. (2013). Autonomous Underwater Vehicle Thermoelectric Power Generation. *Electronic Materials, 42*(7), 2214-2220.

Jaegle, M. (2007). *Simulating Thermoelectric Effects with Finite Element Analysis using COMSOL*. Freiburg: Fraunhofer-Institute for Physical Measurement Techniques.

Jensak Eakburanawat, I. B. (2005). *Development of a thermoelectric battery-charger with microcontroller-based maximum power point tracking technique.* Thonburi: King Mongkuts University of Technology Thonburi.

Jordan, K. C. (1958). *United States of America Patent No. US 2844639.*

Jorge Luis Rosales, V. A. (2018). *United States of America Patent No. US20180351066A1.*

Kar, C. G. (2016). Recent advances in thermoelectric materials. *Materials Science, 83*, 330-382.

Kiekhaefer, E. C. (1965). *United States of America Patent No. US003217696.*

Kim, H. J. (2016). Chemically Exfoliated SnSe Nanosheets and Their SnSe/Poly(3,4-ethylenedioxythiophene):Poly(styrenesulfonate) Composite Films for Polymer Based Thermoelectric Applications. *ACS Nano, 10*(6), 5730-5739.

Lienhard, J. H. (2020). Heat transfer in flat-plate boundary layers: a correlation for laminar, transitional, and turbulent flow. *Journal of Heat Transfer.*

M Ajmi, e. a. (2020). *Convective heat transfer optimization with rib's deployment in a turbulent offset jet flow.* The Japan Society of Fluid Dynamics.

Manuela I. Brunner, D. L. (2021). An extremeness threshold determines the regional response of floods to changes in rainfall extremes. *Springer Nature.*

Marcos Compadre Torrecilla, A. M. (2019). Novel model and maximum power tracking algorithm for thermoelectric generators operated under constant heat flux. *Applied Energy, 256.*

MatMatch. (2022). *ISO 3574 Grade CR4.* Retrieved from MatMatch: https://matmatch.com/materials/minfm56846-iso-3574-grade-cr4

Mayhew, R. &. (1992). *Thermodynamics- Work & Heat Transfer.* Harlow: Pearson Education Limited.

McConkey, E. &. (1993). *Applied Thermodynamics for Engineering Technologies.* Harlow: Pearson Education Limited.

Metals4U. (2022). *1050-a Aluminium.* Retrieved from Metals4U: https://www.metals4u.co.uk/blog/1050a-aluminium

Michael Freunek, M. M. (2009). New Physical Model for Thermoelectric Generators. *Journal of Electronic Materials*, 1214-1220.

Ming He, F. Q. (2013). Towards high-performance polymer-based thermoelectric materials. *Energy Environ. Sci., 6*, 1352-1361.

Mohamed Elkhmri, P. H. (2021). NUMERICAL STUDY OF MIXED CONVECTIVE HEAT TRANSFER FROM NARROW SIDE-UP TWO-SIDED ISOTHERMAL FLAT PLATES. *Proceedings of the Canadian Society for Mechanical Engineering International Congress.* Charlottetown: CSME Congress .

Murat Emre Demira, I. D. (2017). Development of an integrated hybrid solar thermal power system with thermoelectric generator for desalination and power production. *Desalination*, 59-71.

NASA. (2021, May 7). *Reynolds Number: Nasa.* Retrieved from NASA: https://www.grc.nasa.gov/www/BGH/reynolds.html

NCDC. (2020). *How do we know the Earth's climate is warming?* Retrieved from NCDC: https://www.ncdc.noaa.gov/monitoring-references/faq/indicators.php#warming-climate

Nesrine Jaziri, A. B. (2020). A comprehensive review of Thermoelectric Generators: Technologies and common applications. *Energy Reports, 6*, 264-287.

Nesrine Jaziri, e. a. (2021). Low-temperature co-fired ceramic-based thermoelectric generator with cylindrical grooves for harvesting waste heat from power circuits . *Applied Thermal Engineering, 184.*

New World Encyclopedia. (2018, December 12). *North Sea: New World Encyclopedia.* Retrieved from New World Encyclopedia: https://www.newworldencyclopedia.org/entry/North_Sea

Nicholas K. Dulvy, S. I. (2008). Climate change and deepening of the North Sea fish assemblage: a biotic indicator of warming seas. *Journal of Applied Ecology, 45*(4), 1029-1039.

Nuclear Power. (2022). *Boundary Layer Thickness: Nuclear Power.* Retrieved from Nuclear Power: https://www.nuclear-power.com/nuclear-engineering/fluid-dynamics/boundary-layer/boundary-layer-thickness/

Nuclear Power. (2022). *What is the Prandtl Number: Nuclear Power.* Retrieved from Nuclear Power: https://www.nuclear-power.com/nuclear-engineering/heat-transfer/introduction-to-heat-transfer/characteristic-numbers/what-is-prandtl-number/

O. Maganga, N. P. (2014). Hardware implementation of Maximum Power Point. *Journal of Electronic Materials, 43*, 2293-2300.

OED. (2022). *Sustainable: OED.* Retrieved from Oxford English Dictionary: https://www.oed.com/view/Entry/195210?redirectedFrom=sustainable#eid

Oliver Eibl, ,. K. (2015). *Thermoelectric Bi2Te3 Nanomaterials* (1st ed.). Weinheim: John Wiley & Sons, Incorporated.

P. Ziolkowski, P. P. (2010). Estimation of Thermoelectric Generator Performance by Finite Element Modeling. *Journal of Electronic Materials, 39*, 1934-1943.

R. Kiflemariam, M. A. (2014). *Modeling Integrated Thermoelectric Generator-Photovoltaic Thermal (TEG-PVT) System.* Boston: COMSOL Conference.

Raju, D. E. (2022). *Climate change made 2022 UKs heatwave "10 times more likely".* Retrieved from Carbon Brief: https://www.carbonbrief.org/climate-change-made-2022s-uk-heatwave-at-least-10-times-more-likely/

Rama Venkatasubramanian, E. S. (2001). Thin-®lm thermoelectric devices with high room-temperature figures of merit. *Nature, 413*, 597-602.

Rioult, M. (2015, Spetember). *Research Gate.* Retrieved December 20, 2021, from https://www.researchgate.net/figure/Illustrated-scheme-showing-the-Fermi-level-position-within-the-band-gap-in-the-case-of_fig9_283303105

RS Components. (2022). *GM250-127-28-12 Thermoelectric Generator.* Retrieved from RS Components: https://docs.rs-online.com/40a2/0900766b81110d9c.pdf

RS Components. (2022). *Silicone Thermal Grease 5W/mK.* Retrieved from RS Components: https://uk.rs-online.com/web/p/thermal-grease/7074736

S. Mahmoudinezhada, S. A. (2019). Experimental and numerical study on the transient behavior of multi-junction solar cell-thermoelectric generator hybrid system. *Energy Conversion and Management*, 448-455.

Saleh, U. A. (2021). *Analysis of the Performance of Thermoelectric Generators.* Singapore: University Tun Hussein.

Seong Eun Yang, F. K. (2021). Composition-segmented BiSbTe thermoelectric generator fabricated by multimaterial 3D printing. *Nano Energy, 81.*

Seyed Mohsen Pourkiaei, M. H. (2019). Thermoelectric cooler and thermoelectric generator devices: A reviewof present and potential applications, modeling and materials. *Energy, 186*, 1-17.

Snyder G.J., T. E. (2008). Complex thermoelectric materials. *Nature Materials, 7*, 105-114.

Sun Jin Kim, J. H. (2014). A wearable thermoelectric generator fabricated on a glass fabric. *Energy Environment Science*, 1959-1965.

Suski, E. D. (1996). *United States of America Patent No. US5419780A*.

Thielen M., S. L. (2017). Human body heat for powering wearable devices: From thermal energy to application. *Energy Conversion and Management, 131*, 44-54.

Topal, E. T. (2011). *A Flow Induced Vertical Thermoelectric Generator and Its Simulation Using COMSOL Multiphysics*. Boston: COMSOL Conference.

Tulaev, A. T. (2019). Simulation of Si/Ge based thermoelectric generator. *Journal of Physics*.

Uygun, U. (2020, July 22). *Smooth Transition Inflation Option in Ansys*. Retrieved from Mechanical Land: https://mechanicalland.com/smooth-transition-inflation-option-in-ansys-meshing/

Wei He, G. Z. (2015). Recent development and application of thermoelectric generatorand cooler. *Applied Energy, 143*, 1-25.

Wilcox, D. C. (1998). *Turbulence Modelling for CFD*. California: DWC Industries.

WWA. (2022). *Without human-caused climate change temperatures of 40oC in the*. WWA.

X.F. Zheng, C. L. (2014). Experimental study of a domestic thermoelectric cogeneration system. *Appl Therm Eng, 62*, 67-79.

Appendix

The main contour of interest for analysis in the Ansys Fluent study was the temperature in this research, the velocity and pressure contours however give a good understanding as to whether the results will be accurate. The velocity and pressure contours for the longitudinal layout over the fin shows the expected areas of low velocity in the wake of the fin and on its front face. This can be seen in figure 77.
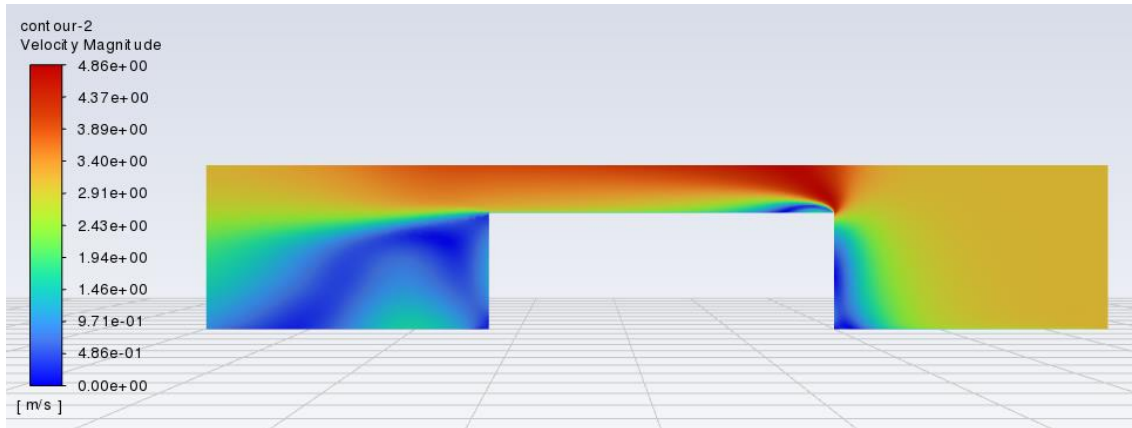

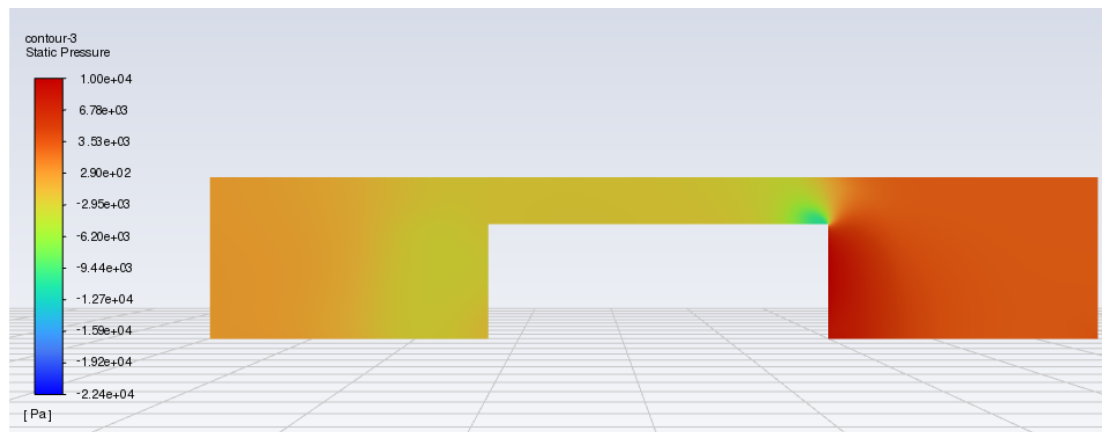*Figure 77: Scaled up model, Longitudinal layout with heat transfer fin, Velocity Contour*

Figure 78: Scaled up model, Longitudinal layout with heat transfer fin, Pressure Contour

As stated in the research two methods were chosen to model the test rig in Ansys, using pipe inlet and using a rectangular inlet with laminar flow. The pipe inlet with turbulent flow was used in the research as it showed a higher accuracy and more similarity to the conditions of the real experiment. Figure 79 shows the results using the rectangular laminar inlet for the aluminium flat heat exchange plate of 6mm thickness.
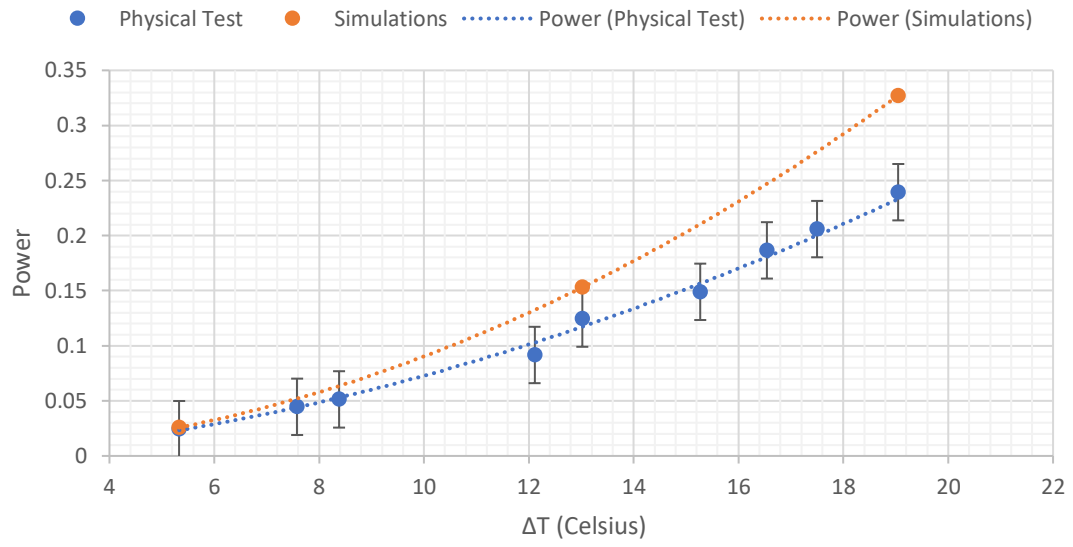
Figure 79: Power comparison for the simulations using a rectangular inlet and outlet with a 0.18475m/s inlet velocity (simplified model), aluminium 6mm flat plate